

# **Crystallisation control for fluorine-free slags using the Single Hot Thermocouple Technique**

To the Program of Postgraduate Studies in Mining, Metals and Materials  
Engineering (PPGE3M)

of the **Universidade Federal do Rio Grande do Sul**

and

to the Faculty of Materials Science and Technology (Faculty 5)

of the **Technische Universität Bergakademie Freiberg**

(bi-national doctorate)

approved

## **THESIS**

to attain the academic degrees of

**Doutor em Engenharia**

**(Dr.)**

and

**Doktor-Ingenieur**

**(Dr.-Ing.)**

submitted

by Engenheiro Metalúrgico Jeferson Leandro Klug

born on October 31<sup>st</sup> 1978 in Camaquã, Brazil

Reviewers: Prof. Dr.-Ing. Antônio C. F. Vilela, Porto Alegre, Brazil  
Prof. Dr.-Ing. Nestor C. Heck, Porto Alegre, Brazil  
Prof. Dr. Hamilton F. Gomes de Abreu, Fortaleza, Brazil  
Prof. Dr.-Ing. Michael Stelter, Freiberg, Germany  
Prof. Dr.-Ing. habil. Christos G. Aneziris, Freiberg, Germany  
Prof. Dr. rer. nat. habil. Jörg Matschullat, Freiberg, Germany

Date of the award: July 2<sup>nd</sup> 2012

## CONTENTS

<b>1. INTRODUCTION</b>	1
1.1 Importance of crystallisation control for mould slags	1
1.2 Mould powders	1
1.3 The necessity of developing F-free mould powders	3
1.4 Control of horizontal heat transfer between steel shell and mould	5
1.5 State-of-the-art studies for solidification behaviour of slags	6
1.5.1 Slags with TiO <sub>2</sub> crystals	6
1.5.2 Slags with varied crystals	6
1.5.3 Effect of water on crystallisation of slags	9
<b>2. MOTIVATION AND OBJECTIVES</b>	11
<b>3. ESSENTIALS ON SOLIDIFICATION BEHAVIOUR OF SLAGS</b>	12
3.1 Glasses	12
3.2 Classical Nucleation Theory	13
3.3 Characteristics of nucleation and growth transformations	14
3.4 Time-temperature-transformation diagrams	15
3.5 Formal theory of transformation kinetics – isothermal transformation	16
<b>4. EXPERIMENTAL WORK</b>	21
4.1 Materials and samples preparation	21
4.2 Single Hot Thermocouple Technique (SHTT)	21
4.2.1 Thermocouple welding	24
4.2.2 Examination of the accuracy of the apparatus	25
4.2.3 Relation between visual observation and T versus t diagrams	26
4.2.4 Effect of atmosphere on CaF <sub>2</sub> crystallisation	29
4.2.5 Procedure for performing experiments using SHTT	30
4.3 Rotation viscometer	31
<b>5. RESULTS AND DISCUSSION</b>	33
5.1 CaO-Al <sub>2</sub> O <sub>3</sub> slag (CA)	33
5.1.1 Results	33
<i>Melting behaviour</i>	33
<i>CCT diagram</i>	33
<i>Viscosity measurements</i>	35
5.1.2 Discussion	36
5.2 CaO-SiO <sub>2</sub> slag (CS)	37
5.2.1 Results	37
<i>CCT diagram</i>	37

	<i>TTT diagram</i>	37
	<i>Conditions for intense crystal growth for CaO-SiO<sub>2</sub> slags</i>	38
	<i>Viscosity measurements</i>	38
5.2.2	Discussion	39
5.3	<b>CaO-SiO<sub>2</sub>-TiO<sub>2</sub> slag (CST_1)</b>	41
5.3.1	Results	41
5.3.2	Discussion	44
5.4	<b>CaO-SiO<sub>2</sub>-TiO<sub>2</sub> slag (CST_2)</b>	44
5.4.1	Results	44
	<i>CCT diagram</i>	45
	<i>TTT diagram</i>	45
	<i>Viscosity measurements</i>	46
5.4.2	Discussion	46
5.5	<b>CaO-SiO<sub>2</sub>-TiO<sub>2</sub>-Na<sub>2</sub>O-Al<sub>2</sub>O<sub>3</sub> slags (CSTNA)</b>	48
5.5.1	Results	48
	<i>Melting behaviour</i>	48
	<i>TTT diagrams</i>	50
	<i>Crystal's morphology</i>	51
	<i>Viscosity measurements</i>	53
5.5.2	Discussion	54
5.6	<b>Thermodynamic calculations</b>	57
5.7	<b>Critical cooling rates</b>	58
5.7.1	Results	58
5.7.2	Discussion	59
5.8	<b>Kinetics of crystal growth</b>	60
5.8.1	Results	60
	<i>CST_2 slag</i>	60
	<i>CSTNA_1 slag</i>	61
5.8.2	Discussion	62
5.9	<b>Relation between basicity index and crystallisation tendency</b>	64
5.10	<b>Solidification behaviour of fluorine-free mould powders for billet casting</b>	66
5.10.1	Laboratory tests	66
	<i>Chemical composition</i>	66
	<i>Melting characteristics</i>	67
	<i>Viscosity</i>	68
	<i>Melting behaviour</i>	69
	<i>Crystallinity analysis</i>	71
5.10.2	Industrial tests	75
6.	<b>CONCLUSIONS</b>	79

<b>REFERENCES</b>	81
<b>EXTENDED ABSTRACT - English</b>	85
<b>EXTENDED ABSTRACT - Português</b>	97
<b>EXTENDED ABSTRACT - Deutsch</b>	109

## 1. INTRODUCTION

### 1.1 Importance of crystallisation control for mould slags

The continuous casting process is applied to the majority of steel grades by most steel manufacturers. Good understanding and control of phenomena in the mould during production of steel are essential to the success of the process. The slags used in the mould are very important when considering casting results, e.g., the quality of the steel slabs and “sticking severity”. The mould slags ultimately have an influence on the capacity of the caster, i.e., how fast it is possible to cast with a good quality and without breakouts caused by sticking [1-4].

During continuous casting process, the presence of crystals in mould slags has a decisive effect on both the lubrication and the heat transfer rate between the mould and the steel strand.

Once the mould powder is melted on the top of the liquid steel and the mould slag infiltrates between the mould and the strand surface, the liquid slag is exposed to different cooling paths that can promote or prevent crystallisation. In fact it is common to see glassy parts of the slag in areas of high cooling rates with crystalline fractions at lower cooling rates [5]. In the following section the functions of mould powders are described with more details.

Considering the development of fluorine-free mould powders for slab casting and thin slab casting, the control of crystallisation is imperative. Therefore, mould powders crystallisation behaviour should be characterised. Time-temperature-transformation (TTT) or continuous-cooling-transformation (CCT) diagrams provide a fundamental understanding of the transformation kinetics. These diagrams can be constructed using the Single Hot Thermocouple Technique (SHTT).

The SHTT is a unique apparatus that enables measurement of the slag sample temperature using a thermocouple while the sample is heated simultaneously. The sample is placed on a thermocouple tip and it can be subjected to rapid cooling rates or heating rates, or to be held under isothermal conditions. The advantage of the SHTT is that it allows for the in situ observation of melting and solidification under various thermal conditions. Due to the low heat capacity of the system (sample and thermocouple) very high heating and cooling rates can be easily obtained (> 3000 °C/min). The SHTT can be applied to slags which are optically transparent or translucent, while the crystalline phase which precipitates upon cooling should be opaque.

### 1.2 Mould powders

Mould powders (or mould fluxes) are synthetic metallurgical slags that should fulfil different functions during the continuous casting of steel: (i) protect the steel meniscus from oxidation, (ii) absorb inclusions that float up from the steel, (iii) provide thermal insulation to prevent the steel from freezing, (iv) provide the optimum level of

horizontal heat transfer between the shell and mould and (v) lubricate the steel shell. The mould slag i.e. the mould powder that was melted in mould during continuous casting is one of the most important slags in the melting shop [2, 6-8].

Once applied in the mould, the mould powder is heated by liquid steel. During heating, the decomposition of carbonates as well as the oxidation of carbon materials used to control the melting behaviour of the mould powder take place. After melting, in contact with the molten steel, the liquid mould slag changes its chemical composition as a function of time, because of (i) absorption of non-metallic inclusions from the liquid steel and (ii) reactions between mould slag and liquid steel during continuous casting. Then, the modified liquid slag infiltrates the gap between the steel strand and mould wall and solidifies [7, 9-12]. The slag film closest to the mould experiences high cooling rates and initially transforms into a glassy layer (typically 2-4 mm thick), while the slag next to the strand (typically 0.1 mm) remains liquid; between these two layers, crystals will start to precipitate, forming a crystalline layer [1, 13]. A very large temperature gradient (approximately 1000 °C) exists across the slag layers. Strand lubrication is provided by the liquid part of the slag film. A schematic representation of the various slag layers in the mould during the continuous casting process is shown in Figure 1 [6].

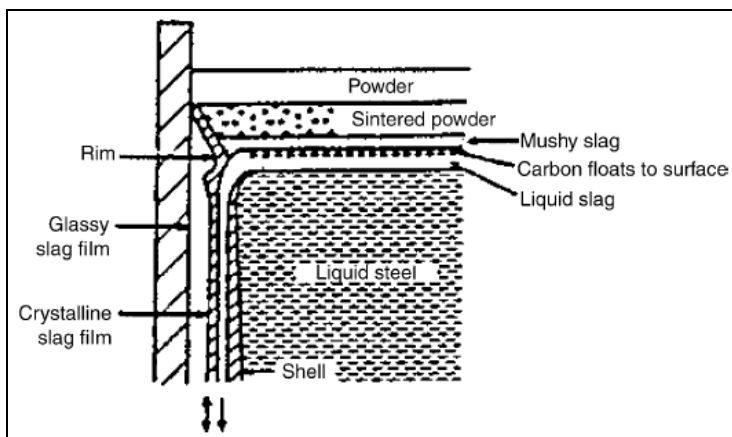


**Figure 1.** Schematic drawing of the various slag layers formed in the mould [6].

Slag film samples were obtained from mould at the end of casting sequences. It was found that the most typical feature in the sampled films was the layer in that the cuspidine phase ( $3\text{CaO}\cdot 2\text{SiO}_2\cdot \text{CaF}_2$ ) was dominant. The films had a crystalline structure that either formed during cooling or via devitrification, i.e., crystallisation from the glassy state. It was observed that the residence time of the slag film, or at least the part of the film in contact with the mould, is very long – up to 10 hours or more [2, 3].

The devitrification of mould slags is similar to that of ordinary glass [14]. Devitrification plays an important role in continuous casting processes because it is related to surface roughness of slag films, that in turn can be related to the interfacial thermal resistance and friction force at the mould/strand interface [2, 15, 16]. It has

been reported that friction in continuous casting moulds depends on the viscosity of the mould slag and on the type of crystalline phases present [8].

With the aid of mould powder, an equal thickness of the solidified shell around the perimeter of the mould can be obtained, thus avoiding areas where shell thickness is less than in the surrounding areas. Deformation of the shell tends to occur chiefly on the thinnest areas and it is caused by shell shrinkage, ferrostatic pressure and bending. It can result in cracks and other consequences [3].

In the upper part of the mould – the most critical zone in the continuous casting process – the liquid metal forms a curved meniscus in contact with molten and solidified mould powder. The surface of the strand is created as the solidification of the metal begins. In general, the beginning of the shell growth is determined by the local heat flow, the strength of the shell and the fluid dynamics. The most common defects on continuously cast material, the oscillation marks, are formed in the meniscus regions. Other important casting defects formed during initial solidification are hot cracks (hot tears) and surface cracks [2].

The performance of mould powders is controlled by three physical and technological properties [6, 17-19]: (i) viscosity (usually at 1300 °C), (ii) crystalline phase fraction developed in the slag film, and (iii) the thickness of both the liquid and solid layers of the slag film that are, in turn, dependent on the break ( $T_{br}$ ) temperature of the mould slag.

The choice of the mould powder for slab casting is a difficult task because of the complicated nature of the powder composition, and because the mould powder has many important functions. Due to the complex requirements in the industrial process the choice is based on trials in the caster, followed by investigations on the quality of the slabs. Normally in the melting shop different compositions – with reasonably small differences – are tested [3, 6].

### **1.3 The necessity of developing F-free mould powders**

Commercial mould powders contain fluorine, typically as calcium fluoride ( $\text{CaF}_2$ ). Fluorine is an essential component since it has a significant influence on mould powder properties, such as (i) to decrease the *liquidus* temperature, important for melting behaviour and lubrication properties of the mould slag; (ii) to decrease the viscosity of the mould slag, important for mould powder consumption (slag infiltration) i.e. the formation of a stable slag film; and (iii) to promote the crystallisation of the slag film, important to control mould heat transfer during casting, forming cuspidine ( $\text{Ca}_4\text{Si}_2\text{O}_7\text{F}_2$ ) crystals [2, 20].

However, the use of fluorine in siliceous melts can lead to the formation of volatile, water-soluble fluorine compounds, in this respect primarily  $\text{SiF}_4$ . In continuous casting machines, fluorine can accumulate in the secondary cooling water, accompanied by a reduction of the pH-value. In such a medium, plant and equipment components are then susceptible to wear [21].

There is a clear trend in industry to eliminate fluorine from slags that are used during the production of steel. Fluorine in mould powders is undesirable from the environmental and health points of view due to the following reasons: (i) evolves easily from slags, producing health-injurious gaseous substances, such as hydrofluoric acid; (ii) creates problems for storage and utilisation of solid waste and (iii) causes machinery corrosion. Regarding machinery corrosion the hydrofluoric acid increases dramatically the corrosion rate especially below the mould where there is a high amount of water accelerating the process [12, 20-22].

Some materials that decrease viscosity strongly could be used to replace F in mould slags, such as  $\text{Li}_2\text{O}$ ,  $\text{B}_2\text{O}_3$  and  $\text{Na}_2\text{O}$ . Considering  $\text{Li}_2\text{O}$ , as a result from an European project [23] it was reported that  $\text{Li}_2\text{O}$  has a strong fluxing ability and can therefore be used in this sense as a fluorine substitute. However, the melting and solidification behaviour show differences with respect to the standard powders. This influences the performance of powders during continuous casting in terms of lubricating ability and steel solidification conditioning. Besides, it was reported [24] that  $\text{Li}_2\text{O}$  and  $\text{B}_2\text{O}_3$  dramatically reduce the melting range, lowering both the softening and the melting temperatures determined by the heating microscope, and also the *liquidus* temperature determined by DTA.

Mixtures with lower fluorides emission potential were studied [20], with the replacement of fluorine and/or sodium by lithium; the replacement of sodium is justified since in this case the formation of  $\text{NaF(g)}$  is avoided. The following advantages for lithium utilisation in mould powders were reported: (i)  $\text{Li}_2\text{O}$  causes significant decrease of *liquidus* temperatures and of viscosity; (ii) with  $\text{Li}_2\text{O}$  slags with better inclusions absorption potential can be produced; (iii)  $\text{Li}_2\text{O}$  is thermodynamically more stable than other alkaline oxides such as  $\text{Na}_2\text{O}$ , and also  $\text{B}_2\text{O}_3$ .

When using boron as substitute of fluorine, there is a risk of redox reactions involving dissolved elements in liquid steel – such as aluminium and silicon –, what would cause boron pick-up [20, 25].

Regarding  $\text{Na}_2\text{O}$ -bearing raw materials, they are interesting to substitute fluorspar because  $\text{Na}_2\text{O}$  decreases viscosity, *liquidus* temperature and it also promotes inclusions absorption, though inclusions absorption when using  $\text{Li}_2\text{O}$  is better (see equation (17) in Section 5.9). It is theoretically possible to increase  $\text{Na}_2\text{O}$  content up to 20%, above this content the solid phase nefeline ( $\text{Na}_2\text{O} \cdot \text{Al}_2\text{O}_3 \cdot 2\text{SiO}_2$ ) precipitates. Frequently  $\text{Na}_2\text{O}$  content in industrial mould powders is high (>10%) [20].

It seems possible to develop and use fluorine-free mould powders for slab casting and thin slab casting. Research on fluorine-free mould powder has to be promoted and plant trials should be organized in order to obtain suitable alternatives to fluorine. This can be realised by collaboration among universities, mould powder suppliers and steel plants [2].



#### 1.4 Control of horizontal heat transfer between steel shell and mould

The main problem related to the development of fluorine-free mould powders for slab casting is effectively controlling the heat transfer between the steel shell and mould. The crystallisation of cuspidine from mould slag is thought to be the most effective way of exerting heat-transfer control. Although the mechanism of heat-transfer control via the crystallisation of cuspidine has not yet been determined, two ideas have been proposed. An idea is that radiation heat flux is decreased by scattering at the boundary between the crystalline and the liquid layers; another idea is that the total heat flux is reduced by the large thermal resistance of the air gap formed as a result of the solidification shrinkage of the solidified slag layer. In any case, the crystallisation of cuspidine from mould slag has a great effect on heat-transfer control [26].

When a layer is formed directly on the mould surface either at the beginning of the casting or later on, it will form at first in a glassy state. If there is enough time and the temperature is sufficiently high, devitrification of the layer will take place, resulting in a crystalline phase. The presence of crystals in the liquid layer increases the friction between the mould and strand, leading to a higher incidence of sticker breakouts. On the other hand, a high crystallisation tendency is beneficial in the casting of peritectic steel grades. The formation of a significant crystal fraction in the mould slag film between mould and strand reduces the heat transfer rate and helps alleviate problems associated with longitudinal cracking that arises from the mismatch in the thermal contraction coefficients of  $\delta$ -ferrite and austenite. This mismatch results in strains on the growing shell, and to minimise these strains, it is important to decrease the heat flux. Anyway, it is clear that in the continuous casting mould slags crystallisation control is a matter of utmost importance. For example, for high speed thin slab casting, mould powder design concentrates on mild cooling i.e. specific values of basicity and break temperature, promoting the crystallisation of cuspidine [2, 3, 13].

As a rule of thumb low values of basicity ( $\text{CaO}/\text{SiO}_2 < 1.0$  for thin slab casting) will result in the formation of a more glassy slag film and consequently, improved lubrication and increased mould heat transfer. Increased values of basicity ( $\text{CaO}/\text{SiO}_2 > 1.0$  for thin slab casting) will generally result in a more crystalline and rigid slag film and consequently, decreased values for mould heat transfer and strand lubrication. A balance must be found between strand lubrication (glassy slag) and the control of mould heat transfer (crystalline slag) [2].

The heat transfer reduction would be possible according to the following mechanism: crystallisation of slag film increases the reflectivity of the crystalline slag layer in the film owing to enhanced scattering of light by introduction of crystal grain boundaries, and thereby more radiation energy returns from the crystalline slag layer to the steel, leading to reduction in the total heat flux across the film [27].

For the thin slab casting process, where the slag films are thin (approximately 200  $\mu\text{m}$ ) and the surface roughness has very low values, reflection of radiation at the

interface of the crystalline layers seems to be a plausible mechanism to explain the control of mould heat transfer during casting [2].

## 1.5 State-of-the-art studies for solidification behaviour of slags

### 1.5.1 Slags with $\text{TiO}_2$ crystals

There are some papers indicating that  $\text{TiO}_2$ -bearing raw materials can be used to replace fluorine-bearing raw materials, by forming  $\text{TiO}_2$  crystals instead of cuspidine [26, 28, 29] to allow for heat-transfer control.

Nakada and Nagata [26] analysed the basic system  $\text{CaO-SiO}_2\text{-TiO}_2$  evaluating the possibility of having it as a candidate for fluorine-free mould powder through the crystallisation of  $\text{CaO.SiO}_2\text{.TiO}_2$ , determining the time-temperature-transformation (TTT) diagram of two slag compositions through differential thermal analysis (DTA). They concluded that it is possible to obtain the heat transfer control function, but the thickness of the crystalline layer was found to be smaller than that of the crystalline layer resulting from cuspidine precipitation obtained under similar thermal conditions. Then, they suggested that it is worth investigating the effect of  $\text{Na}_2\text{O}$  addition in the  $\text{CaO-SiO}_2\text{-TiO}_2$  slags, since in this way it would be possible to decrease the incubation time of the crystals and consequently to increase the thickness of the crystalline layer.

Wen *et al.* [28] evaluated titanium-bearing blast furnace slags as a base material to develop F-free mould powders, evaluating their properties and their performance through laboratory experiments and plant trials. According to them the industrial trials indicated that F-free mould powders can effectively control mould heat transfer through perovskite ( $\text{CaO.TiO}_2$ ) precipitated in the infiltrated slag layer instead of cuspidine in fluorine-bearing powder, with better slab surface quality than fluoride-bearing powders in terms of crack index.

Qi, Wen and Tang [29] studied mould slags using a device that simulates the heat flux through the mould slag film, based on the copper finger method, and reported that when increasing  $\text{TiO}_2$  content in fluorine-free mould powders the activation energy for crystallisation from glassy solid slag and the activation energy for crystallisation from liquid slag are reduced. Thus, according to their report, from the perspective of the activation energy for crystallisation the fluorine-free mould powders containing  $\text{TiO}_2$  have already reached the level of industrial mould slags containing fluorine, and can be used to replace them.

### 1.5.2 Slags with varied crystals

Besides  $\text{TiO}_2$ -bearing slags, there are also other reports on the solidification behaviour of mould powders without fluorine or with relatively low fluorine contents using different crystals. For example, a  $\text{CaO-SiO}_2\text{-Na}_2\text{O}$  slag with low fluorine content was studied and compared with a  $\text{CaO-SiO}_2\text{-CaF}_2$  slag [30], measuring melting temperature, viscosity, crystallisation temperature by differential scanning

calorimetry, crystallisation ratio, and crystalline phases by X-ray diffraction. The compositions of these slags are in Table 1. It was concluded that they have similar behaviour according to these parameters, and then the CaO-SiO<sub>2</sub>-Na<sub>2</sub>O slag could be used for peritectic steel grades sensitive to longitudinal cracking. The crystals for the CaO-SiO<sub>2</sub>-CaF<sub>2</sub> slag are cuspidine, whereas the crystals for the CaO-SiO<sub>2</sub>-Na<sub>2</sub>O slag are Na<sub>2</sub>O.CaO.3SiO<sub>2</sub>.

**Table 1.** Mould powders composition (wt%) studied in [30].

Mould powder	CaO/SiO <sub>2</sub>	Al <sub>2</sub> O <sub>3</sub>	MgO	Fe <sub>2</sub> O <sub>3</sub>	F	Na <sub>2</sub> O + K <sub>2</sub> O + Li <sub>2</sub> O + MnO
CaO-SiO <sub>2</sub> -Na <sub>2</sub> O	0.8	3.0	2.0	1.0	1.0	24.0
CaO-SiO <sub>2</sub> -CaF <sub>2</sub>	1.3	1.5	1.7	0.6	6.5	7.9

Confocal scanning laser microscopy (CSLM) and single hot thermocouple technique (SHTT) were used to construct TTT diagrams in the CaO-SiO<sub>2</sub>-B<sub>2</sub>O<sub>3</sub>-Na<sub>2</sub>O-Al<sub>2</sub>O<sub>3</sub> system for different basicities, and also studying the effect of ZrO<sub>2</sub> addition on the crystalline behaviour of F-free mould powders [31]. It was found that the crystallisation temperature increases whereas the incubation time decreases with increasing basicity, i.e. increasing the basicity enhances the tendency of crystallisation, considering the systems in Table 2. This can be explained by the structure of the silicate molten slag. They also reported that the crystallisation temperature increased when adding 2% ZrO<sub>2</sub> (wt%), since ZrO<sub>2</sub> particles act as heterogeneous nucleation sites due to its limited solubility in molten slag. The following crystals were detected through X-ray diffraction and scanning electron microscope: CaSiO<sub>3</sub> in the slags CS-1 and CS-2, Ca<sub>3</sub>Si<sub>2</sub>O<sub>7</sub> and CaSiO<sub>3</sub> in the slag CS-3, and Ca<sub>2</sub>SiO<sub>4</sub> in the slag CS-4.

**Table 2.** Mould powders composition (wt%) studied by SHTT and CSLM in [31].

Slag	CaO/SiO <sub>2</sub>	Al <sub>2</sub> O <sub>3</sub>	Na <sub>2</sub> O	B <sub>2</sub> O <sub>3</sub>	ZrO <sub>2</sub>
CS-1	0.7	3.21	6.70	5.67	0
CS-2	0.8	2.87	6.56	5.02	0
CS-3	1.2	3.12	6.45	4.70	0
CS-4	1.3	2.62	6.53	4.70	0
CS-5	1.2	3.12	6.45	4.70	2.02

Regarding crystal morphologies, it was reported in [31] that for the systems in Table 2 they depend on the basicity and isothermal temperature, where equiaxed crystals are observed in a slag melt with high basicity and high isothermal temperature, and columnar crystals grow along the thermocouple at low isothermal temperature. The individual equiaxed crystals were observed when the isothermal temperature was higher than 1100 °C for all the slags. The crystals with columnar structure were observed when the isothermal temperature was lower than 1050 °C.

The hot-stage equipped Confocal Scanning Laser Microscope was used to build TTT diagrams in synthetic slags of the systems CaO-SiO<sub>2</sub>-FeO and CaO-SiO<sub>2</sub>-FeO-MnO

[32], analyzing the crystallisation kinetics. After melting, the samples were slowly cooled to certain temperatures, and then the temperature was maintained constant. Then the isothermal transformations were observed, the times for the first crystals precipitation were registered, and TTT diagrams were constructed. The effect of basicity in these systems was investigated – the higher the basicity, the faster the crystal precipitation. An increase in basicity for the studied systems would decrease viscosity of the molten slag, due to changes in structure and therefore in mass transport and precipitation kinetics.

In another study [33] two slags, a F-bearing and a F-free, whose compositions are in Table 3, were compared. Both presented similar behaviour regarding melting temperature, viscosity (at 1300 °C, break temperature, and similar  $\eta$ -T curve), crystallisation temperature tested by differential scanning calorimetry, and crystal ratio of slag by air cooling. The crystallized mineral phase of the F-free slag was mainly  $\text{Na}_2\text{O} \cdot 2\text{CaO} \cdot 3\text{SiO}_2$ . Further research was suggested on the basis of this F-free slag.

**Table 3.** Mould powders composition (wt%) studied in [33].

	CaO/SiO <sub>2</sub>	CaO	SiO <sub>2</sub>	Al <sub>2</sub> O <sub>3</sub>	MgO	MnO	F	B <sub>2</sub> O <sub>3</sub>	Li <sub>2</sub> O+Na <sub>2</sub> O
<b>F-bearing</b>	1.4	43.4	30.5	2.5	0.8	-	10.4		12.4
<b>F-free</b>	0.8	31.2	36.8	3	2	8	-	2	16

F-free mould powders were examined in the system  $\text{CaO-SiO}_2\text{-Al}_2\text{O}_3\text{-Na}_2\text{O-B}_2\text{O}_3$  measuring the parameters viscosity, thermal conductivity, crystallisation behaviour, and comparing with commercial mould powders used in high speed continuous casting [34]. In this work B<sub>2</sub>O<sub>3</sub> was added instead of F, and the viscosity was controlled changing the ratio CaO/SiO<sub>2</sub>. Thermal conductivities were measured by the Hot-Disk Method Thermal Analyzer (TDA-501); the hot-disk method utilizes a thin disk-shaped sensor (hot-disk sensor) to measure the thermal conductivity (W/m.K). The crystallisation behaviour were studied by single hot thermocouple technique in the following way: glass samples were heated (200 seconds) and melted at 1400 °C for 30 seconds; then the samples were quenched (2 seconds) and measured at testing temperature (900 °C, 1000 °C and 1100 °C) for 1000 seconds. The beginning time of crystallisation was defined as the time when the first crystalline phase was observed in the sample. In Table 4 the composition of a commercial F-bearing mould powder used for peritectic steel (F-bearing) and a F-free mould powder that was considered as having similar properties is shown. The critical beginning points for the F-free from the SHTT experiments were 10 seconds at 900 °C, 4 seconds at 1000 °C, 3 seconds at 1100 °C ; and for the F-bearing 12 seconds at 900 °C, 5 seconds at 1000 °C, and 3 seconds at 1100 °C. According to the XRD pattern for a F-free sample treated at 1150 °C for 1 hour, the crystals  $\text{CaB}_2\text{SiO}_7$  and  $\text{CaAl}_{14}\text{B}_2[\text{SiO}_4]_8$  were identified.

**Table 4.** Mould powders composition (wt%) studied in [34] .

	CaO/SiO <sub>2</sub>	Al <sub>2</sub> O <sub>3</sub>	MgO	Na <sub>2</sub> O	B <sub>2</sub> O <sub>3</sub>	F
<b>F-bearing</b>	1.3	3.52	3.67	8.88	-	10.18
<b>F-free</b>	1.7	2.45	1.53	8.47	31.02	-

The effect of La<sub>2</sub>O<sub>3</sub> on crystallisation behaviour and heat transfer character were studied through differential scanning calorimetry, thermal gravimetric analyzer, a self-made mould simulator to calculate heat flow densities, and an energy disperse spectrometer attached to a scanning electron microscope [35]. It was reported that when increasing the proportion of La<sub>2</sub>O<sub>3</sub> in free-fluoride mould powders the thickness and crystallisation ratio of slag film is increased.

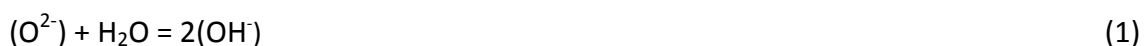
### 1.5.3 Effect of water on crystallisation of slags

Regarding the effect of humidity on crystallisation behaviour, it was reported that the critical cooling rate required for glass formation for the slag 50% CaO - 50% Al<sub>2</sub>O<sub>3</sub> increased from 300 °C/min to 600 °C/min , when changing the atmosphere from dry to humid. On the other hand, when adding 9% MgO in this slag the effect of humidity on crystallisation behaviour was eliminated, according to TTT diagrams that were constructed through DHTT [36].

The effect of water vapour on an industrial mould powder was studied; it was observed that the existence of H<sub>2</sub>O increased the crystallisation temperature, the rate of crystal growth, and the density of nucleated crystals [13].

In another work the crystallisation behaviour of an experimental mould slag (39.58% CaO, 40.94% SiO<sub>2</sub>, 6.94% Al<sub>2</sub>O<sub>3</sub>, 9.57% Na<sub>2</sub>O, 1.00% CaF<sub>2</sub>) was studied in a dry atmosphere and in the presence of water vapour, building TTT diagrams using the DHTT [37]. The presence of water vapour increased the nucleation rate and crystal growth rate significantly when compared to experiments carried out in a dry atmosphere. Precipitation of solid crystals occurred at a temperature above the equilibrium *liquidus* temperature (1260 °C) that is measured in a dry atmosphere. It was suggested that there is significant interaction between water vapour and liquid slags at high temperatures and that the phase diagram for these slags is very sensitive to the equilibrium partial pressure of water vapour in the surrounding atmosphere. Thus, the influence of humidity of the atmosphere on mould slags crystallisation behaviour cannot be neglected.

It is known that it is H<sub>2</sub>O, and not H<sub>2</sub>, that dissolves into molten silicates and glasses [37]. The solubility is proportional to the square root of the partial pressure of H<sub>2</sub>O. Depending on the degree of polymerization of the slag, the absorbed H<sub>2</sub>O will behave either as an acid oxide or as a basic oxide. Since H<sub>2</sub>O is absorbed as hydroxyl group in both acidic and basic melts, the overall absorption reaction can be written as



If it is assumed that crystal growth rate is limited by mass transfer in the liquid, then the increased crystal growth rate that is found in the humid atmosphere can be explained by a viscosity reduction in the melt due to the incorporation of OH<sup>-</sup> ions into the slag melt. Diffusivity in the slag melts is often related to the inverse of viscosity through the Stoke-Einstein relation, i.e. a decrease in viscosity leads to an increase in the mass-transfer rate:

$$D = \frac{kT}{6\pi r\eta} \quad (2)$$

where  $D$  is the diffusion constant,  $k$  is the Boltzmann constant,  $T$  the absolute temperature,  $r$  the radius of the spherical particle, and  $\eta$  the liquid viscosity.

## 2. MOTIVATION AND OBJECTIVES

The motivation for the present work is to provide fundamental information related to crystallisation control for the development of fluorine-free mould powders for continuous casting of steel, studying the crystallisation behaviour of slags through the Single Hot Thermocouple Technique (SHTT).

The objectives are the following:

(i) To perform a basic and systematic study evaluating the crystallisation behaviour of slags in the systems  $\text{CaO-Al}_2\text{O}_3$ ,  $\text{CaO-SiO}_2$ ,  $\text{CaO-SiO}_2\text{-TiO}_2$ , and  $\text{CaO-SiO}_2\text{-TiO}_2\text{-Na}_2\text{O}$ , building TTT and CCT curves, analysing the kinetics of crystals growth and crystals morphology;

(ii) To study the solidification behaviour of a new industrial fluorine-free mould powder to be used at steelworks during continuous casting of billets.

### 3. ESSENTIALS ON SOLIDIFICATION BEHAVIOUR OF SLAGS

#### 3.1 Glasses

Glass formation and crystallisation are competitive processes. Controlled nucleation and crystallisation of glasses underlay the production of glass-ceramics invented in the mid-1950s, that are widely used in both domestic and high-technology applications [38].

Glasses can be defined as non-crystalline solids that undergo a glass transition in the course of their preparation. The traditional method of vitrification consists in supercooling a liquid escaping crystallisation. Thus, when a liquid is cooled down at sufficiently high rates, crystallisation can occur to a limited degree or can be completely arrested down to temperatures corresponding to very high viscosities, in the range  $\eta \geq 10^{13}$ - $10^{12}$  Pa.s  $\sim \eta(T_g)$ , where  $T_g$  is the glass transition temperature. Below this temperature, the viscosity is so high that large-scale atomic rearrangements of the system are no longer possible within the time-scale of typical experiments, and the structure freezes-in. This process of freezing-in the structure of an undercooled liquid transforming it into a glass is commonly denoted as glass transition. Typical glass-forming liquids, such as silicate melts, are usually characterized by: (i) relatively high viscosities ( $\eta > 100$  Pa.s) at the melting point or *liquidus* and (ii) a steep increase of the viscosity with decreasing temperature. These properties favour vitrification. The mechanism above sketched leads to the conclusion that the glass structure must be similar to that of the parent undercooled liquid at temperatures near  $T_g$  and, indeed, this similarity has been experimentally observed [38, 39].

The most striking feature of the glass transition is the abrupt change in the properties of a liquid, such as the thermal expansion coefficient and the heat capacity, as it is cooled through the range of temperature where its viscosity approaches  $10^{12}$  Pa.s [38, 39].

Figure 2 shows the change in volume,  $V$ , of a glass forming liquid during cooling through the transition region. If the liquid is cooled slowly (path b) it may crystallize at the melting point,  $T_m$ . If the cooling rate is fast enough to avoid crystal nucleation and growth, a supercooled liquid would be produced (path a). As the temperature drops, the time required to establish the equilibrium configuration of the liquid increases, and eventually the structural change cannot keep pace with the rate of cooling. At that point a transition temperature,  $T_g$ , is reached below which the atoms are frozen into fixed positions (only thermal vibrations remain) and glass is formed. Thus, glass formation from the liquid state is feasible if path (a) is followed. On the other hand, all the glasses heated to a temperature between  $T_g$  and  $T_m$  tend to crystallize to achieve thermodynamical equilibrium [39].



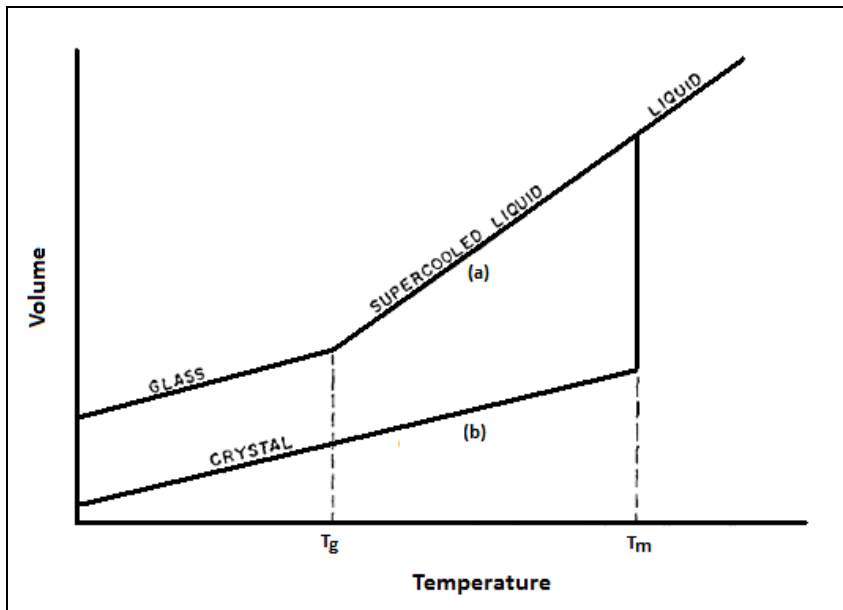


**Figure 2.** Schematic representation of the glass transition (a) and crystallisation from liquid (b) [39].

At room temperatures glasses can exist for extremely long periods of time because their high viscosity inhibits structural rearrangements required for crystal nucleation and growth. However, when a glass is heat-treated for a sufficiently long time at temperatures within or above the glass transition range, devitrification readily starts, as a rule, from the surface and sometimes in the bulk via heterogeneous or homogeneous nucleation [38, 39].

### 3.2 Classical Nucleation Theory

In its original form, the Classical Nucleation Theory is based on the thermodynamic description of heterogeneous systems developed by Gibbs. Following Gibbs, a real inhomogeneous system is replaced by a model system consisting of two homogeneous phases divided by a mathematical surface of zero thickness. While the properties of the ambient phase are known, the bulk properties of the critical clusters are determined via Gibbs' equilibrium conditions. A detailed analysis shows that the cluster bulk properties determined in such way are widely identical to the properties of the newly evolving macroscopic phase coexisting in stable equilibrium with the ambient phase at a planar interface. The free energy of the heterogeneous system – consisting of a cluster of the newly evolving phase in the ambient phase – is expressed as the sum of the bulk contributions of the nucleus and the ambient phase. These bulk terms are supplemented by interfacial contributions, the main one is given by the product of the interfacial area and specific surface energy. When applying the theory to cluster formation, these surface terms initially result in an increase of the characteristic thermodynamic potential, which leads to the existence of a critical cluster size. Only clusters with sizes larger than the critical size are capable to grow up to macroscopic dimensions in a deterministic way. The change of the characteristic

thermodynamic potential resulting from the formation of clusters of critical size is commonly denoted as the work of critical cluster formation. This quantity reflects the thermodynamic aspects in the description of nucleation. In addition to thermodynamic aspects of nucleation, the dynamics of cluster formation and growth must be appropriately incorporated into the theory. Different approaches have been studied depending on the particular problem being analyzed, for example considering the nucleation in condensed systems [38].

With the Classical Nucleation Theory it is not possible quantitatively to describe crystal nucleation rates in silicate glasses. The crystal nucleation rates calculated with it are many orders of magnitude smaller than the experimental values for inorganic glasses. Despite of getting significant progress in understanding crystal nucleation in glasses in the last years, many problems still exist and this is likely to remain a highly interesting subject for both fundamental and applied research for a long time [38-40].

### 3.3 Characteristics of nucleation and growth transformations

Nucleation, i.e. the process of formation of the precursors of the crystalline phases, may occur by different mechanisms. Commonly one divides these processes into homogeneous and heterogeneous nucleation. Homogeneous nucleation is a stochastic process occurring with the same probability in any give volume (or surface) element. Alternatively, nucleation occurring on preferred nucleation sites, such as pre-existing interfaces, previously nucleated phases, and surface defects, is denoted as heterogeneous nucleation [38].

Either the nucleation rate or the growth rate may be effective in determining the overall kinetics of a heterogeneous transformation. The net transformation rate will depend mainly on the slower of the two stages [41] (p. 10).

In silicate glasses, in many respects the nucleation stage determines the pathways of overall crystallisation [38].

In typical “nucleation and growth” transformations the new phase grows at the expense of the old by the relatively slow migration of the interphase boundary, and growth results from atom by atom transfers across this boundary. The atoms move independently and at a rate which varies markedly with the temperature. At a given temperature, the reaction proceeds isothermally, and the amount of new phase formed increases with time [41] (p. 5).

Two extreme cases can be distinguished in principle: interface-controlled and diffusion-controlled. In the first one there is a boundary which moves very slowly, even under the influence of very high driving forces. The ratio of motion will then be largely independent of the diffusion rate. The second one – diffusion-controlled – is where the boundary is highly mobile when compared with the rate of diffusion, so that it will move as rapidly as the required segregation can be accomplished. The growth rate is then determined almost entirely by diffusion conditions [41] (p. 7).

In some transformations, there is no doubt that thermal fluctuations resulting in atomic rearrangements are responsible for the appearance of stable nuclei of a new phase. Such fluctuations may occur randomly throughout the volume of the assembly, or at preferred sites where impurities or structural defects act as catalysts for the phase change. Many solid assemblies contain defects which are not in thermal equilibrium with the structure but are “frozen in”. Non-equilibrium defects of this kind may be able to form suitable nuclei for some changes without the aid of thermal agitation [41] (p. 10).

The assumption of linear growth law (constant growth rate) for isothermal transformation kinetics is appropriate under all circumstances in which the interface advances into a region of matrix of constant mean composition, so that the rate of the process controlling the growth is independent of the interface position, and hence of the time. However, this situation does not necessarily apply when an isolated precipitate particle  $\beta$  grows into a phase  $\alpha$  of different composition. If  $\beta$  is richer in solute atoms, there may be a region depleted in solute formed around the  $\beta$  particles as growth proceeds; and if  $\beta$  is poorer in solute atoms, then the region around the  $\beta$  particle may be enriched. In either case, the continual growth of the particle requires chemical diffusion in the surrounding phase, and as the particle increase in size, the effective distances over which diffusion takes place may also increase. When the particle is first formed, it is probable that processes near the interface will control the net rate of growth, but the volume diffusion will eventually become the dominant factor if the interface is reasonably high. The particle will then grow just as fast as the diffusion rate allows [41] (p. 486).

### 3.4 Time-temperature-transformation diagrams

If the kinetics of a transformation is found experimentally at a number of different constant temperatures, a complete isothermal transformation diagram may be drawn. This diagram is the time-temperature-transformation (TTT) diagram. It gives the relation between the temperature and the time for fixed fractional amounts of transformation to be attained. Frequently, the time for the beginning of the transformation (incubation time) is given [41] (p. 546).

If given sufficient time, the transformation will, in principle, continue until complete. The velocity of transformation varies enormously, and for any transformation a temperature can be found below which the change proceeds at a negligible rate. For nucleation and growth reactions, the rate of reaction is zero at the thermodynamical transformation temperature. On cooling, as the temperature is lowered, the free energy of formation of a critically sized nucleus decreases much more rapidly than does the available thermal energy. The probability of nucleation may thus increase rapidly with decreasing temperature, at least until very low temperatures are reached. In condensed phases, however, the formation energy of the critical nucleus constitutes only part of the required activation energy, and there

may be additional terms representing the energy needed for an atom to cross the interphase boundary or for interdiffusion of the species, where a composition change is involved. [41] (p. 11).

When both the nucleation and growth rates are temperature dependent, the isothermal transformation rate will depend on other parameters. In very many reactions on cooling, the nucleation rate is determined mainly by a Boltzmann type equation with an activation energy which decreases exponentially with temperature. This gives a rapidly increasing nucleation rate as the undercooling (or supersaturation) increases. The growth rate, in contrast, is controlled by an activation energy which is nearly independent of the temperature, and hence the rate decreases as the temperature decreases. These opposing factors give an overall transformation rate which first increases and then decreases again as the temperature falls, leading to the C curves characteristic of TTT diagrams. At sufficiently low temperatures, the nucleation rate may be so large that the nucleation sites saturate early in the reaction. The growth rate alone then controls the overall reaction rate. In this way, the decreasing formation energy and decreasing growth rate produce a characteristic dependence of reaction velocity on temperature, in which the rate increases to a maximum at a temperature below the equilibrium transformation temperature, and then decreases again [41] (p. 547).

The isothermal reaction curves are usually interpreted in terms of Avrami equation, equation (3), which in many situations is a good approximation in almost all modes of transformation (in the next section more details about this equation are given). For most transformations, the value of  $n$  is independent of temperature over appreciable temperature ranges [41] (p. 547).

$$\zeta(t) = 1 - \exp(-Kt^n) \quad (3)$$

where

$\zeta$  is crystals volume fraction,

$t$  is time,

$n$  represents the mechanism of crystal growth, and

$K$  represents nucleation and growth mechanisms.

### 3.5 Formal theory of transformation kinetics – isothermal transformation

In the following there is a description got from the formal theory of transformation kinetics, for the relation between the fraction of the assembly transformed and the time at constant temperature [41] (p. 17).

Considering a nucleation and growth reaction, a individual transformed region is formed at a time  $t = \tau$  (incubation time), and thereafter its size increases continuously. At a time  $t$  the untransformed volume is  $V^\alpha$ , and between times  $t = \tau$ ,  $\tau + d\tau$  a number of new regions are nucleated (i.e. reach some arbitrary minimum size).

The nucleation rate per unit volume is  $I$ . Thus, in the whole assembly, the number of new  $\beta$  regions nucleated in the time interval between  $\tau$  and  $\tau + d\tau$  is  $I V^\alpha d\tau$ .

Assuming an isotropic growth rate  $\gamma$  the transformed region  $\beta$  is spherical. That is a good approximation in many actual changes. The volume of a transformed region, originating at time  $t = \tau$  is zero to  $t < \tau$ , and to  $t > \tau$  is

$$v\tau = \left(\frac{4\pi}{3}\right) \gamma^3 (t - \tau)^3 \quad (4)$$

During the initial stages of transformation, when  $V^\beta \ll V^\alpha$ , the nuclei are widely spaced, and the interference of neighbouring nuclei is negligible. Under these conditions, the transformed volume at time  $t$  resulting from regions nucleated between times  $\tau$  and  $\tau + d\tau$  is

$$dV^\beta = v\tau I V^\alpha d\tau \quad (5)$$

Since  $V^\alpha$  is effectively constant and equal to  $V$ , the total volume transformed at time  $t$  is

$$V^\beta = \frac{4\pi V}{3} \int_{\tau=0}^t I \gamma^3 (t - \tau)^3 d\tau \quad (6)$$

However, in a more exact treatment, the mutual interference of regions growing from separate nuclei must also be considered. When  $t$  becomes large the growth rate is reduced due to the mutual impingement of regions transforming from separate nuclei, which must ultimately interfere with each other's growth. In solid transformations, the two regions develop a common interface, over which growth ceases, although it continues normally elsewhere. This problem is primarily geometrical.

During the time  $d\tau$ , when  $I V^\alpha d\tau$  new transformed regions are nucleated, it is also possible to consider that  $I V^\beta d\tau$  regions would have nucleated in the transformed portion of the assembly, had not transformation previously occurred there. Avrami described these as "phantom nuclei", and he defined an "extended" volume of transformed material,  $V^\beta \text{ ext}$ , by the relation

$$dV^\beta \text{ ext} = v\tau I (V^\alpha + V^\beta) d\tau \quad (7)$$

or

$$V^{\beta} \text{ ext} = \frac{4\pi V}{3} \int_0^t \gamma^3 I(t-\tau)^3 d\tau \quad (8)$$

$V^{\beta} \text{ ext}$  differs from the actual volume of transformed material in two ways. Firstly, phantom regions were counted, nucleated in already transformed material. Secondly, all regions were treated as though they continued growing, irrespective of other regions. The extended volume can thus be visualized as a series of volume elements having the same limiting surface as the actual transformed volume but all growing “through” each other, see Figure 3. Some elements of the transformed volume are counted twice, others three times, and so on, in order to obtain the extended volume. It follows that the extended volume may be larger than the real volume of the whole assembly  $V$ . The significance of  $V^{\beta} \text{ ext}$  is that it is simply related to the kinetic laws of growth, which may thus be separated from the geometrical problem of impingement.

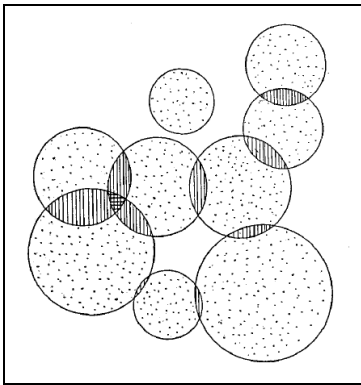


**Figure 3.** Schematic figure for the extended volume ( $V^{\beta} \text{ ext}$ ), as described by Avrami [41].

A relation must be found between  $V^{\beta} \text{ ext}$  and  $V^{\beta}$ . Considering any small random region, of which a fraction  $(1 - V^{\beta}/V)$  remains untransformed at time  $t$ , during a further time  $dt$ , the extended volume of  $\beta$  in the region will increase by  $dV^{\beta} \text{ ext}$ , and the true volume by  $dV^{\beta}$ . Of the new elements of volume which make up  $dV^{\beta} \text{ ext}$ , a fraction  $(1 - V^{\beta}/V)$  on the average will lie in previously untransformed material, and thus contribute to  $dV^{\beta}$ , whilst the remainder of  $dV^{\beta} \text{ ext}$  will be in already transformed material. This result clearly follows only if  $dV^{\beta} \text{ ext}$  can be treated as a completely random volume element, and it is for this reason that phantom nuclei have to be included in the definition of  $V^{\beta} \text{ ext}$ .

The above arguments are based on the assumption that nucleation is random, in the sense that if the assembly is divided into small equal volume elements, the probability of forming a nucleus in unit time is the same for all these elements. The treatment does not preclude the possibility that nuclei form preferentially at certain sites in the  $\beta$  phase, but as developed here, it may be applied to experimental observations only if the minimum resolvable  $\beta$  volume contains several such sites. All

equal volume elements of size greater than this observational limit then have equal nucleation probabilities. In practice, nucleation may occur preferentially along macroscopic surfaces (grain boundaries) of the assembly, so that volume elements in different regions may have quite different nucleation probabilities. The formal theory can be extended to cover such cases; more details can be found in [41] (Chapter 12).

The relation between  $V^\beta$  and  $V^\beta ext$  can be written in the form

$$dV^\beta = \left(1 - \frac{V^\beta}{V}\right) dV^\beta ext \quad (9)$$

or

$$V^\beta ext = -V \ln\left(1 - \frac{V^\beta}{V}\right) \quad (10)$$

Substituting equation (10) into equation (8)

$$-\ln(1 - \zeta) = \frac{4\pi}{3} \gamma^3 \int_0^t I (t - \tau)^3 d\tau \quad (11)$$

Where  $\zeta$  is  $V^\beta/V$ , i.e., volume fraction transformed at time  $t$ .

The equation (11) may be integrated by making specific assumptions about the variation of  $I$  with time. In particular, if  $I$  is constant

$$\zeta = 1 - \exp\left(\frac{-\pi \gamma^3 I t^4}{3}\right) \quad (12)$$

In general  $I$  may not be constant, but may either increase or decrease with time. Equations (11) and (12) must be used for  $\zeta$  in the general case [41] (p. 19).

Avrami used a alternative assumption, supposing that nucleation occurs only at certain preferred sites in the assembly which are gradually exhausted [41] (p. 20). From this assumption it was proposed that for a three-dimensional nucleation and growth process the general relation (Avrami equation) should be used

$$\zeta(t) = 1 - \exp(-Kt^n) \quad (3)$$

where  $3 \leq n \leq 4$ . This should cover all cases in which  $I$  is some decreasing function of time, up to the limit when  $I$  is constant.

The equation (3) can also be written as

$$\ln(-\ln(1-\zeta)) = \ln K + n \ln t \quad (13)$$

In the general form of equation (3) the above theory applies to many real transformations. However, it cannot be safely applied in practice unless the assumptions about  $I$  and  $\gamma$  can be verified. The Avrami theory assumes that the nucleation frequency is either constant, or else is a maximum at the beginning of the transformation and decreases (slowly or rapidly) during the course of transformation. In contrast to this, there may be an operational rate of nucleation which increases with time [41] (p. 21).

The Avrami equation is also often applied to transformations in which the growth rate is diffusion-controlled, but in most cases there is no adequate theoretical sanction for this. These questions are discussed with details by Christian [41] (Chapter 12).



## 4. EXPERIMENTAL WORK

### 4.1 Materials and samples preparation

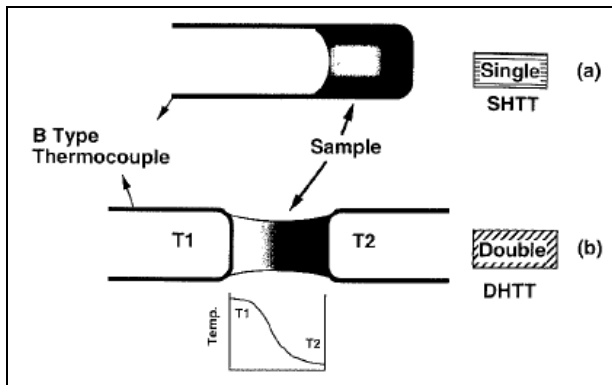
The slags were produced from reagent-grade  $\text{CaCO}_3$ ,  $\text{SiO}_2$ ,  $\text{TiO}_2$ ,  $\text{Na}_2\text{CO}_3$  and  $\text{Al}_2\text{O}_3$ . They were pre-melted in graphite crucibles heated in an induction furnace, milled, decarburised at  $700^\circ\text{C}$  for 5 hours in a muffle furnace (except CST\_1 and CST\_2) and analysed through X-ray fluorescence (XRF). Carbon was analysed with the combustion infrared detection technique (LECO CS 244). The results of the analyses for the slags used with the SHTT are shown in Table 5.

**Table 5.** Compositions of the slags used for SHTT analyses (wt%). B is the ratio  $\% \text{CaO} / \% \text{SiO}_2$ .

	$\% \text{CaO}$	$\% \text{SiO}_2$	$\% \text{TiO}_2$	$\% \text{Na}_2\text{O}$	$\% \text{Al}_2\text{O}_3$	$\% \text{C}$	<b>B</b>
<b>CA</b>	43.7				56.3	0.074	
<b>CS</b>	41.7	58.3				0.063	0.7
<b>CST_1</b>	41.1	29.1	29.8			-	1.4
<b>CST_2</b>	35.6	46.3	18.1			0.590	0.8
<b>CSTNA_1</b>	33.6	41.3	16.5	7.1	1.5	0.073	0.8
<b>CSTNA_2</b>	30.1	46.8	16.4	5.4	1.3	0.034	0.6
<b>CSTNA_3</b>	31.6	48.1	15.5	3.7	1.1	0.032	0.7
<b>CSTNA_4</b>	30.9	42.3	15.2	6.4	5.2	0.038	0.7

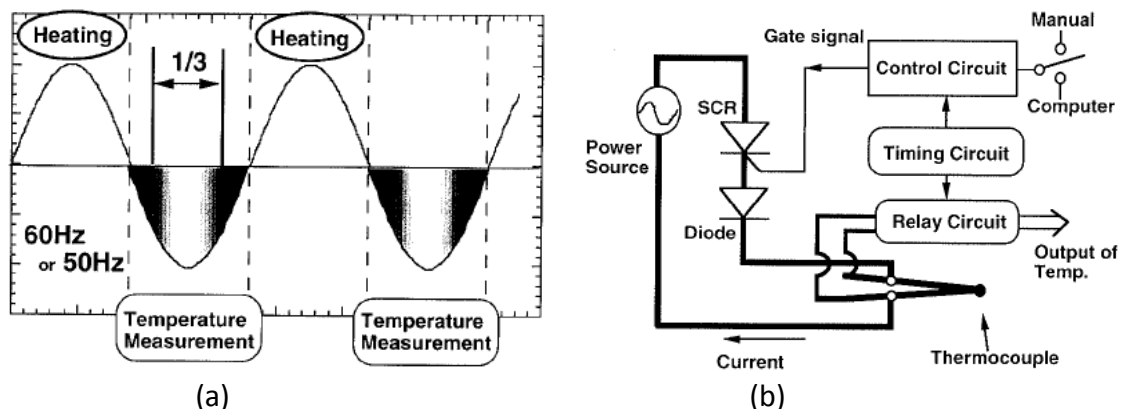
### 4.2 Single Hot Thermocouple Technique (SHTT)

Single and double hot thermocouple techniques (SHTT and DHTT) were developed for in situ observation and measurement of mould slag crystallisation, overcoming the limitations of differential thermal analysis (DTA) and direct casting experimentation [5, 42]. The SHTT allows a sample to be subjected to rapid cooling rates or to be held under isothermal conditions. The DHTT allows large temperature gradients to be developed between the two thermocouples and allows a simulation of the transient conditions which can occur in the infiltrated slag film that occur between the mould and the solidifying shell in the mould of a continuous caster. These techniques can be applied to mould slags which are optically transparent or translucent at steelmaking temperatures, while the crystalline phase which precipitates upon cooling should be opaque. In this way it is possible to describe the conditions under which glass formation is possible, the conditions for the initiation of solidification, the crystal morphology, growth rate and the time evolution of the fraction of solid. Figure 4 shows an illustration.



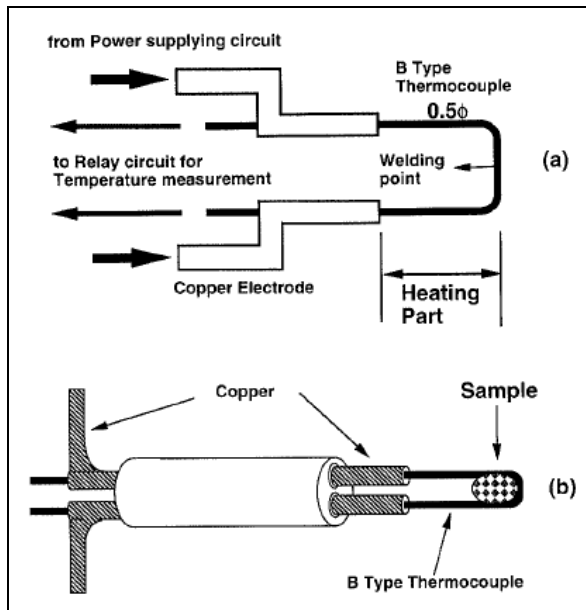
**Figure 4.** Illustration of (a) single hot thermocouple technique (SHTT) and (b) double hot thermocouple technique (DHTT) [42].

The apparatus is a unique system that enables simultaneous measurement of temperature while a thermocouple is heated. Figure 5a illustrates the principle of the hot-thermocouple controller. The electric current is rectified into a half-wave by a silicon controlled rectifier (SCR, a type of thyristor), so that the heating cycle occurs for a maximum length of  $1/120$  seconds followed by a similar period with no current input where the temperature of the thermocouple is measured using a relay circuit. Figure 5b shows a circuit schematic of the hot thermocouple controller. The main circuit is the power supply circuit having a SCR and a diode. To control the SCR the gate signal is supplied from the power control circuit, or temperature control circuit, which is operated by means of a computer or a potentiometer. The output of electromotive force from thermocouple is connected to the relay circuit [42].



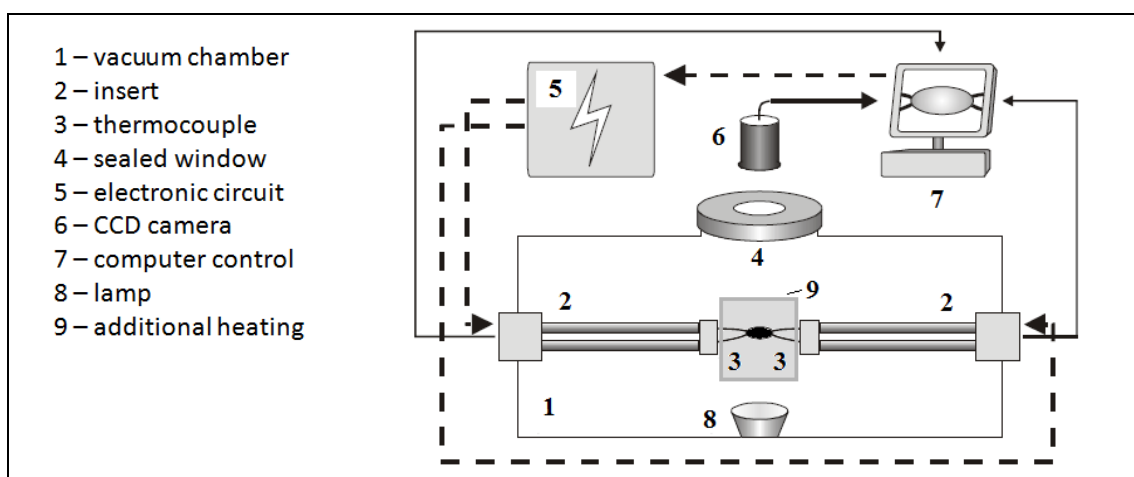
**Figure 5.** (a) Principle of the hot thermocouple controller, (b) circuit diagram of the hot thermocouple controller [42].

Figure 6 shows schematics of the electrode assembly and electrode used to hold a thermocouple. It is very important to weld the thermocouple maintaining the same diameter. The wider or smaller diameter would result in a nonuniform heat generation. Tight contact between the thermocouple and copper electrode is important for noiseless measurement [42].



**Figure 6.** Schematic of (a) electrode conjunction and (b) electrode assembly for hot thermocouple technique [42].

The apparatus used in the present work was constructed at the Technische Universität Bergakademie Freiberg [43]. A schematic view of the apparatus is shown in Figure 7. It consists of two systems: an observation system and a thermocouple system. In a vacuum chamber, there are two water-cooled inserts, one on the left and another on right. Both of them hold a B-type thermocouple at the tips. Each thermocouple is connected to a separate thermocouple controller. The material under study is melted directly on the thermocouple in the vacuum chamber. The thermocouples remain inside an additional heating element (i.e., a kanthal coil), which reduces heat losses from the sample to the surroundings, maintaining a temperature of approximately 500 °C around the sample.



**Figure 7.** Schematic view of the experimental set-up used in the present work.

Figure 8 shows a photo of an industrial mould powder sample at 1400 °C (completely melted) on a B-type thermocouple in the additional heating element.

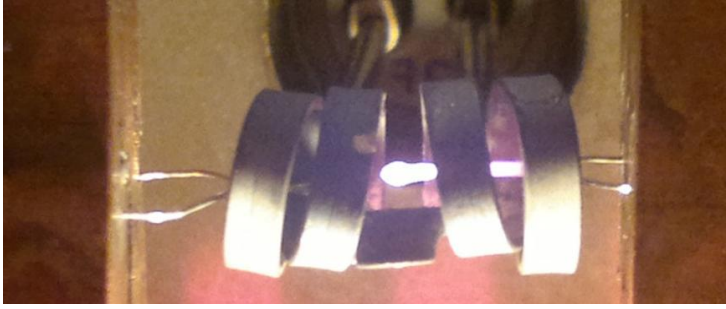


**Figure 8.** Industrial mould powder sample completely melted at 1400 °C on a thermocouple tip in the additional heating element (right side).

With this experimental set-up, it is possible to measure the sample temperature with a thermocouple while it is heated simultaneously. A computer manages the two thermocouple controllers, controlling the heating and cooling conditions individually. A software program superimposes information regarding time, temperature and sample images on video files in a real-time system. Due to the low mass of the system (sample and thermocouple) high heating and cooling rates can be easily obtained. This is useful for determination of TTT and CCT diagrams where fast cooling rates are required.

#### 4.2.1 Thermocouple welding

The thermocouple is a B-type (up to 1800°C). It is built using two platinum wires measuring 0.5 mm in diameter and approximately 25 mm in length: Pt30Rh and Pt6Rh. The tips of the wires are welded to obtain one thermocouple. To obtain a geometrically perfect weld there is a special device, see Figure 9, where the wires are fixed in copper tubes using a propane-butane gas mixture (1925°C).

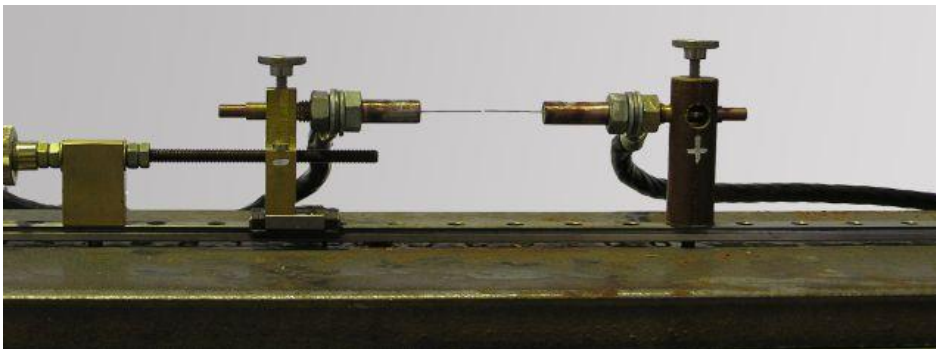


**Figure 9.** Device used to weld platinum wires (25 mm each).

Before installation in the device of the Figure 9 the platinum wires tips (which touch each other) must be well polished, having flat surfaces. When applying a voltage in the system it is possible to get a weld at the tips, with a special technique; see Figure 10(a). Figure 10(b) shows a typical thermocouple.

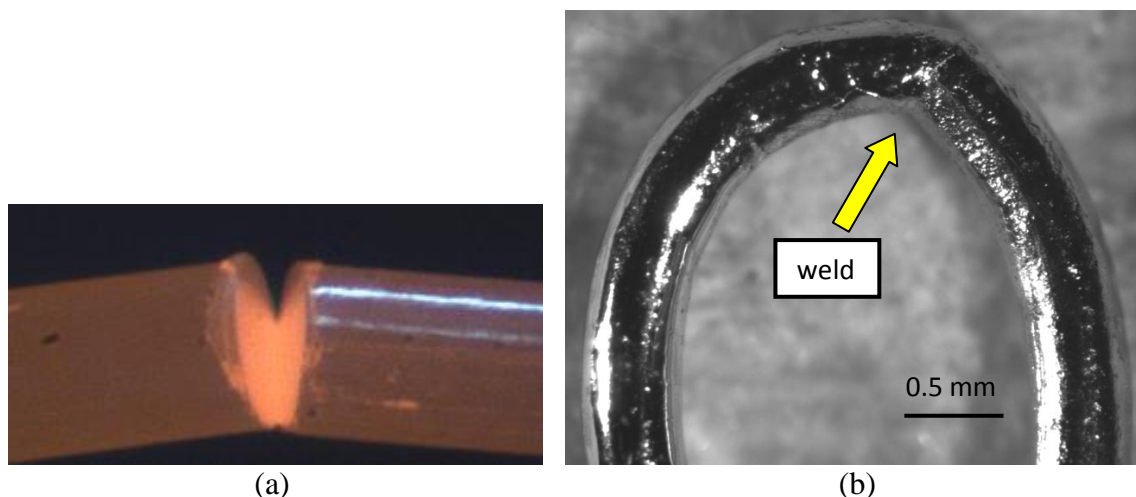


**Figure 10.** (a) Beginning of the welding (Pt30Rh-Pt6Rh wires), (b) the tip of a typical thermocouple showing the region where slags samples are melted and held together by surface tension.

#### 4.2.2 Examination of the accuracy of the apparatus

The accuracy of the apparatus was verified by measuring the crystallisation temperature ( $T_{\text{cryst.}}$ ) of  $\text{CaF}_2$ ,  $\text{Na}_2\text{SO}_4$  and  $\text{K}_2\text{SO}_4$ . The  $T_{\text{cryst.}}$  is defined here as the temperature at which the first crystals can be observed at a particular cooling rate.

With the substances in the vacuum chamber, a pressure of 10 mbar was applied for 5 minutes. Then, the vessel was filled with Ar, maintaining a flux of 300 L/h during the measurements. Afterwards, the substances were melted at  $100^\circ\text{C}$  above their melting points and cooled at a rate of  $30^\circ\text{C}/\text{min}$ . Their melting points are  $\text{CaF}_2$  -  $1418^\circ\text{C}$ ,  $\text{Na}_2\text{SO}_4$  -  $884^\circ\text{C}$ , and  $\text{K}_2\text{SO}_4$  -  $1069^\circ\text{C}$  [44].

The three materials used for calibration have the following specifications from the manufacturers:

- Calcium fluoride ( $\text{CaF}_2$ ): free Ca (not in  $\text{CaF}_2$ ) 0.2%,  $\text{SiO}_2$  0.1%;
- Sodium bisulphate ( $\text{NaHSO}_4$ ) and potassium pyrosulphate ( $\text{KHSO}_4$ ): reagent grade.

Figure 11 shows the differences between the reported melting points [44] and  $T_{\text{cryst.}}$ . Twelve experiments were performed for each substance (experiments 1-6 with the left thermocouple and experiments 7-12 with the right thermocouple; see Figure 7).

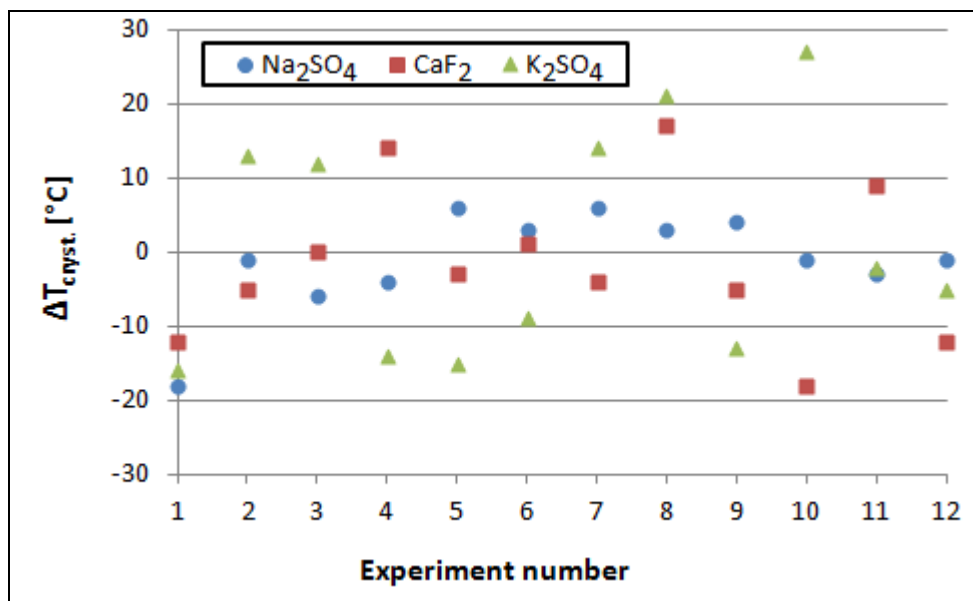


**Figure 11.** Comparison between literature results [44] and the results of the present work.  $\Delta T_{\text{cryst.}}$  is the difference between the reported melting point and the crystallisation temperature that was measured by SHTT.

Assuming a normal distribution for  $\Delta T_{\text{cryst.}}$ , the average values of  $T_{\text{cryst.}}$  for the three substances used for calibration can be calculated; see Table 6. The average values of  $T_{\text{cryst.}}$  are very close to the melting points reported in the literature, and the scattering is low. The small observed differences can be related to certain conditions required for heterogeneous nucleation. For  $\text{CaF}_2$  and  $\text{Na}_2\text{SO}_4$ , the crystallisation is intense and takes place suddenly; in this case, it is easy to accurately define the beginning of crystallisation. For  $\text{K}_2\text{SO}_4$ , the substance that presents the highest standard deviation, the crystallisation is not particularly intense and normally takes a few seconds to finish.

**Table 6.** Comparison between the literature-reported [44] melting points and the crystallisation temperatures measured by SHTT ( $T_{\text{cryst.}}$ ). For each substance, 12 measurements were performed.

	m.p. literature [44]	average $T_{\text{cryst.}}$	standard deviation $T_{\text{cryst.}}$
$\text{CaF}_2$	1418 °C	1417 °C	10.6 °C
$\text{Na}_2\text{SO}_4$	884 °C	883 °C	6.6 °C
$\text{K}_2\text{SO}_4$	1069 °C	1071 °C	15.4 °C

#### 4.2.3 Relation between visual observation and T versus t diagrams

The results summarised in Table 6 were obtained through video-file analysis. The apparatus also registers the evolution of temperature with time, in a similar manner to differential thermal analysis (DTA). It was verified during calibration that the visually observed crystallisation corresponds to peaks in the T versus t diagrams. Figure 12 shows where the energy-liberation rate during cooling is sufficiently high to produce observable peaks, for  $\text{CaF}_2$ .

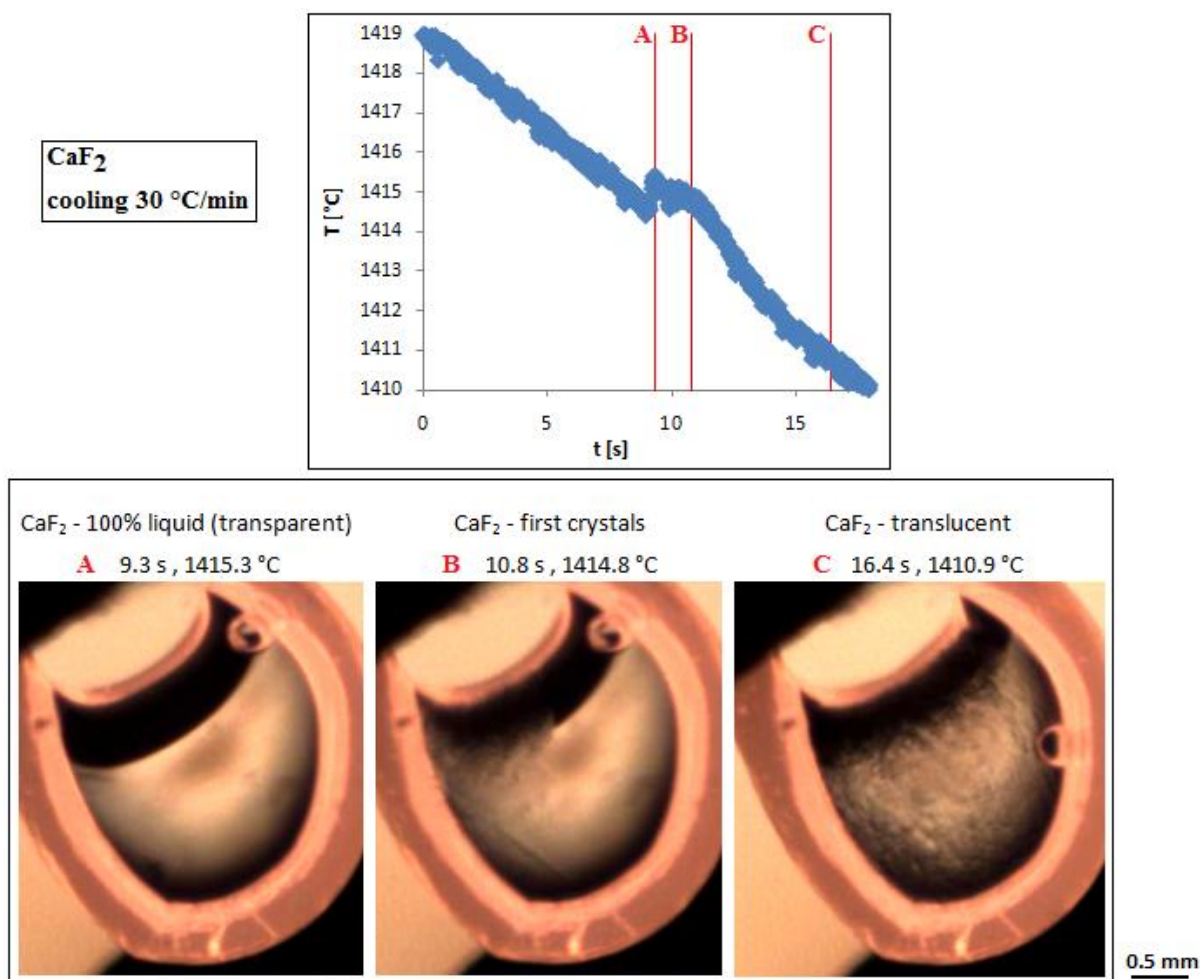


**Figure 12.** Relation between the CaF<sub>2</sub> crystallisation peak in the T versus t diagram during cooling (above) and the visually determined start of crystallisation (below).

More T versus t diagrams in Figure 13. K<sub>2</sub>SO<sub>4</sub>, the substance with the highest standard deviation in Table 6, presents different crystallisation behaviour, since for it the crystals growth rate is lower. For Na<sub>2</sub>SO<sub>4</sub> the crystallisation is intense and happens suddenly, with low standard deviation. The “first crystals” in the diagrams refer to the temperatures at which it is possible to observe the first crystals.

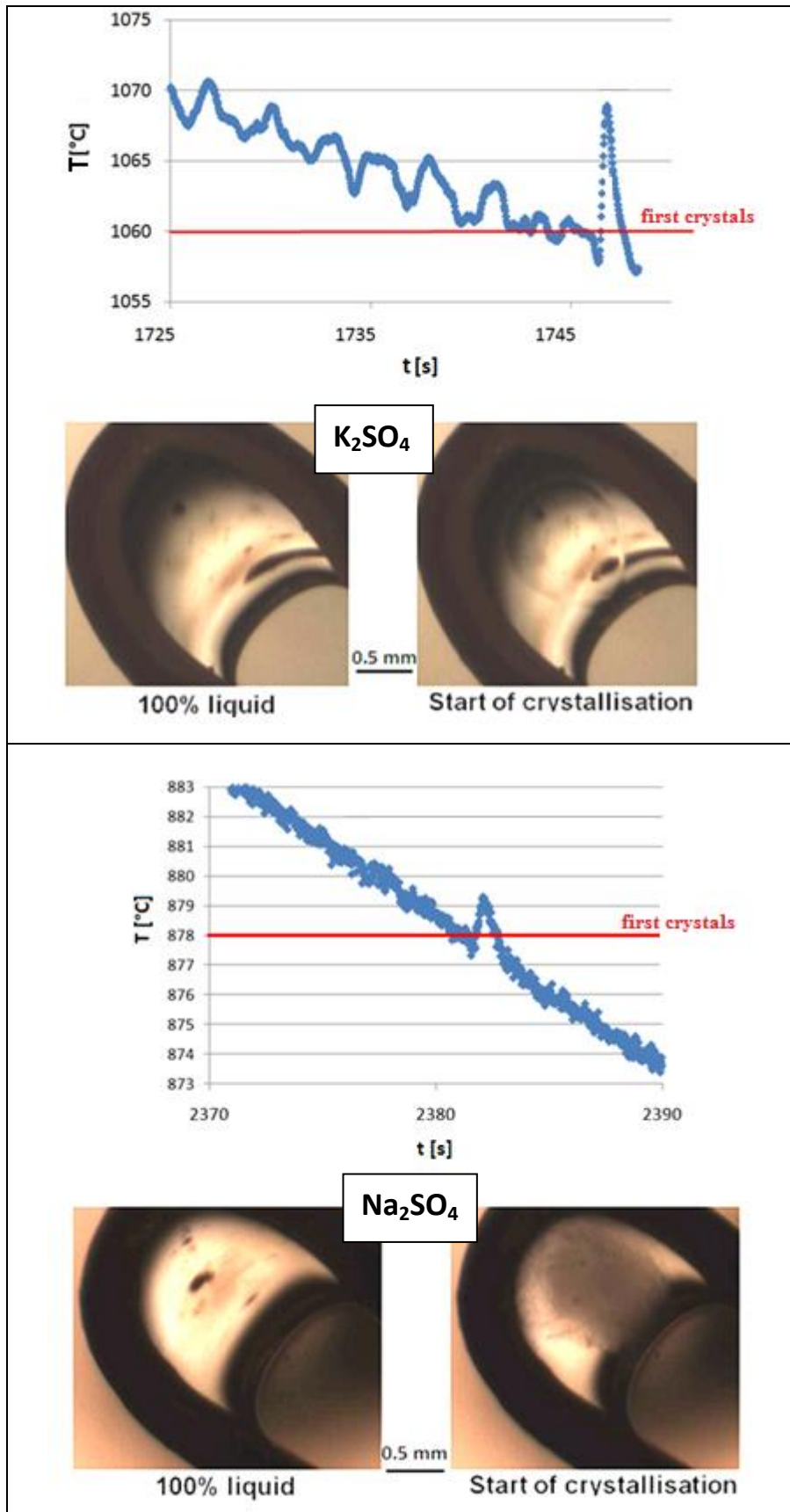
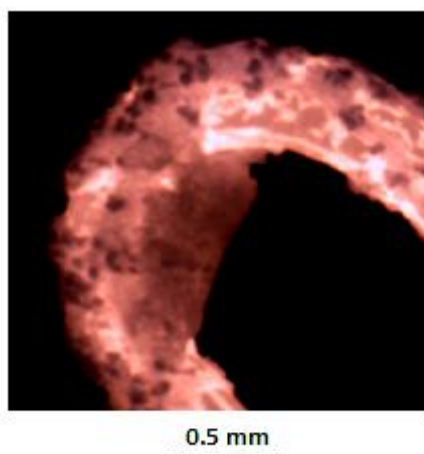


Figure 13. T versus t diagrams for  $K_2SO_4$  (above) and  $Na_2SO_4$  (below). Cooling rate 30  $^{\circ}C/min$ .



#### 4.2.4 Effect of atmosphere on CaF<sub>2</sub> crystallisation

Some experiments were performed in air to evaluate the effect of atmospheric conditions on CaF<sub>2</sub> crystallisation. Under these conditions, when performing measurements on CaF<sub>2</sub>, several lumps on the thermocouple and on the sample were observed. The mass of these lumps increased with time, and it was not possible to melt them, even by maintaining a temperature of 1700 °C for a long time; see Figure 14. These particles are most likely the result of the reaction between water vapour and CaF<sub>2</sub> because when evacuating the system before the experiments the lumps were not formed and the CaF<sub>2</sub> sample melted easily at 1518 °C.



**Figure 14.** Thermocouple at 1700 °C covered with several lumps (i.e., solid particles that cannot be melted even by maintaining the sample at this high temperature for several minutes).

In a previous work using a similar apparatus [45], it was observed that when taking measurements in air, the CaF<sub>2</sub> crystallisation temperature tended to decrease. Lumps were also observed, and they were collected and analysed through X-ray diffraction; CaO(s) and CaF<sub>2</sub>(s) were detected. Thus, the lumps can be attributed to the reaction between water vapour and liquid calcium fluoride:  $\text{CaF}_2(\text{l}) + \text{H}_2\text{O}(\text{g}) = \text{CaO}(\text{s}) + 2\text{HF}(\text{g})$ . In the Slag Atlas [46], the CaF<sub>2</sub>-CaO phase diagram shows that when increasing the CaO content from pure CaF<sub>2</sub>, the *liquidus* temperature initially decreases and then increases (Figure 15). Therefore, the existence of solid lumps can be explained by the formation of CaO crystals.

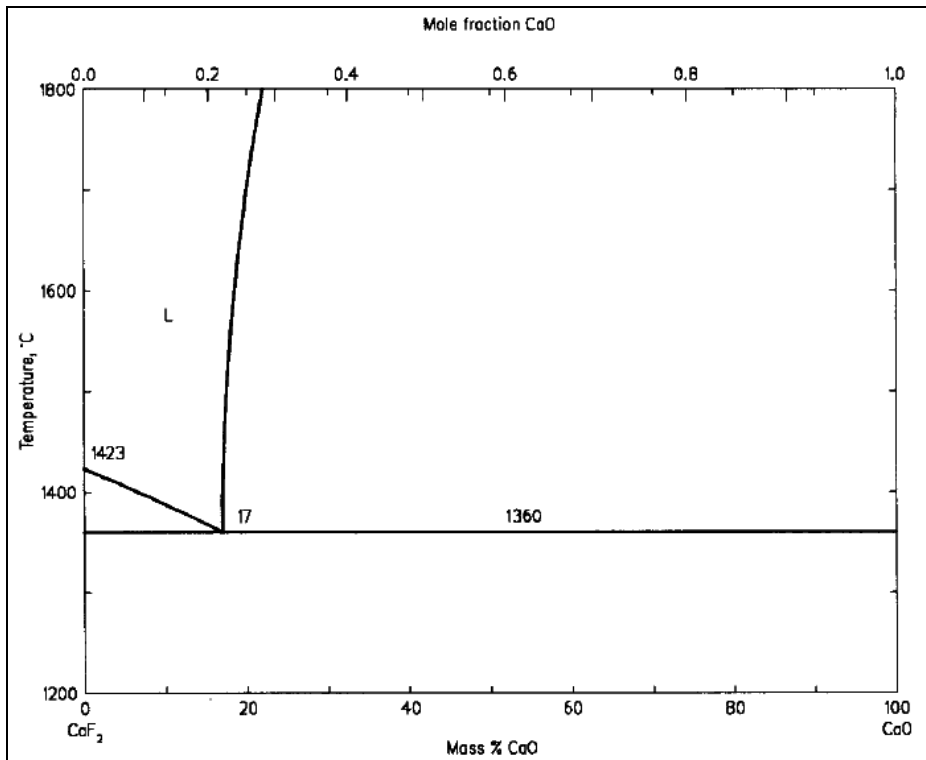


Figure 15. CaF<sub>2</sub>-CaO phase diagram, from Slag Atlas [46].

It was observed that it is important to apply suitable vacuum times, in this case approximately 10 mbar for 5 minutes, before the measurements. When working with lower vacuum times, e.g., 1 minute at 10 mbar, the CaF<sub>2</sub> crystallisation temperatures tend to fall outside of the  $1418 \pm 20$  °C range.

#### 4.2.5 Procedure to construct CCT and TTT curves for slags

To perform the experiments using SHTT small portions of premelted slags (5-10 mg) are pressed and placed on thermocouple tips. With the substances in the vacuum chamber, a pressure of 10 mbar is applied for 5 minutes. Then, the vessel is filled with Ar, maintaining a flux of 300 L/h during the measurements. The additional heating element is turned on, maintaining a temperature of approximately 500 °C around the thermocouple. The slag samples are heated and melted directly on the thermocouple tip, using one thermocouple per slag sample. During the operation, lime slurry is held at the gas exit. The experiments are recorded as video files.

To produce time-temperature-transformation (TTT) diagrams, after melting, very high cooling rates (higher than 3000 °C/min) are applied down to the desired temperature, as illustrated in Figure 16(a). Then, the incubation time, i.e., the time required to obtain the first crystals, is measured by direct observation. Using the incubation times for different temperatures, TTT diagrams are constructed.

To create continuous-cooling-transformation (CCT) diagrams, after melting, a particular cooling rate is applied, as illustrated in Figure 16(b). Then, the solidification behaviour is observed. Using different cooling rates, a CCT curve can be constructed.

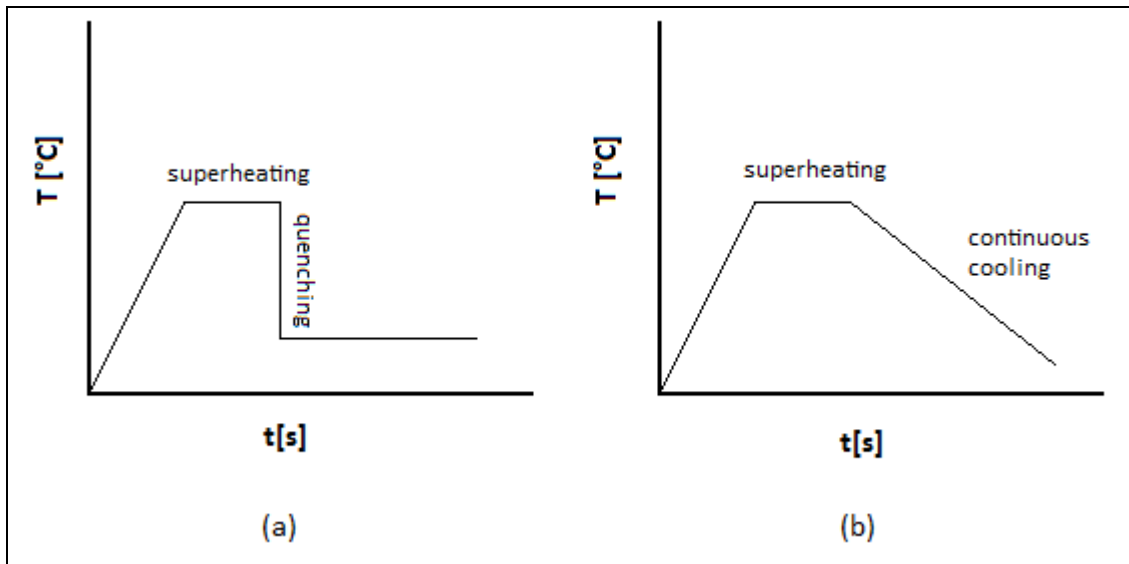


**Figure 16.** Typical thermal courses used to obtain data for TTT (a) and CCT (b) diagrams.

### 4.3 Rotation viscometer

Viscosity measurements were performed using a rotation viscometer (Anton Paar MC 301) at the Technische Universität Bergakademie Freiberg [47].

The mass of the samples – which were specifically prepared to perform viscosity measurements in a manner similar to that described in section 4.1 – was 30 grams. The idea was to produce a larger amount of slag to measure the viscosity of the materials that were analysed via the SHTT. Then, new slags of similar composition were obtained. These slags were melted in a crucible in an induction furnace under an Ar atmosphere. Then, from the liquid slag, a cooling rate of 10 °C/min was applied, measuring the viscosity at a rotation speed of 15 rpm. The measurements were stopped when the torque exceeded 2000  $\mu\text{Nm}$ .

The inner cylinder and the crucible are made of molybdenum; the dimensions are shown in Figure 17.

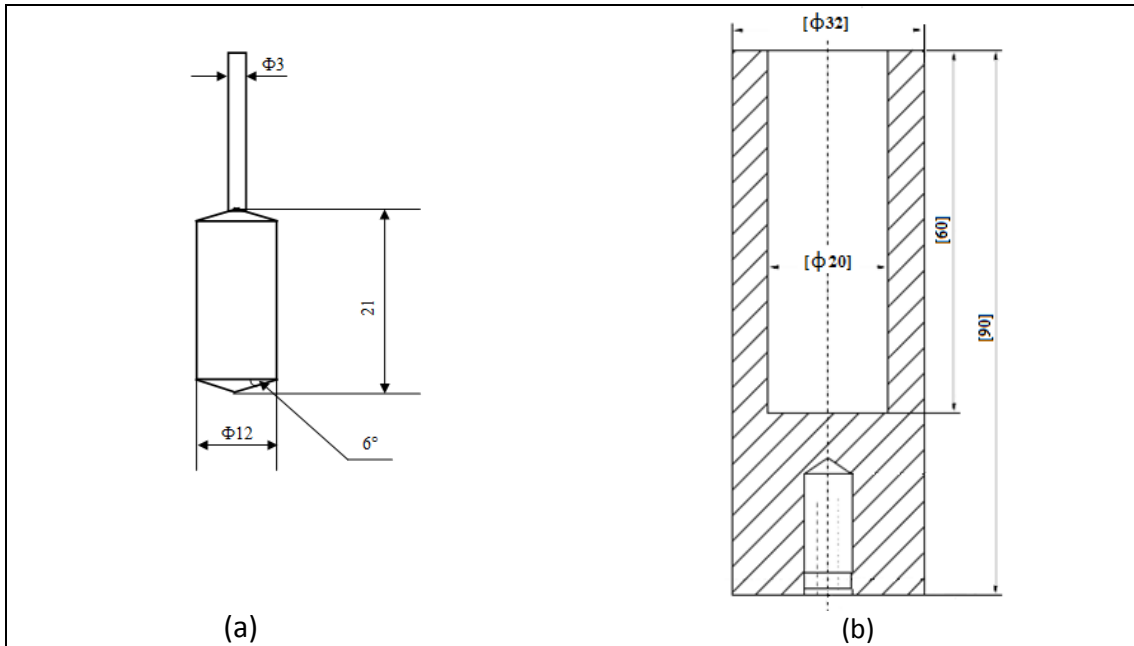


**Figure 17.** Dimensions of (a) the inner cylinder and (b) the crucible used for the measurements with the rotation viscometer [mm] [47].

## 5. RESULTS AND DISCUSSION

### 5.1 CaO-Al<sub>2</sub>O<sub>3</sub> slag (CA)

#### 5.1.1 Results

The CaO-Al<sub>2</sub>O<sub>3</sub> slag, herein referred to as CA, containing 43.7% CaO and 56.3% Al<sub>2</sub>O<sub>3</sub>, was studied with the SHTT. The *liquidus* temperature for this slag according to FactSage 6.1 is 1518 °C, and the first crystal during cooling is CaAl<sub>2</sub>O<sub>4</sub>. The second crystal during cooling is Ca<sub>3</sub>Al<sub>2</sub>O<sub>6</sub>, which precipitates at 1362 °C (*solidus* temperature).

#### *Melting behaviour*

In Figure 18 the melting behaviour for a CA sample, that was heated at 1000 °C/min from room temperature up to 1700 °C. When the sample is completely melted the slag becomes transparent, i.e. the conditions to determine the start of crystallisation become good. The time to melt the sample depends on its mass. The lower the mass of the sample, the faster the sample becomes liquid.

During melting some bubbles were observed, remaining in the slag even after long time at high temperatures. This slag was well decarburized. Bubble formation was observed for this sample and for all experiments of the present work during the first melting. They may originate from decomposition of carbonates or moisture pickup in the powders used to mix slags [13]. The bubble residence time in slags is long if slag viscosity is high. Their origin is not clear, since the samples were decarburized and vacuum was applied before the experiments.

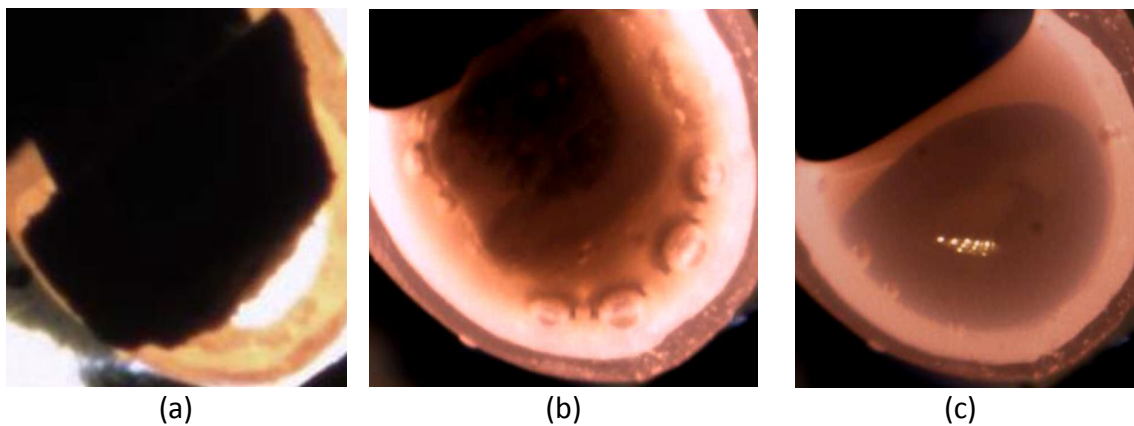


**Figure 18.** CA melting behaviour, heating rate 1000 °C/min from room temperature up to 1700 °C. (a) 1329 °C, below *solidus*; (b) 1700 °C, above *liquidus*, many bubbles can be observed, and part of the sample remains solid (centre); (c) 1700 °C, the sample becomes fully liquid and transparent after 5 minutes at this temperature.

#### *CCT diagram*

It was constructed a CCT diagram for the CA slag; see Figure 19. The samples were maintained at 1700 °C for 60 seconds before the cooling at different cooling

rates. The red triangles mean the point of first crystals precipitation for the CA slag. The crystallisation starts far from the *liquidus*. It can be observed that the crystallisation temperature is a function of the cooling rate; the critical cooling rate for the slag is 1700 °C/min, i.e. with higher cooling rates no crystal is observed. For the lower cooling rates in a few seconds the sample is 100% crystalline (after the beginning of crystallisation).

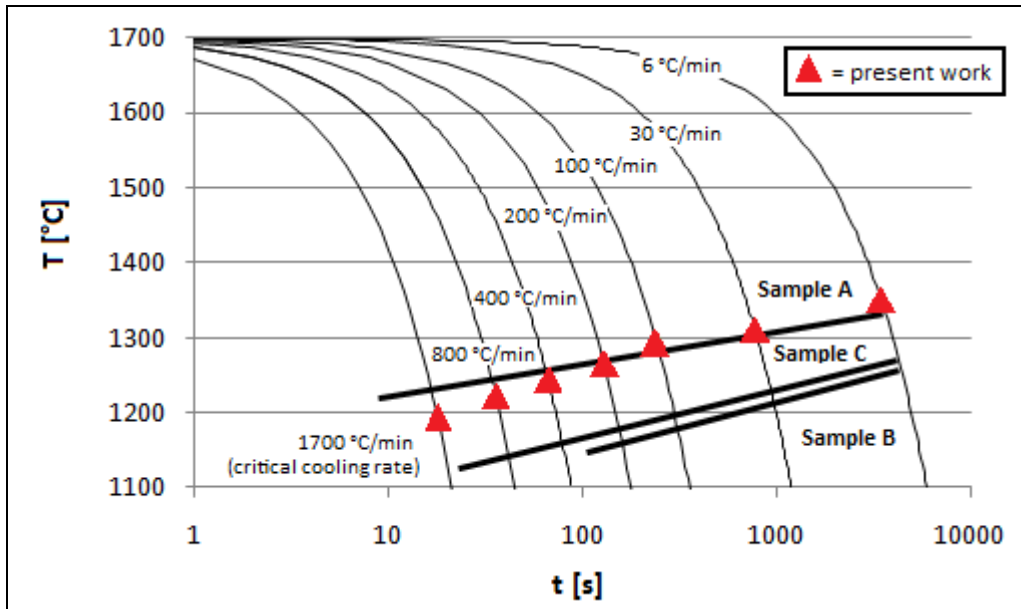


**Figure 19.** CCT diagram for the CA slag, obtained from SHTT. The red triangles mean the point of first crystals precipitation (crystallisation temperature) for the slag of the present work (44% CaO, 56% Al<sub>2</sub>O<sub>3</sub>). Samples A, B and C are calcium aluminate slags containing 48% CaO, 50% CaO and 53% CaO respectively, whose CCT diagrams were also determined through the hot thermocouple technique in a previous work [36].

The sample showed in Figure 20 – cooled at 30 °C/min from 1700 °C – at 1330 °C is still transparent (Figure 20a). The lamp below the sample is on, and because of that there are some optical effects, but they do not disturb the analysis. At 1310 °C the first crystals were registered (Figure 20b). At 1280 °C the sample is opaque, i.e. full crystallisation (Figure 20d).

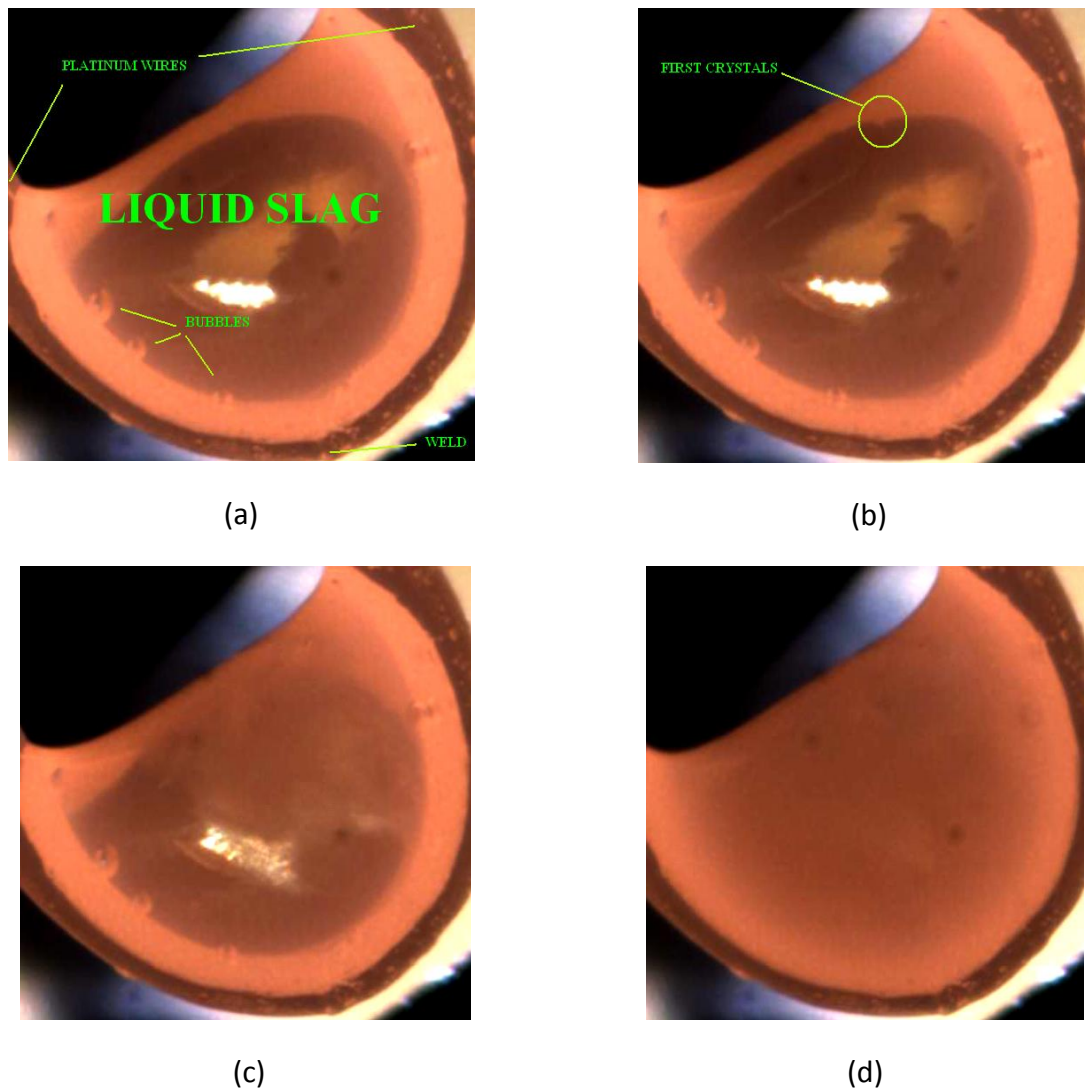


**Figure 20.** Crystallisation of the slag CA under a cooling rate of 30 °C/min from 1700 °C. (a) 1330 °C, no crystal; (b) 1310 °C, start of crystallisation; (c) 1292 °C, high %crystallinity; (d) 1280 °C, full crystallisation.

#### *Viscosity measurements*

Figure 21 shows results of viscosity measurements taken using a rotation viscometer (three measurements), for a slag whose composition is close to that of the CA slag (46.1 %CaO, 53.9% Al<sub>2</sub>O<sub>3</sub>). The measured viscosity for this slag at 1550 °C is 3.2 P. According to Slag Atlas [46] the viscosity for it (mole fraction CaO = 0.62 , page 356) at 1550 °C is approximately 2 P.

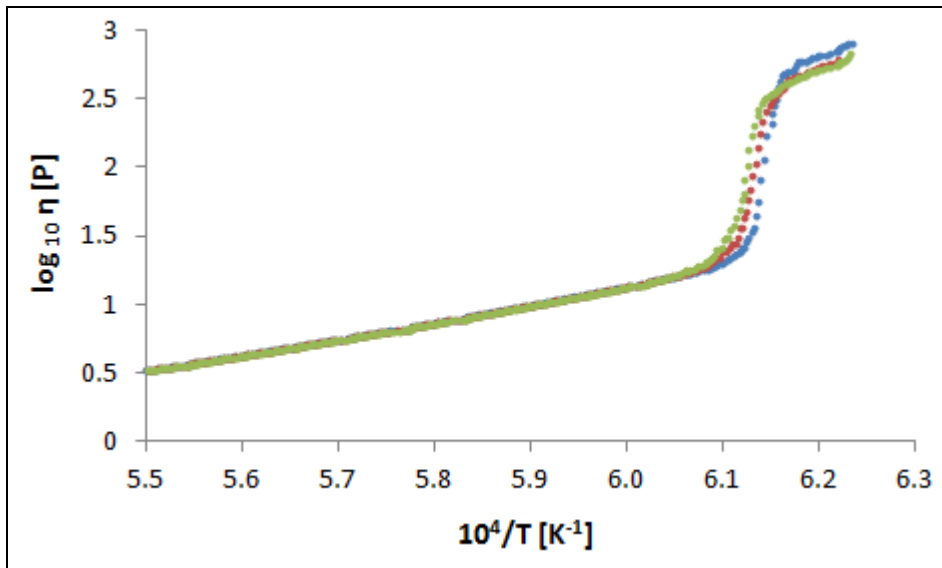


**Figure 21.** Viscosity measurements taken using a rotation viscometer, for a slag whose composition is close to that of the CA slag (46.1 %CaO, 53.9% Al<sub>2</sub>O<sub>3</sub>).

### 5.1.2 Discussion

Prapakorn and Cramb [36] showed CCT diagrams for calcium aluminate slags which were named as Sample A = 48% CaO, Sample B = 50% CaO and Sample C = 53% CaO; see Figure 19. The CCT diagrams for these slags were also determined through the hot thermocouple technique. According to their observations it is easiest to form a glass at the eutectic composition, i.e. 50% CaO.

The slag CA studied in the present work has got 44% CaO and presents a CCT curve more similar to Sample A. Thus, the comparison with these results is coherent.

From the viscosity measurements, see Figure 21, it can be observed that the break temperature, i.e. the point where there is a sudden increase of the viscosity due to crystals precipitation, is in the range 1350 - 1375 °C. According to the SHTT the point where the first crystals were detected for this CA slag at the lower cooling rate, 6 °C/min, is 1350 °C. Thus, for this slag there is a correspondence between break temperature obtained from viscometer and crystallisation temperature obtained from SHTT.

In Figure 21 it can also be observed that after the beginning of crystallisation the slope of the curve decreases. A possible explanation for this fact would be decrease of viscosity of the liquid slag caused by increase of temperature, which would happen due to liberation of energy during cooling, as it was registered in Figures 12 and 13 for CaF<sub>2</sub>, K<sub>2</sub>SO<sub>4</sub> and Na<sub>2</sub>SO<sub>4</sub>.



## 5.2 CaO-SiO<sub>2</sub> slag (CS)

### 5.2.1 Results

The slag CaO.SiO<sub>2</sub> with basicity %CaO/%SiO<sub>2</sub> (wt%) = 0.7, herein referred to as CS, has the following characteristics according to FactSage 6.1: *liquidus* temperature, 1500 °C; first solid phase during cooling, CaSiO<sub>3</sub>; and *solidus* temperature, 1437 °C, where the second crystal (SiO<sub>2</sub>) precipitates.

Figure 22 shows the melting behaviour of the CS slag.

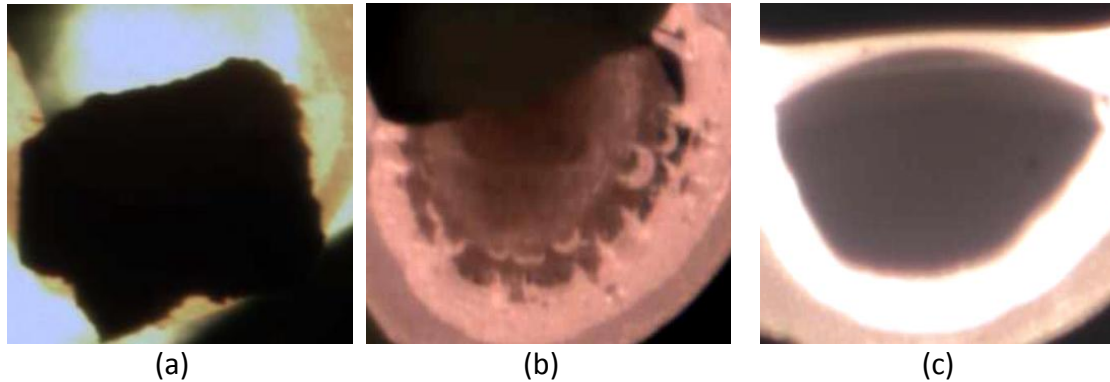


**Figure 22.** CS melting behaviour, heating rate 1000 °C/min from room temperature up to 1700 °C. (a) 1427 °C, below *solidus*; (b) 1700 °C, above *liquidus*, many bubbles can be observed, and part of the sample remains solid (centre); (c) 1700 °C, the sample becomes fully liquid and transparent after 5 minutes at this temperature (with a small bubble observed at the right).

#### *CCT diagram*

Regarding the CCT experiments (continuous cooling), no crystallisation is observed, even at very low cooling rates. The samples were completely melted, then maintained at 1700 °C for 5 minutes, and finally cooling rates of 30 °C/min and 10 °C/min were applied down to 700 °C.

#### *TTT diagram*

For TTT experiments (isothermal transformation), the samples were completely melted and then maintained at 1700 °C for 5 minutes. Then, a very high cooling rate (> 3000 °C/min) was applied. When the desired temperatures were reached – 900 °C, 950 °C, 1000 °C, 1050 °C, 1100 °C, 1150 °C, and 1200 °C – the samples were maintained at those temperatures for up to 1000 seconds. Crystallisation was observed only at 1000 °C occurring at 76 seconds (average for 6 experiments, standard deviation 27 seconds).

### Conditions for intense crystal growth for CaO-SiO<sub>2</sub> slags

In addition to the CCT and TTT experiments, another type of thermal cycle was applied:

- (i) The sample was maintained at 1700 °C for 5 minutes, i.e., completely melted;
- (ii) Quenching (> 3000 °C/min) down to particular temperatures (900 °C, 950 °C, 975 °C, 1000 °C, 1025 °C, 1050 °C, 1100 °C, 1150 °C, 1200 °C, 1300 °C);
- (iii) Maintenance at the particular temperature for 60 seconds, and
- (iv) Heating again at a rate of 1000 °C/min up to 1700 °C.

With respect to this special thermal cycle, crystallisation was observed to occur intensely during heating at a rate of 1000 °C/min but only when starting (after quenching) at 1000 °C or below. The crystallisation occurs intensely in the range 1069 - 1125 °C when starting at 900 °C, 950 °C, 975 °C, and 1000 °C. Thus, it is clear that when increasing the temperature after reaching a particular range of lower temperatures, good conditions for crystals growth can be obtained for the CaO-SiO<sub>2</sub> slag. Figure 23 shows an example, which is the result of maintaining a sample at 900 °C for 60 seconds and then heating at a rate of 1000 °C/min. This slag is transparent, i.e. the conditions to determine the start of crystallisation are good.

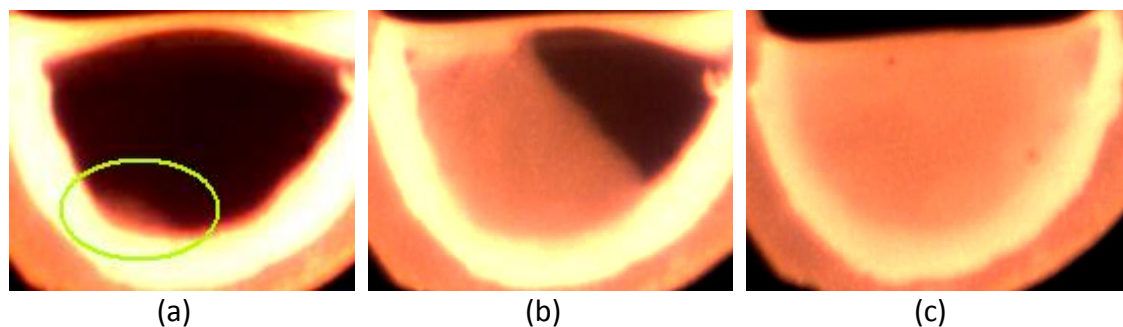


**Figure 23.** Crystallisation of the CS slag (basicity = 0.7) when increasing the temperature at a heating rate of 1000 °C/min, after maintaining the sample at 900 °C for 60 seconds. (a) 1079 °C, start of crystallisation; (b) 1202 °C, 7 seconds after the start of crystallisation; (c) 1297 °C, 13 seconds after the start of crystallisation (full crystallisation).

### Viscosity measurements

In Figure 24 the results for a slag whose composition is close to that of the CS slag (43.3 %CaO, 56.7 %SiO<sub>2</sub>). At temperatures of approximately 1350 °C, the viscosity increased very quickly. For this apparatus, the measurement is automatically terminated when the torque exceeds 2000 μNm.

The measured viscosity for this CaO-SiO<sub>2</sub> slag at 1600 °C is 3.1 P. According to Slag Atlas [46], the viscosity of this slag at 1600 °C is 4.4 P.

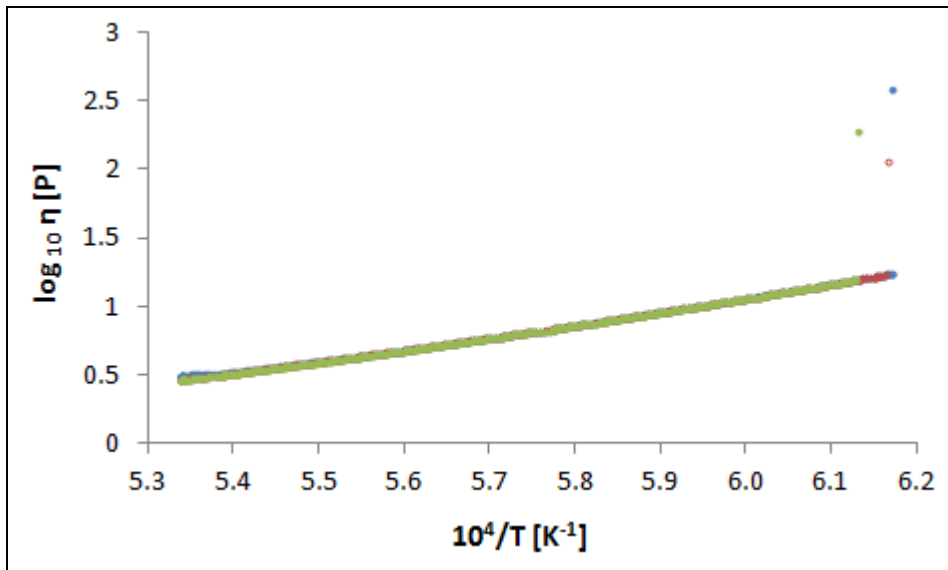


**Figure 24.** Viscosity measurements taken using a rotation viscometer, for a slag whose composition is close to that of the CS slag (43.3 %CaO, 56.7 %SiO<sub>2</sub>).

### 5.2.2 Discussion

The sudden increase in viscosity shown in Figure 24 was surprising because for the SHTT at 10 °C/min – the same continuous cooling rate used during the viscosity measurement – no crystal was observed. For this CS composition – 43.3 %CaO, 56.7 %SiO<sub>2</sub> (wt%) – according to the phase diagram [46] above 870 °C it is possible to have wollastonite, CaO.SiO<sub>2</sub>, and tridymite, SiO<sub>2</sub>. The precipitation of small transparent crystals at high temperature would explain this sudden increase in viscosity and the SHTT observations; see Figure 25.

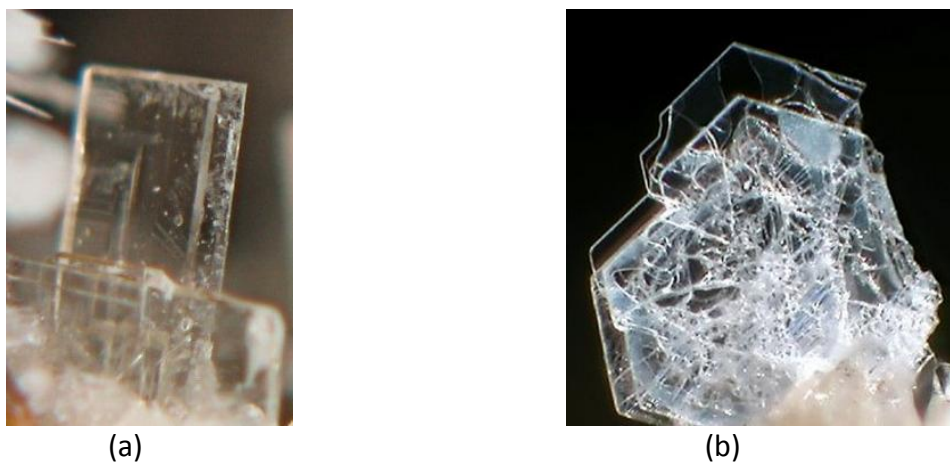


**Figure 25.** Crystals of wollastonite (a) and tridymite (b). Images got from [www.mindat.org](http://www.mindat.org) on 17.11.2011.

For the CaO-SiO<sub>2</sub> slag, no crystal was detected during experiments with SHTT at continuous cooling rates, even at very low cooling rates. This result is in agreement with the results of other reports for CaO-SiO<sub>2</sub> slags with basicity 0.8, 1.0 and 1.2, in which no crystal was detected when performing CCT experiments [43].

However, in the present study, it was observed that it is possible to obtain intense crystallisation for a low-basicity CaO-SiO<sub>2</sub> slag, depending on the thermal cycle. This intense crystallisation can be explained by the fact that the optimum range of temperatures for crystal nucleation is lower than the optimum range of temperatures for crystal growth. Thus, crystals cannot be detected through CCT experiments, even at very low cooling rates. This idea is related to the fact that the rate of crystal growth is not the only factor determining the ability of a melt to form crystals because crystals grow from a certain number of nuclei, and in many respects, the nucleation stage determines the pathways of overall crystallisation in silicate glasses [38].

It is well known that crystallisation can be divided into two processes: (i) formation of nuclei and (ii) crystal growth. The rates of both processes are temperature-dependent, with maxima at certain supercooling values. These maxima are separated in glass-forming materials suitable for the preparation of glass ceramics, allowing for control over glass crystallisation [48].

Crystallisation from a glassy state is qualitatively explained by the nucleation rate and crystal growth rate as a function of temperature for ordinary glass, according to Figure 26 – the hatched zone represents the temperature range in the present work. This schematic diagram shows that the driving force for nucleation increases with decreasing temperature. The mobility of atoms or ions decreases with decreasing temperature. Therefore, the nucleation rate exhibits a maximum at a certain temperature. The growth rate also exhibits a maximum at a certain temperature. The nucleation rate is high and the crystal growth rate is low at relatively low temperature, for example, at T<sub>1</sub> in Figure 26. On the other hand, the nucleation rate is low and the crystal growth rate is high at a relatively high temperature (e.g., at T<sub>2</sub>). It was observed that the crystallisation of mould powders from the glassy state agrees with the qualitative representations shown in Figure 26 [14]. Therefore, it was concluded that the crystallisation of mould powders from the glassy state is similar to that of ordinary glass.

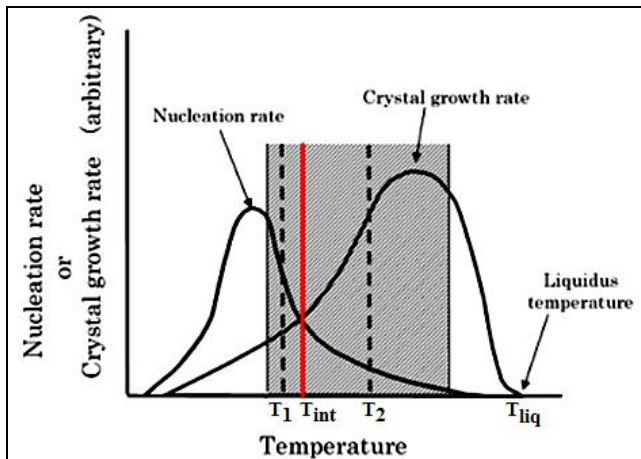


**Figure 26.** Schematic curves of the nucleation rate and the crystal growth rate as a function of temperature (adapted from [14]). The temperature range in the present work is represented by the hatched zone. There is an intermediate temperature where the nucleation rate and the crystal growth rate would be sufficiently high to promote crystallisation under isothermal conditions.

Considering the aforementioned discussion, the observation of crystals during isothermal experiments at 1000 °C for the CS slag is explained by the fact that 1000 °C is an intermediate temperature ( $T_{int}$ ), at which both the nucleation rate and growth rate are sufficiently high.

In a general way crystals can grow from supercooled slag or solid glass (devitrification), according to Figure 2. With SHTT it is difficult to determine if the crystals grow from supercooled slag or solid glass. Anyway, for transparent materials crystallisation can be observed in both situations (if the crystals are opaque), though at lower temperatures the conditions for visibility are not ideal.

### 5.3 CaO-SiO<sub>2</sub>-TiO<sub>2</sub> slag (CST\_1)

#### 5.3.1 Results

The slag of the CaO-SiO<sub>2</sub>-TiO<sub>2</sub> system, herein referred to as CST\_1, was used to study the effect of the duration of superheating on incubation times. The composition (wt%) of CST\_1 is 41.1 %CaO, 29.1 %SiO<sub>2</sub>, and 29.8 %TiO<sub>2</sub>. The *liquidus* temperature for this slag is very high, approximately 1600 °C. The first phase formed during cooling from liquid slag is CaO.TiO<sub>2</sub>. According to the CaO-SiO<sub>2</sub>-TiO<sub>2</sub> phase diagram, the possible phases are CaO.TiO<sub>2</sub>, CaO.SiO<sub>2</sub>, and CaO.SiO<sub>2</sub>.TiO<sub>2</sub> [46].

To study the effect of the duration of superheating on incubation times, a special thermal cycle was applied. This thermal cycle, which was repeated several times for each sample, is described in the following:

(i) The samples were held in the temperature range of 1650 °C - 1680 °C for different periods (the samples always completely melted and became transparent within a few seconds);

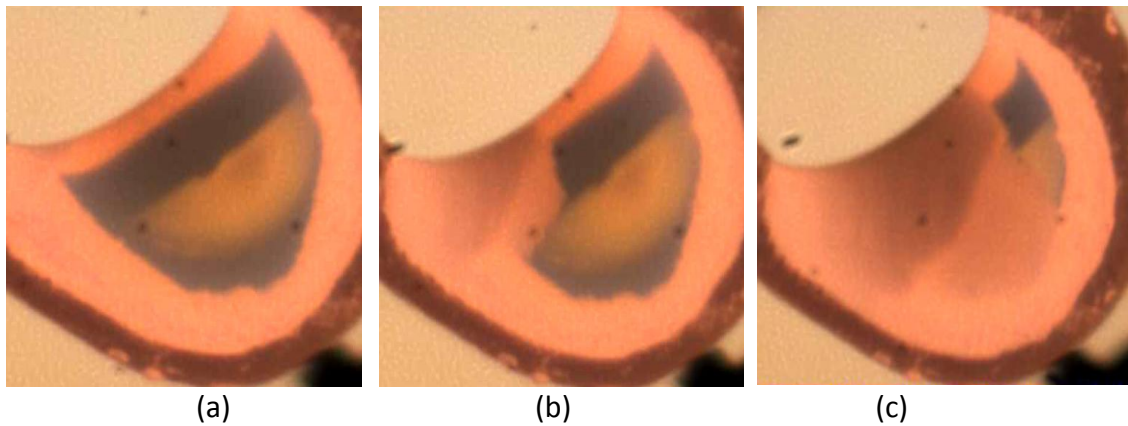
- (ii) Quenching down to 1400 °C at the highest cooling rate (> 3000 °C/min);
- (iii) Measurement of the incubation time, i.e., when the first crystals could be observed;
- (iv) Quenching down to a temperature of 1200 °C, which was held for 60 seconds to guarantee full crystallisation of the sample.
- (v) Heating up to 1650 °C - 1680 °C.

Table 7 shows the results in chronological order for a sample with 2.3 mg. For “Sequence 1” it can be observed that the initial holding time is very long: 1800 s. This very long holding time was necessary to melt completely CST\_1. The expression “> 1000 [s]” in Table 7 means that no crystal was observed at 1400 °C up to 1000 seconds. That was the limit for the observation time. It is clear that the duration of superheating completely changed the crystallisation behaviour of the CST\_1 slag, assuming that the initial conditions before melting were the same. When the holding time is 60 seconds, the incubation times tend to be shorter than when the holding time is 600 seconds (it is notable that no crystals was observed up to 1000 seconds). The TTT diagrams when using different holding times are very different. Another sample with a mass of 1.4 mg was also analysed in the same conditions, and the results have the same tendency. For this slag it was necessary to use samples with lower mass to get fast melting.

**Table 7.** Results for CST\_1 (2.3 mg). “Sequence” means chronological order. Between each measurement the sample was maintained at 1200 °C for 60 seconds to guarantee full crystallisation.

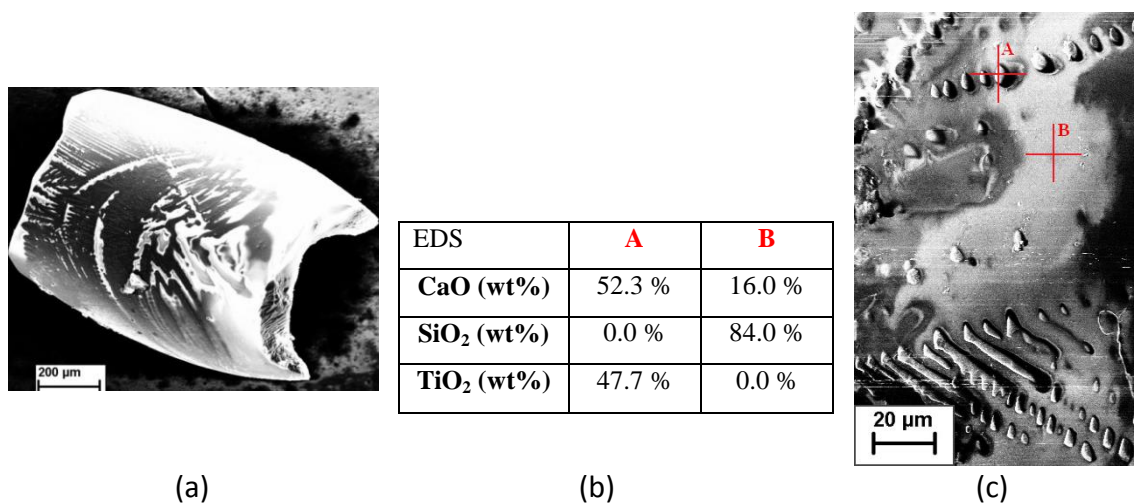
Sequence	Duration of superheating at 1650°C-1680°C [s]	Incubation time at 1400°C [s]
1	1800	> 1000
2	60	5
3	600	> 1000
4	60	11
5	600	> 1000
6	600	> 1000
7	60	> 1000
8	600	> 1000
9	60	12

Figure 27 shows the isothermal transformation at 1400 °C of the sample with a mass of 2.3 mg when the duration of the superheating is 60 s.



**Figure 27.** Crystallisation of CST\_1 slag at 1400 °C, when the duration of the superheating is 60 s, in the range 1650 °C - 1680 °C. After the fast quenching, the measured incubation time is approximately 10 s. (a) No crystal; (b) and (c) crystallisation in progress.

After the SHTT experiments, a sample that suffered thermal treatment at 1200 °C for 60 seconds was detached and analysed by scanning electron microscopy; see Figure 28. A dendritic structure can be observed. Using energy-dispersive X-ray spectroscopy, a qualitative analysis was performed, comparing crystals and the regions nearby. Point A is most likely a perovskite crystal particle ( $\text{CaO}\cdot\text{TiO}_2$ ), growing into a phase of different composition. Point B represents a region depleted of  $\text{TiO}_2$  formed around the particle, which features a higher  $\text{SiO}_2$  content. It is known that in this case the continual growth of the particle requires chemical diffusion in the surrounding phase, and as the particle increases in size, the effective distances over which diffusion takes place may also increase [41].



**Figure 28.** (a) CST\_1 sample after thermal treatment at 1200 °C for 60 seconds (it appears completely crystalline according to visual observation with SHTT); (b) EDS analysis results for two points; (c) crystals and a region of remaining slag with high  $\text{SiO}_2$  content.

### 5.3.2 Discussion

It is known that a new phase is nucleated by nuclei that already exist in the old phase and whose effective number per unit nucleation region can be altered by the temperature of superheating and the duration of superheating. There are indications that, for given supercooling or superheating, the nuclei grow or diminish considerably more slowly than grains of visible size. These nuclei, which may be heterogeneities of any sort, would usually consist of small particles of the subcritical phase or tough films of the latter surrounding foreign inclusions [49].

Thus, it can be concluded that there is a relation between the duration of superheating, incubation times, and number of nuclei. The longer the duration of superheating is, the lower the number of nuclei per unit nucleation region is, and consequently, the longer the incubation time becomes.

At any temperature, the nuclei grow (supercooling) or diminish (superheating) more slowly than grains of measurable size (in the  $\mu\text{m}$  range). This tendency was confirmed for nuclei growth, i.e., supercooling [40]. The crystallisation behaviour of the  $\text{Li}_2\text{O} \cdot 2\text{SiO}_2$  glass was studied with special emphasis on the induction period for crystallisation. Detailed nucleation, growth and overall crystallisation data were obtained for  $\text{Li}_2\text{O} \cdot 2\text{SiO}_2$  glass at  $500\text{ }^\circ\text{C}$ , employing reflected-light and transmitted-light microscopy.

It was demonstrated [40] for  $\text{Li}_2\text{O} \cdot 2\text{SiO}_2$  glass, which crystallises through homogeneous nucleation, that the times required to grow super-critical nuclei (nm range) to sizes detectable by optical microscopes ( $\mu\text{m}$  range) are long, appearing as induction times in length versus time plots. The apparent induction periods determined by three independent kinetic measurements were in the range of 1-4 hours. The glassy samples were maintained at  $500\text{ }^\circ\text{C}$  for 75 hours, reaching volume crystal fractions of up to 26%. It was concluded that the time required for the first crystal to grow to detectable sizes is the main component of the experimental apparent observed induction periods.

## 5.4 CaO-SiO<sub>2</sub>-TiO<sub>2</sub> slag (CST\_2)

### 5.4.1 Results

The composition for the slag of the CaO-SiO<sub>2</sub>-TiO<sub>2</sub> system, herein referred to as CST\_2, is 35.6 %CaO, 46.3 %SiO<sub>2</sub>, 18.1 %TiO<sub>2</sub> (wt%). The *liquidus* temperature is  $1366\text{ }^\circ\text{C}$  according to FactSage 6.1. This slag has higher carbon content (0.590 %) since for this slag the decarburization step in the furnace at  $700\text{ }^\circ\text{C}$  for 5 hours was not applied. Thus, the carbon from carbonates was removed only during pre-melting.

From the CaO-SiO<sub>2</sub>-TiO<sub>2</sub> phase diagram [46] after complete solidification the possible phases for CST\_2 are: CaO.SiO<sub>2</sub>, CaO.SiO<sub>2</sub>.TiO<sub>2</sub> and SiO<sub>2</sub>. This slag is translucent, i.e. the conditions to determine the start of crystallisation are not ideal.



This was surprising, because the other TiO<sub>2</sub>-bearing slag (CST\_1) is transparent when melted.

#### CCT diagram

Some continuous cooling rates were applied using the SHTT – 60, 30, 20 and 10 °C/min. No crystal was observed.

#### TTT diagram

The TTT diagram for the slag CST\_2 was constructed; see Figure 29. It can be observed that the crystallisation starts far below the *liquidus*. For each temperature six measurements were done, i.e. the diagram was constructed from 102 measurements. The averages and standard deviations were calculated assuming a normal distribution, and they are shown in Figure 29. The experiments were executed considering the maximum holding time of 1000 s.

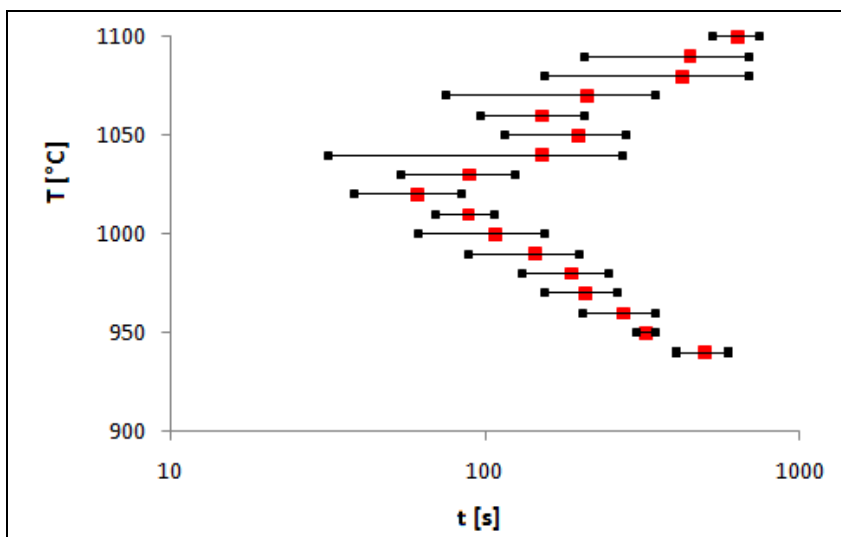


**Figure 29.** TTT diagram for the slag CST\_2 – 35.6 %CaO, 46.3 %SiO<sub>2</sub>, 18.1 %TiO<sub>2</sub> (wt%), obtained from SHTT. For each temperature six measurements were done. The averages and standard deviations are shown.

Different ways of crystallisation were observed. In the range 940 °C - 1030 °C crystallisation always occurred on the surface of the thermocouple advancing to the bulk of the sample. The surface of the thermocouple most likely facilitates heterogeneous nucleation.

In the range 1040 °C - 1070 °C crystallisation occurred in two different forms: (i) from the surface of the thermocouple advancing to the bulk of the sample and (ii) in the bulk of the sample in an relatively intense way.

In the range 1080 °C - 1100 °C crystallisation occurred (i) also from the surface of the thermocouple advancing to the bulk of the sample and (ii) in the bulk of the

sample, but not in an intense way, since it were observed small blocks of crystals growing very slowly.

#### Viscosity measurements

Figure 30 shows results for a slag whose composition is close to that of the CST\_2 slag (36.4 %CaO, 45.9 %SiO<sub>2</sub>, 17.7 %TiO<sub>2</sub>). The temperature where the viscosity increases suddenly is approximately 1250°C.

The measured viscosity for this slag at 1400 °C is 3.9 P. According to Schenck and Froberg [50] the viscosity of this slag at 1400 °C is approximately 10 P.

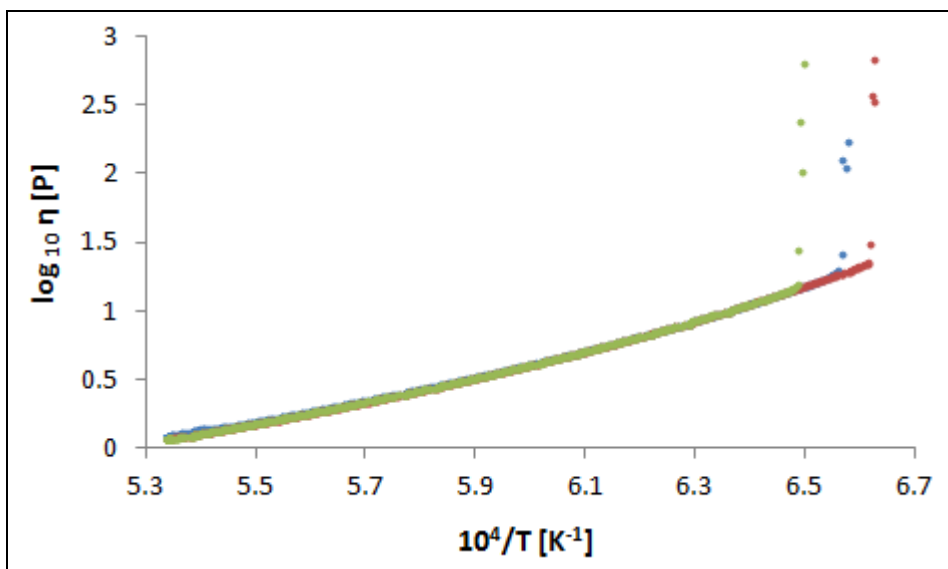


**Figure 30.** Viscosity measurements taken using a rotation viscometer for a slag whose composition is close to that of the CST\_2 slag (36.4 %CaO, 45.9 %SiO<sub>2</sub>, 17.7 %TiO<sub>2</sub>), for three measurements.

#### 5.4.2 Discussion

Figure 31 compares the TTT diagram for the CST\_2 slag with two other TTT diagrams for slags from literature. The “CST literature” is a slag of similar composition, also in the primary crystallisation field of CaO.SiO<sub>2</sub> in the CaO-SiO<sub>2</sub>-TiO<sub>2</sub> diagram. The TTT diagram of the “CST literature” was constructed through Differential Thermal Analysis (DTA) [26].

The slag “commercial” is an industrial mould powder normally employed in the continuous casting of stainless steels, which contains CaF<sub>2</sub> and Na<sub>2</sub>O, without TiO<sub>2</sub>, and whose TTT diagram was also constructed through SHTT [5]. For the “CST literature” and “commercial” the reported melting points are 1296 °C and 1262 °C respectively [26].

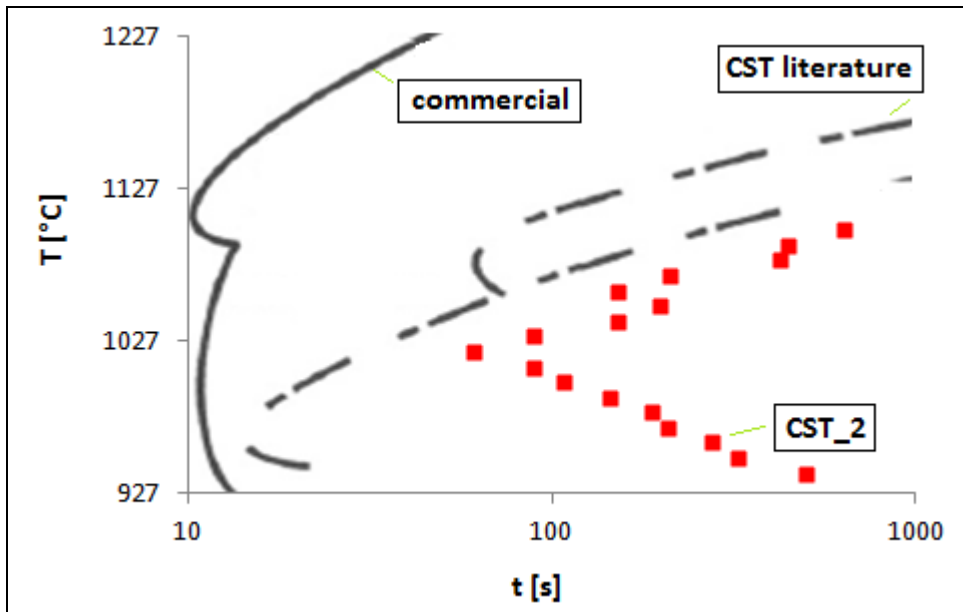


**Figure 31.** TTT diagram of the slag CST\_2 constructed through SHTT. The TTT diagrams for the slags “commercial” [5] and “CST literature” [26] are also shown.

It is required that the crystals of the  $\text{CaO-SiO}_2\text{-TiO}_2$  system precipitate as the phase cuspidine in commercial mould powders, replacing the system  $\text{CaO-SiO}_2\text{-CaF}_2$ . However, the incubation times for the slag CST\_2 are much longer than of the industrial mould slag.

An interesting point is that the TTT diagram of the “CST literature” was obtained through DTA, and the TTT diagram of the CST\_2 slag was obtained through SHTT. Even with so different experimental setups the result is similar. According to the researchers who studied the “CST literature” [26] their TTT diagram was obtained in the following way: the continuous-cooling- transformation diagram (CCT) was experimentally determined by using DTA, and then it was transformed into TTT diagram by using the additivity rule of Scheil. The crystallisation temperature was defined considering the temperature observed at the exothermic peak during the continuous cooling process. Besides, the melting point was determined by the heating process of the DTA measurement.

The TTT curve for the CST\_2 slag was constructed through SHTT by visual analysis using recorded video files. The starting point for crystallisation was considered as the point where undoubtedly crystallisation is perceived, using appropriate light conditions.

The slags “CST literature” and CST\_2 are similar considering the following aspects: chemical composition, basicity (V-ratio), both are in the primary crystallisation field of wollastonite, and the possible phases after solidification are the same according to the phase diagram [46]. Besides, they have similar *liquidus* temperatures and viscosities. Then, considering these similarities, it is expected a similar crystallisation behaviour, as it is shown in Figure 31. See Table 8 for more details.

**Table 8.** Properties of the slags CST\_2 (present work) and “CST literature” [26].

	CST literature	CST_2
%CaO (wt%)	37.0%	35.6%
%SiO <sub>2</sub> (wt%)	47.2%	46.3%
%TiO <sub>2</sub> (wt%)	15.8%	18.1%
Basicity (%CaO/%SiO <sub>2</sub> )	0.78	0.77
<i>Liquidus</i> , FactSage 6.0	1387 °C	1366 °C
<i>Solidus</i> , FactSage 6.0	1339 °C	1339 °C
Melting point, from [26]	1296 °C	-
Viscosity of the liquid slag at 1400°C [P], from [50]	approx. 10 P	approx. 10 P

However, despite of the similar crystallisation behaviour the incubation times are different below 1020 °C. Regarding the kinetics related to CST\_2 and “CST literature”, different conditions for heterogeneous nucleation can exist depending on the raw materials and on the experimental set-up.

It is known that phase boundaries and foreign solid particles may favour nucleation. This effect is due mainly to the diminished thermodynamic barrier as compared to that for homogeneous nucleation, owing to a decrease of the contribution of the effective surface energy to the work of critical cluster formation. Catalyzing surfaces may also be represented by dispersed solid particles that act as nucleation sites. In this case, their curvature and number may strongly affect the nucleation kinetics [38]. The raw materials for production of the slags in the present work are reagent grade, *i.e.* there are some impurities (for the slag CST\_2 for example there are 0.62% impurities according to XRF, e. g. little amounts of Fe<sub>2</sub>O<sub>3</sub>, MgO, Al<sub>2</sub>O<sub>3</sub>, etc.).

It was suggested that it would be worth to investigate the effect of Na<sub>2</sub>O addition in CaO-SiO<sub>2</sub>-TiO<sub>2</sub> slags [26], since in this way it would be possible to decrease the incubation times of the crystals, getting a fluorine-free mould powder with crystallisation behaviour more similar to an industrial one.

## 5.5 CaO-SiO<sub>2</sub>-TiO<sub>2</sub>-Na<sub>2</sub>O-Al<sub>2</sub>O<sub>3</sub> slags (CSTNA)

### 5.5.1 Results

#### *Melting behaviour*

In Figure 32 some pictures of a CSTNA\_1 sample (compositions of the CSTNA slags are shown in Table 5) that was heated from room temperature at the rate 1000 °C/min up to 1600 °C, and then maintained at this temperature for 60 seconds before the fast quenching, are shown. This slag is transparent; the conditions to determine the start of crystallisation are good. Eventually a few bubbles remained stuck to the thermocouple, as it can be observed in Figure 32 at 1600 °C, where there is a bubble at

the left side even after maintaining the sample at 1600 °C for 60 seconds. At higher temperatures bubbles movement is observed due to the relatively low viscosity of the sample.

After maintaining the sample at 1600 °C for 60 seconds the sample becomes transparent, and then the isothermal experiments can begin, performing fast quenching ( $> 3000$  °C/min) down to the desired temperature.

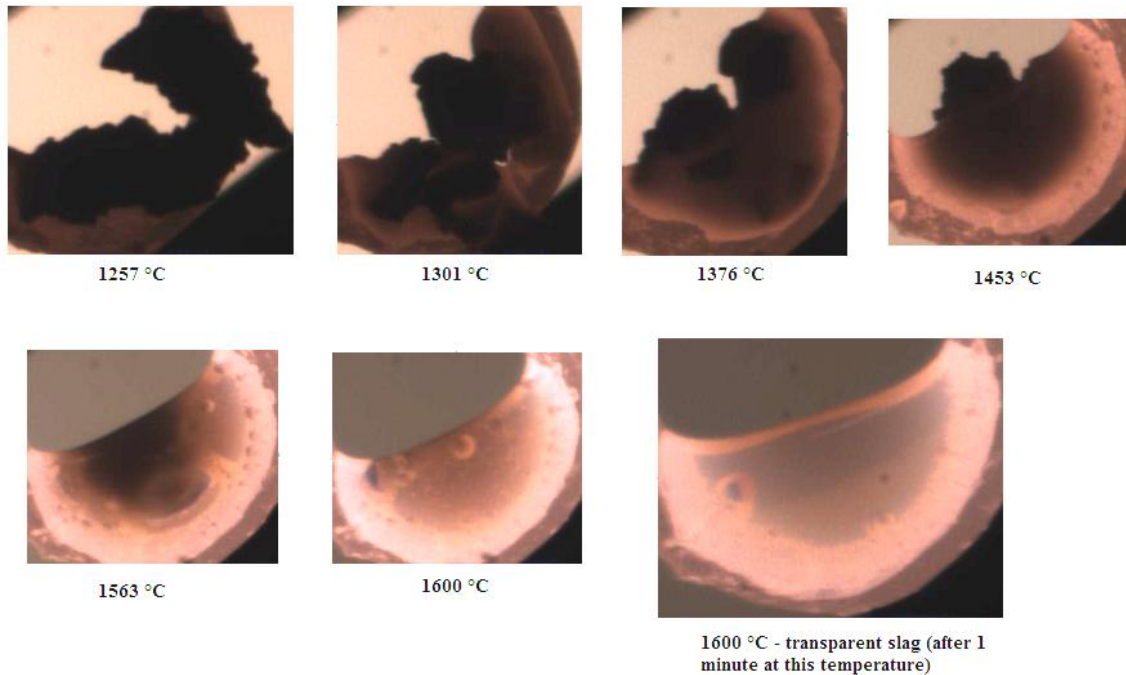


**Figure 32.** Pictures got from video files for a CSTNA\_1 slag sample (composition in Table 5) which was heated from room temperature with 1000 °C/min up to 1600 °C, and then maintained at this temperature for 60 seconds.

The temperature course for melting of the CSNTA\_1 slag is shown in Figure 33. The beginning of the melting i.e. the point when first liquid can be seen was observed at 1257 °C.

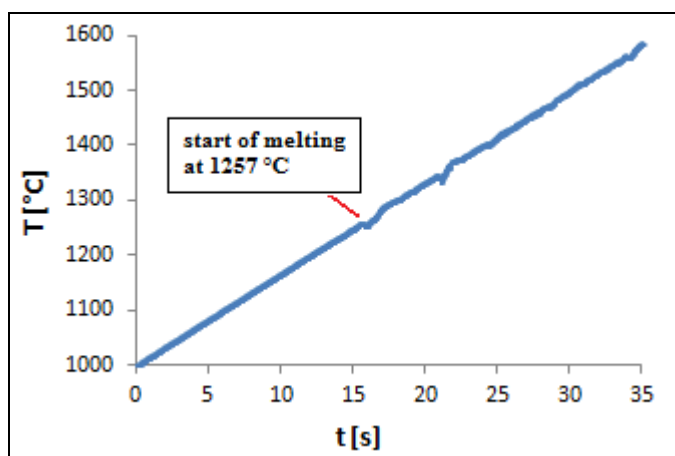


**Figure 33.** Temperature course for melting the sample described in Figure 32, from data file generated during the experiment.

### TTT diagrams

For the CSTNA slags the samples were maintained at 1600 °C for 60 seconds after heating at a rate of 1000 °C/min. At this high temperature, the samples are completely melted within a few seconds. It was clearly observed that if the same sample is used to do many determinations at the same temperature the incubation times became longer. The reason for this effect is Na<sub>2</sub>O loss at high temperatures, assuming that the higher the %Na<sub>2</sub>O content the higher the crystallisation tendency. To avoid this problem the maximum number of measurements per sample was ten.

The slag CSTNA\_1 was designed to have basicity and TiO<sub>2</sub> content similar to the slag CST\_2; see Table 5. The TTT diagrams for the slags CST\_2 and CSTNA\_1 are in Figure 34, in logarithmic scale. The Na<sub>2</sub>O-bearing slag CSTNA\_1 has higher crystallisation rate. Na<sub>2</sub>O addition shortens intensely the incubation times from the CaO-SiO<sub>2</sub>-TiO<sub>2</sub> slag system.

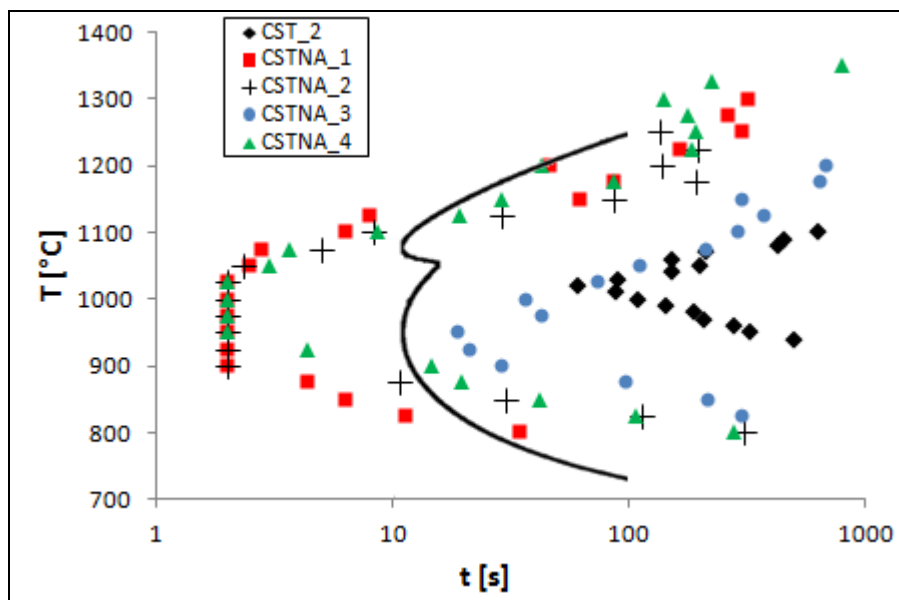


**Figure 34.** TTT diagrams for slags in the CaO-SiO<sub>2</sub>-TiO<sub>2</sub>-Na<sub>2</sub>O-Al<sub>2</sub>O<sub>3</sub> system (composition in Table 5) obtained from SHTT and for a F-bearing industrial slag [5] (continuous line also obtained from SHTT).

With this new finding i.e. the fact that there is a great increase of the crystallisation rate when adding Na<sub>2</sub>O in the CaO-SiO<sub>2</sub>-TiO<sub>2</sub> system, other slags were produced with a lower Na<sub>2</sub>O content to study the possibility of controlling the crystallisation. From CSTNA\_1 were produced CSTNA\_2 and CSTNA\_3, maintaining basicity and TiO<sub>2</sub> content in similar levels. As expected shorter incubation times were observed, especially to CSTNA\_3 which has lower Na<sub>2</sub>O content.

Industrial mould slags contain Al<sub>2</sub>O<sub>3</sub> and because of this fact CSTNA\_4 was also produced, which is a slag with composition similar to CSTNA\_1 but containing more Al<sub>2</sub>O<sub>3</sub>. Despite of having a higher Al<sub>2</sub>O<sub>3</sub> content the incubation times are similar, except at lower temperatures where there is some difference.

### *Crystal's morphology*

It was observed for all the slags that the morphology of the crystals varies with temperature. Columnar grains (which seem to grow unidirectionally from surface to centre of the sample) and equiaxed grains (which seem to grow radially in the liquid slag) were observed. It was reported that, for crystallisation in mould powders, both columnar and equiaxed grains grow dendritically [14].

The crystals show dendritic structure at higher temperatures and become small and dense at lower temperatures. For these last crystals, which are formed in the middle of the liquid slag for higher degree of undercooling, they can be explained by homogeneous nucleation.

Figure 35 shows some images obtained from recorded video files, for the slag CSTNA\_1.

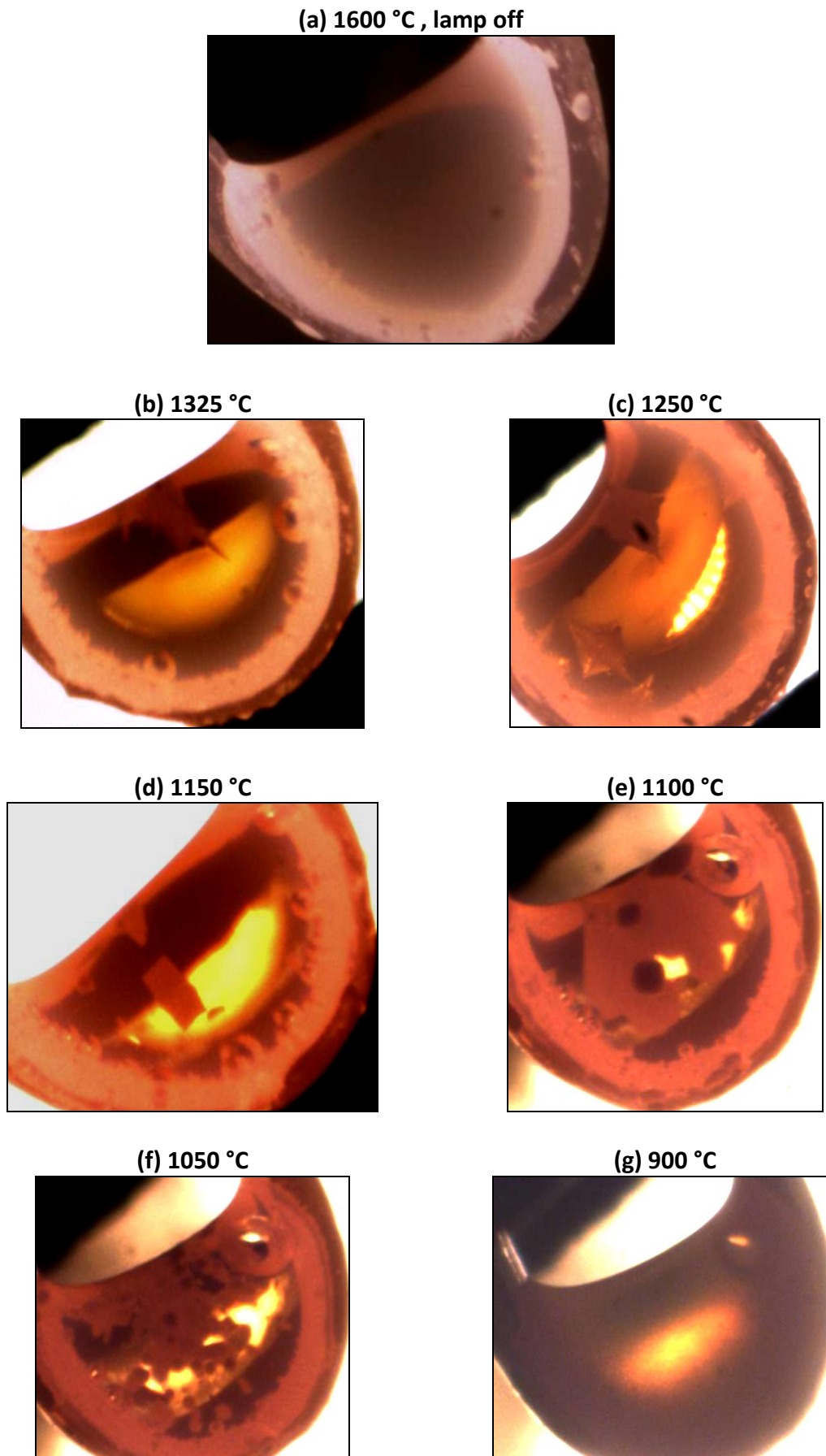


**Figure 35.** Images from experiments performed with the slag CSTNA\_1 at different temperatures.



Firstly, in Figure 35(a) it is shown an image of a slag completely liquid at 1600 °C, with the lamp below the sample off. Normally there are some bubbles around the thermocouple borders, even using decarburized samples – the reason for their formation is not clear. For all the experiments the lamp below the sample was turned on, because in this way the image resolution is higher.

At higher temperatures – Figures 35(b), 35(c) and 35(d) – normally there are dendrites nucleating from thermocouple borders or sample borders. These temperatures correspond to longer incubation times and consequently to lower crystallisation rates. At lower temperatures – Figures 35(e) and 35(f) – there are equiaxed grains growing from different points in the sample.

At 900 °C the samples are translucent, see Figure 35(g). The incubation time is 2 seconds and the samples are completely opaque in only 4 seconds. The crystals are very fine and the density of crystals increases until it appeared “cloud-like” (a similar result is reported in [51] p. 433).

In thermocouple techniques it is common to see at higher temperatures solidification occurring on the thermocouples as the platinum/rhodium of the thermocouple wire is a heterogeneous nucleation point for solidification of the oxide. However, as the temperature decreases the effect of the thermocouple as a nucleating agent diminishes until eventually there is no effect and solid is seen to precipitate and grow within the bulk of the liquid [51].

A further analysis using an optical microscope was performed with a CSTNA\_1 crystalline sample collected after a SHTT experiment; see Figure 36. This sample was maintained at 1200 °C for some minutes up to full crystallisation, then a cross-section was polished and analysed. Dendritic structure can be observed.

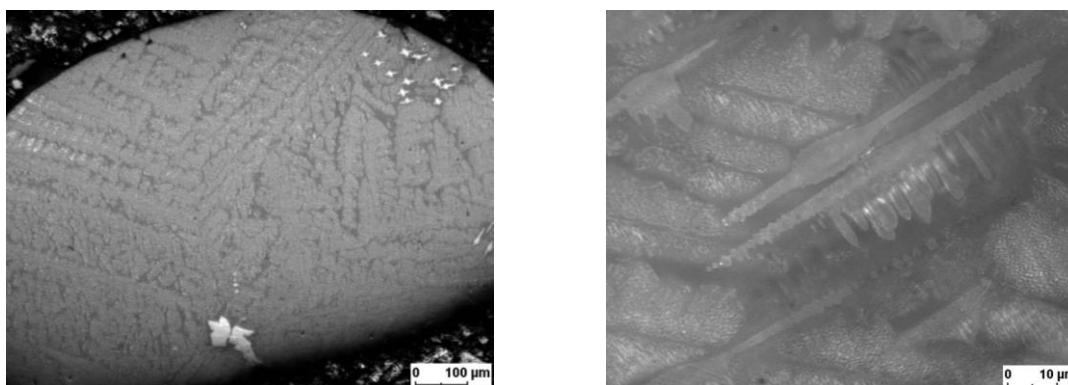


**Figure 36.** CSTNA\_1 crystalline sample (cross-section) at 1200 °C; images obtained using an optical microscope.

#### *Viscosity measurements*

For the viscosity measurements a slag whose composition is close to that of the CSTNA\_1 slag was used – 33.5 %CaO, 41.9 %SiO<sub>2</sub>, 16.3 %TiO<sub>2</sub>, 8.2 %Na<sub>2</sub>O, 0.1 %Al<sub>2</sub>O<sub>3</sub> (wt%); see Figure 37.

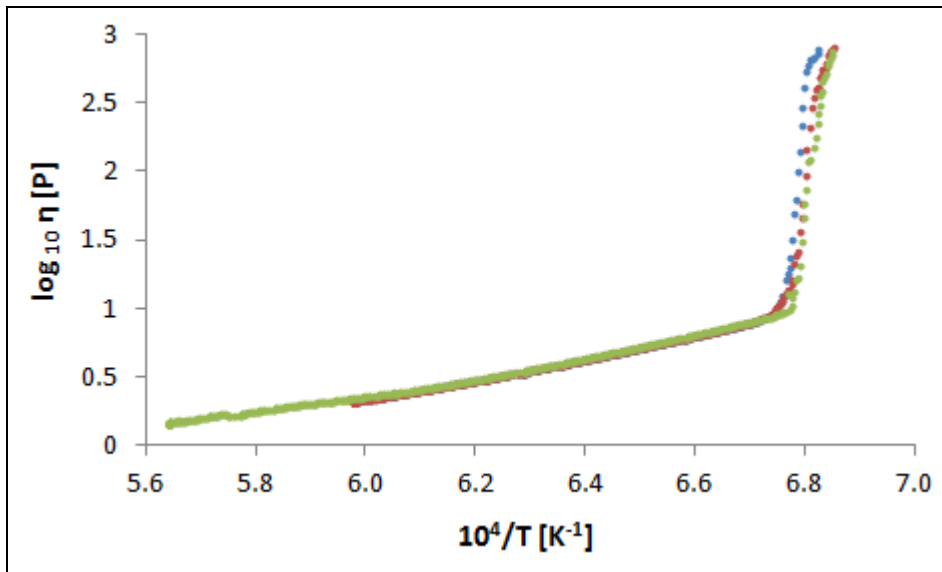


**Figure 37.** Viscosity measurements taken using a rotation viscometer for a slag whose composition is close to that of the CSTNA\_1 slag (33.5 %CaO, 41.9 %SiO<sub>2</sub>, 16.3 %TiO<sub>2</sub>, 8.2 %Na<sub>2</sub>O, 0.1 %Al<sub>2</sub>O<sub>3</sub>), for three measurements.

### 5.5.2 Discussion

In Figure 34 it can be observed the TTT diagram of a commercial mould powder normally employed in the continuous casting of stainless steels, which contains CaF<sub>2</sub> and Na<sub>2</sub>O, without TiO<sub>2</sub> – it was also shown in Figure 31. For F-bearing mould powders, it is known that the presence of alkali oxides (Na<sub>2</sub>O, K<sub>2</sub>O, and Li<sub>2</sub>O) enhances cuspidine crystallisation, both by lowering the melting temperature and by increasing the mobility within the mould slag. Cuspidine is the main phase normally found in slag films taken from the mould [2].

Na<sub>2</sub>O has an important role related to crystallisation behaviour. The TTT diagrams show that it is possible to control the crystallisation tendency changing the Na<sub>2</sub>O content in CaO-SiO<sub>2</sub>-TiO<sub>2</sub> slags.

The effect of Na<sub>2</sub>O content on incubation times was shown in literature using the Hot Thermocouple Technique for some simple slags (%CaO/%SiO<sub>2</sub> =1 and %Al<sub>2</sub>O<sub>3</sub> in the range 6%-7%) [42, 52]. It can be observed in TTT diagrams that Na<sub>2</sub>O shortens the incubation times for these slags; see Figure 38.

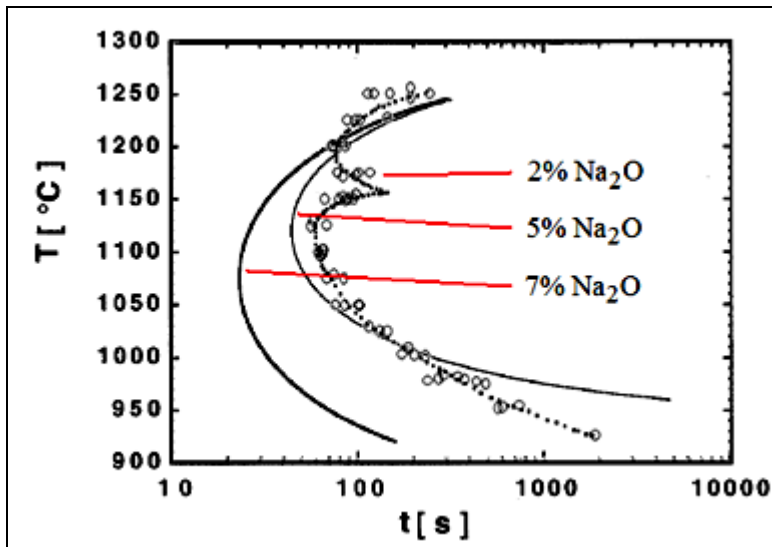


**Figure 38.** Effect of  $\text{Na}_2\text{O}$  on incubation times of slags with  $\text{CaO}/\text{SiO}_2 = 1$ , and  $\% \text{Al}_2\text{O}_3$  in the range 6%-7% [42, 52].

$\text{Na}_2\text{O}$  has an important role regarding mould slag viscosity. It is known that the lower the viscosity the easier the crystallisation. In Figure 39 a summary for the viscosity measurements, which were performed with materials whose composition is close to that of the slags used for the SHTT analyses. It can be observed that:

- (i) When adding  $\text{TiO}_2$  in a  $\text{CaO-SiO}_2$  slag (43.3 % $\text{CaO}$ , 56.7 % $\text{SiO}_2$ ), the viscosity decreases for all the range of temperatures, and
- (ii) Afterwards, when adding  $\text{Na}_2\text{O}$  in a  $\text{CaO-SiO}_2\text{-TiO}_2$  slag (36.4 % $\text{CaO}$ , 45.9 % $\text{SiO}_2$ , 17.7 % $\text{TiO}_2$ ) obtaining in this way a  $\text{CaO-SiO}_2\text{-TiO}_2\text{-Na}_2\text{O}$  slag (33.5 % $\text{CaO}$ , 41.9 % $\text{SiO}_2$ , 16.3 % $\text{TiO}_2$ , 8.2 % $\text{Na}_2\text{O}$ , 0.1 % $\text{Al}_2\text{O}_3$ ) the viscosity decreases more, for all the range of temperatures, and the slope of the curve becomes lower.

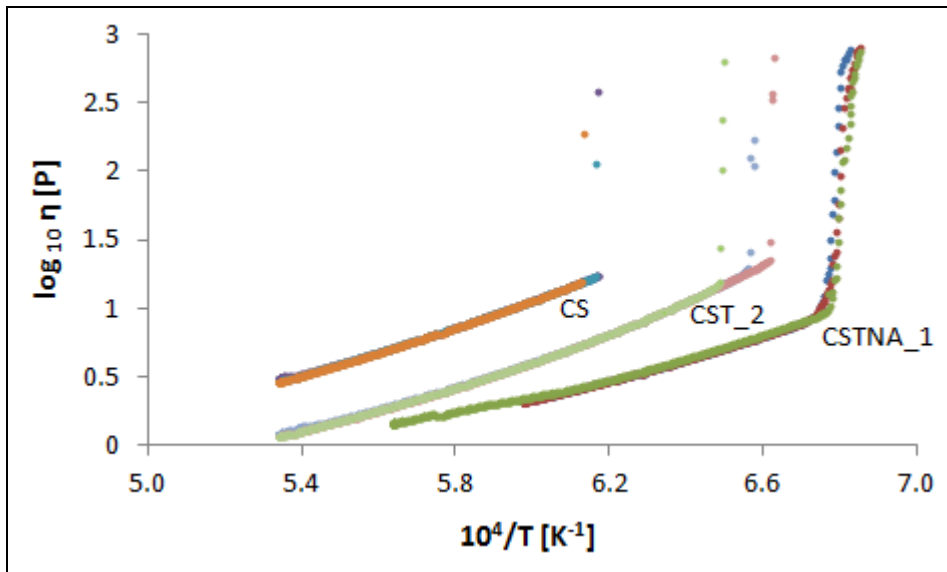


**Figure 39.** Viscosity measurements taken using a rotation viscometer (three measurements per composition). The compositions of the materials used for the viscosity measurements are close to that of the slags (CS, CST\_2, CSTNA\_1) used for the SHTT. CS - 43.3 %CaO, 56.7 %SiO<sub>2</sub>; CST\_2 - 36.4 %CaO, 45.9 %SiO<sub>2</sub>, 17.7 %TiO<sub>2</sub>; CSTNA\_1 - 33.5 %CaO, 41.9 %SiO<sub>2</sub>, 16.3 %TiO<sub>2</sub>, 8.2 %Na<sub>2</sub>O, 0.1 %Al<sub>2</sub>O<sub>3</sub>.

Samples were collected after viscosity measurements and analysed by X-ray fluorescence. In Table 9 the variation after viscosity measurements when comparing with the original composition.

**Table 9.** Variation after viscosity measurements when comparing with the original composition (wt%).

	%CaO	%SiO <sub>2</sub>	%TiO <sub>2</sub>	%Na <sub>2</sub> O	%Al <sub>2</sub> O <sub>3</sub>
CA	0.2				-0.2
CS	0.2	-0.2			
CST_2	0.2	-0.2	0.0		
CSTNA_1	0.0	0.4	0.0	-0.4	

Regarding the effect of TiO<sub>2</sub> on the silicate network, the Raman spectra of quenched silicotitanate melts indicate two monomer units (SiO<sub>4</sub><sup>4-</sup> and TiO<sub>4</sub><sup>4-</sup>), two types of chain units (Si<sub>2</sub>O<sub>6</sub><sup>4-</sup> and Ti<sub>2</sub>O<sub>6</sub><sup>4-</sup>), and two sheet units (Si<sub>2</sub>O<sub>5</sub><sup>2-</sup> and (Si,Ti)<sub>2</sub>O<sub>5</sub><sup>2-</sup>). The presence of discrete titanate complexes indicated by the Raman spectroscopic data suggests that the titanate complexes must compete with silicate complexes to coordinate metal cations. Hence, the addition of TiO<sub>2</sub> to basic silicate melts polymerizes a portion of the silicate network [53].

Because the Ti<sup>4+</sup> cation is larger than the Si<sup>4+</sup> cation, the Ti-O-Al and Ti-O-Ti bonds are expected to be weaker than Si-O-Al and Si-O-Si bonds. Therefore, the addition of TiO<sub>2</sub> to highly polymerized aluminosilicate melts will decrease their viscosity, although the overall NBO/T ratio decreases with increasing TiO<sub>2</sub> content of

the melt. This deduction from structural considerations is consistent with rheological data for TiO<sub>2</sub>-bearing aluminosilicate melts [53].

For sodium silicate glasses, the structure of silicate glasses and melts deduced from X-ray diffraction measurements is shown in Figure 40 in two dimensions, together with the structure of pure silica for comparison. The atom ratio O/Si is greater than 2; therefore, part of the oxygen atoms are bonded between two silicon atoms and part to only one silicon atom. There is a gradual breakdown of the silicate network with the addition of Na<sub>2</sub>O to molten silica [53, 54].

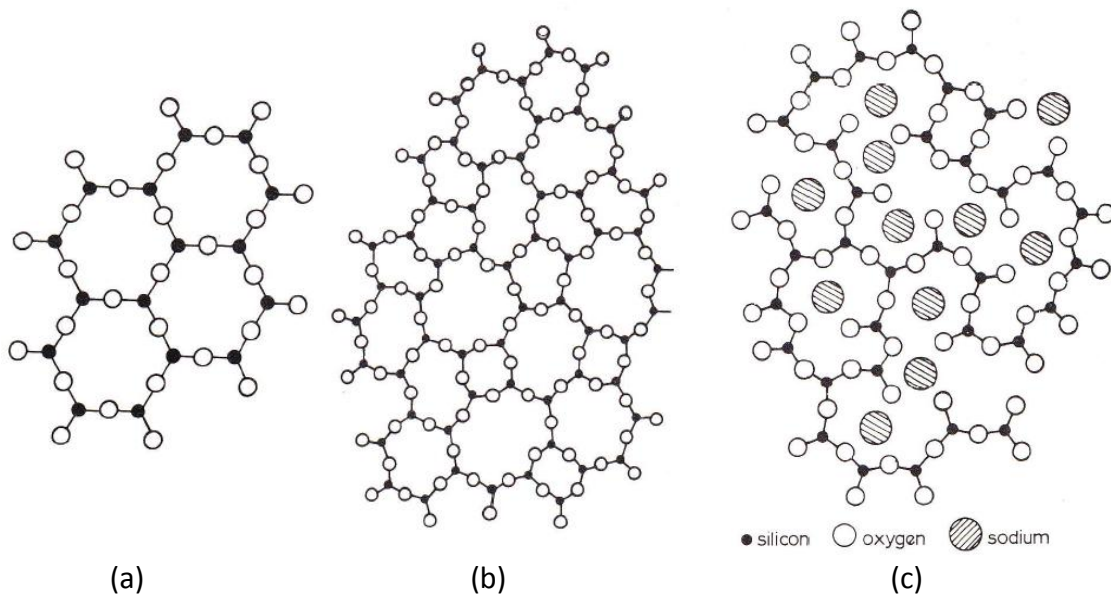


**Figure 40.** Schematic representation in two dimensions of: (a) the structure of silica in the crystalline state, (b) the structure of silica in the glassy state, and (c) the structure of sodium silicate glasses and melts [53, 54].

Industrial mould slags would be more complex than the CSTNA slags, since they have more components. Anyway, the present study can be used as a reference for future developments when designing fluorine-free mould powders for slab casting, where the control of crystallisation is imperative.

## 5.6 Thermodynamic calculations

For the slags of the present work thermodynamic simulations were performed with FactSage 6.1. The results are summarised below in Table 10.

**Table 10.** Calculations with FactSage 6.1 for the slags CST\_2 and CSTNA ( $pO_2 = 0.21$  atm).

$T$	%Na <sub>2</sub> O	0%	3.7%	5.4%	6.4%	7.1%
		CST_2	CSTNA_3	CSTNA_2	CSTNA_4	CSTNA_1
	<i>liquidus</i>	1366 °C	1320 °C	1311 °C	1409 °C	1399 °C
	1 <sup>st</sup> crystal	CaO.SiO <sub>2</sub>	CaO.SiO <sub>2</sub> .TiO <sub>2</sub>	CaO.TiO <sub>2</sub>	CaO.TiO <sub>2</sub>	CaO.TiO <sub>2</sub>
	2 <sup>nd</sup> crystal	CaO.SiO <sub>2</sub> .TiO <sub>2</sub> (1348 °C)	CaO.SiO <sub>2</sub> (1308 °C)	CaO.SiO <sub>2</sub> .TiO <sub>2</sub> (1309 °C)	CaO.SiO <sub>2</sub> (1256 °C)	CaO.SiO <sub>2</sub> (1269 °C)
	3 <sup>rd</sup> crystal	SiO <sub>2</sub> (1339 °C)	Na <sub>2</sub> Ca <sub>3</sub> Si <sub>6</sub> O <sub>16</sub> (1039 °C)	CaO.SiO <sub>2</sub> (1273 °C)	CaO.SiO <sub>2</sub> .TiO <sub>2</sub> (1165 °C)	CaO.SiO <sub>2</sub> .TiO <sub>2</sub> (1151 °C)

Table 10 shows that for CSTNA slags with lower Na<sub>2</sub>O contents (0.0% and 3.7%) the TiO<sub>2</sub>-bearing phase at high temperatures is only CaO.SiO<sub>2</sub>.TiO<sub>2</sub>. However, the higher the Na<sub>2</sub>O content is (5.4%, 6.4% and 7.1%), the easier the formation of CaO.TiO<sub>2</sub> instead of CaO.SiO<sub>2</sub>.TiO<sub>2</sub> becomes. At lower temperatures Na<sub>2</sub>O-bearing crystals (e.g., Na<sub>2</sub>Ca<sub>3</sub>Si<sub>6</sub>O<sub>16</sub>) could exist, according to the calculations.

There are few thermodynamic data in the literature for the system CaO-SiO<sub>2</sub>-TiO<sub>2</sub>-Na<sub>2</sub>O. Because of that, these calculated results are not accurate.

For a slag with composition similar to the CST\_2 (37.0% CaO, 47.2% SiO<sub>2</sub>, 15.8% TiO<sub>2</sub>), using XRD and EPMA, the following crystals were found: CaO.SiO<sub>2</sub>.TiO<sub>2</sub>, CaO.SiO<sub>2</sub> and SiO<sub>2</sub> [26]. These reported results agree with the thermodynamic simulations.

An important point is the variation of the slag chemical composition during the precipitation of solid phases. In the continuous casting process the viscosity of the liquid slag due to crystallisation can vary due to the precipitation of TiO<sub>2</sub>-bearing phases. The crystallisation of CaO.SiO<sub>2</sub>.TiO<sub>2</sub> and CaO.SiO<sub>2</sub> consume both CaO which is a basic oxide and SiO<sub>2</sub> which is an acidic oxide, thus in this way the viscosity of the remaining slag would not increase largely when comparing with the crystallisation of slags with CaO.TiO<sub>2</sub> precipitation. Thus, regarding the lubrication ability of the remaining slag the crystallisation of CaO.SiO<sub>2</sub>.TiO<sub>2</sub> would be preferred [26].

## 5.7 Critical cooling rates

### 5.7.1 Results

The critical cooling rate is the cooling rate required for complete glass formation, avoiding crystallisation. It can be calculated using the equation below [52]:

$$R_c = \Delta T / t_{nose} = (T_{liq} - T_{nose}) / t_{nose} \quad (14)$$

where  $R_c$  = critical cooling rate [°C/s],  $T_{liq}$  = *liquidus* temperature [°C],  $T_{nose}$  = nose temperature [°C], and  $t_{nose}$  = nose time [s]. The nose time is the shortest incubation time in the TTT diagram, and the corresponding temperature is called the nose temperature.

In Table 11, the critical cooling rates ( $R_c$ ) for the slags studied in the present work (Table 5) are shown. They were calculated by obtaining  $T_{nose}$  and  $t_{nose}$  from the TTT curves and calculating  $T_{liquidus}$  using FactSage 6.1.

For the slags CST\_2 and CSTNA, Table 11 shows that the higher the  $Na_2O$  content is, the higher  $R_c$  becomes. For these slags, the ratio  $\%CaO/\%SiO_2$  is in the range 0.6-0.8,  $\%TiO_2$  in the range 15.2%-18.1%, and  $\%Al_2O_3$  in the range 1.1%-5.2%.

**Table 11.** Critical cooling rates for the slags studied in the present work (compositions in Table 5).

	$R_c$ [ $^{\circ}C/s$ ]	$\%Na_2O$ (wt%)	$t_{nose}$ [s]	$T_{nose}$ [ $^{\circ}C$ ]	$T_{liquidus}$ [ $^{\circ}C$ ]	$T_{nose} / T_{liquidus}$
CS	7	0%	76	1000	1500	0.67
CST_2	6	0%	61	1020	1366	0.75
CSTNA_1	218	7.1%	2	963	1399	0.69
CSTNA_2	174	5.4%	2	963	1311	0.73
CSTNA_3	20	3.7%	19	950	1320	0.72
CSTNA_4	211	6.4%	2	988	1409	0.70

The influence of sodium on increasing critical cooling rate is clear; see Figure 41.

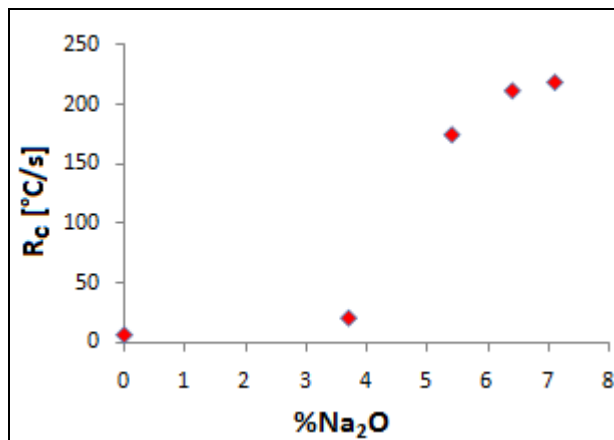


**Figure 41.** Effect of  $\%Na_2O$  on critical cooling rate, for the slags CST\_2 and CSTNA (compositions in Table 5).

### 5.7.2 Discussion

Direct crystallisation of mould slag during continuous casting will not occur when the cooling rate exceeds the critical cooling rate. In this situation, the mould slag will quench as a glass, followed by devitrification. In a thin-slab caster (Direct Sheet Plant), an estimate of the cooling rate of mould slag along the longitudinal (casting) direction is between approximately 35 and 40  $^{\circ}C/s$ . The local cooling rate, especially near the meniscus, will be considerably higher [2].

Because the cooling rates during continuous casting range from less than 1  $^{\circ}C/s$  to 100  $^{\circ}C/s$  [2, 43], it can be concluded that for  $Na_2O$ -bearing slags with higher sodium

content (CSTNA\_1, CSTNA\_2, CSTNA\_4) crystallisation during cooling cannot be avoided.

The ratio  $T_{\text{nose}} / T_{\text{liquidus}}$  is shown in Table 11. The temperature of the nose can be estimated as  $0.77T_{\text{liquidus}}$ , as suggested by Uhlmann and Yinnon (*apud* [55]). This approximation is helpful in classifying the relative ability of different compositions to form glassy phases, but it is not accurate enough to be quantitatively predictive [55].

## 5.8 Kinetics of crystal growth

### 5.8.1 Results

In the following, the kinetics of crystal growth for the CST\_2 and CSTNA\_1 slags (composition in Table 5) are analysed. The overall crystallisation can be described by determining the volume fraction of the transformed phase during isothermal transformation,  $\zeta(t)$ .

#### *CST\_2 slag*

For the CST\_2 slag, during the isothermal transformation at 1170 °C, images were obtained from video files. From these images (bitmap files), the area  $A$  of the crystallised fraction was measured using a software program. The particles were treated as spheres. The volume  $V$  is

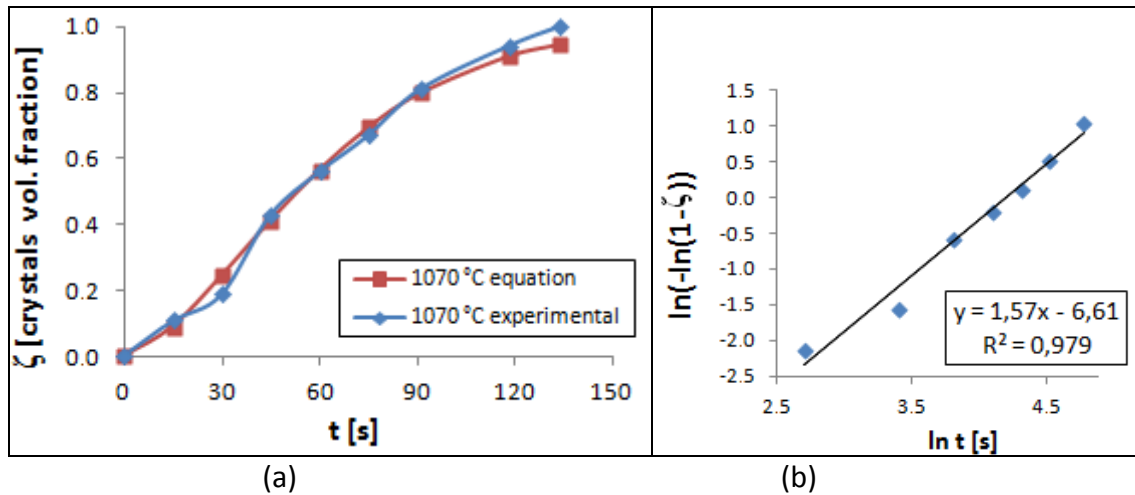
$$V = \frac{4\pi}{3} \left( \frac{A}{\pi} \right)^{\frac{3}{2}} \quad (15)$$

and it is denoted in Figure 42a as “1070 °C experimental”. Using equation (13), the parameters  $n$  and  $K$  can be obtained:  $n = 1.57$  and  $K = 0.00135$ , and the Avrami equation is

$$\zeta(t) = 1 - \exp(-0.00135t^{1.57}) \quad (16)$$

which is plotted in Figure 42a as “1070 °C equation”. The typical S-shape can be observed.

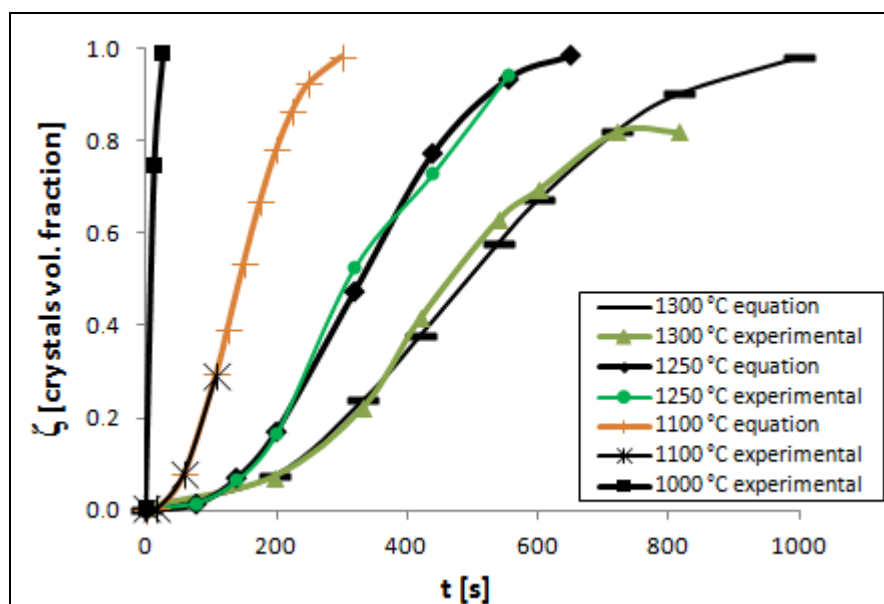




**Figure 42.** (a) Crystal volume fraction ( $\zeta$ ) versus time for the isothermal transformation at 1070 °C for the slag CST\_2; (b) determination of the parameters  $n$  and  $K$  of the Avrami equation for the slag CST\_2 at 1070 °C.

#### CSTNA\_1 slag

For the slag CSTNA\_1, during isothermal transformation at different temperatures, the same aforementioned procedure was applied. The results are summarised in Figure 43. The characteristic S-shape can be observed.



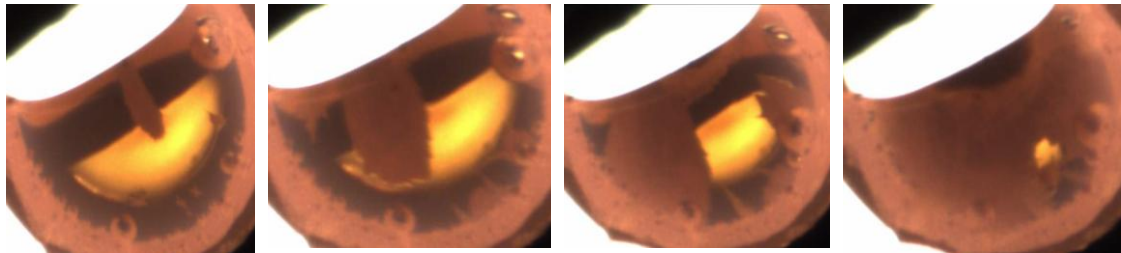
**Figure 43.** Crystals volume fraction versus time for the isothermal transformation at different temperatures, for the slag CSTNA\_1.

Table 12 shows the parameters  $n$  and  $K$  of the Avrami equations for the slag CSTNA\_1, related to Figure 43.

**Table 12.** Parameters  $n$  and  $K$  of the Avrami equations for the slag CSTNA\_1.

	$n$	$K$
1300 °C	2.38	2.71E-7
1250 °C	2.63	1.68E-7
1100 °C	2.36	5.18E-6

Figure 44 shows images of an isothermal transformation at 1250 °C, for the slag CSTNA\_1.



**Figure 44.** Isothermal transformation for the slag CSTNA\_1 at 1250 °C observed during an experiment using the Single Hot Thermocouple Technique.

### 5.8.2 Discussion

The JMAK theory was developed in the late 1930s by Kolmogorov, Johnson and Mehl, and Avrami, for overall crystallisation kinetics under isothermal conditions. It is used to study the mechanisms of phase transformation in metals. More recently, the JMAK theory has been employed by polymer and glass scientists studying, for example, glass-ceramic materials [38, 39, 41] and the kinetics of crystal growth for mould powders and slags using the Single Hot Thermocouple Technique [5, 56-58].

The assumptions of the JMAK theory are [39, 41, 49, 59, 60]:

(i) Nucleation is random, i.e., the probability of forming a nucleus in unit time is the same for all infinitesimal volume elements of the assembly.

(ii) Nucleation occurs from a certain number of embryos, which are gradually exhausted. The number of embryos decreases in two ways: by growing to critical sizes (becoming critical nuclei) and by absorption by the growing phase.

(iii) The growth rate is constant, until the growing regions impinge on each other and growth ceases at the common interface, although it continues normally elsewhere.

Table 13 shows values of  $n$  for different transformation mechanisms, for the Avrami equation (equation 3). If spherical particles grow in the internal volume of the sample, then  $n$  should vary from 1.5 to 4. If growth proceeds from the external surfaces towards the centre (columnar shape) then  $n$  would be different [39]. Thus, for CST\_2 ( $n=1.6$ ), according to Table 13, the parameter  $n$  would be related to diffusion-controlled growth, decreasing  $I$  (nucleation rate per unit volume) and for CSTNA\_1 ( $n$  approx. 2.5) the parameter would be related to diffusion-controlled growth, constant  $I$ . For CSTNA\_1 the value of  $n$  is independent of temperature.

**Table 13.** Avrami parameters,  $n$ , for several mechanisms (spherical growth) [39].

	Interface-controlled growth	Diffusion-controlled growth
Constant $I$	4	2.5
Decreasing $I$	3-4	1.5-2.5
Constant number of sites	3	1.5

However, the CST\_2 slag presents complex crystallisation behaviour, i.e., more than one crystal phase, with different morphologies that seem to be a combination of bulk and surface crystallisation. In this case, the physical meaning of the values of  $n$  and  $K$  of the Avrami equation obtained from numerical fitting is unknown<sup>1</sup>. Thus, it is not possible to obtain information regarding the transformation mechanism, which makes it unclear whether the crystal growth is controlled by the interface or by diffusion. For the CSTNA slags, similar ambiguities arise.

The complex crystallisation behaviour of the system CaO-SiO<sub>2</sub>-TiO<sub>2</sub> was demonstrated [26]. It was reported that phase separation is a common phenomenon in CaO.SiO<sub>2</sub>.TiO<sub>2</sub> glasses because TiO<sub>2</sub> induces liquid-liquid immiscibility. Moreover, considering the fact that normally crystalline phases growing in viscous liquids are spherulitic, i.e., only partially crystalline, in such cases the “crystallinity” values depend on the experimental technique employed. In this way, the values can be different when comparing optical microscopy and X-ray diffraction; this fact was reported for a BaO.2SiO<sub>2</sub> glass [61].

The JMAK theory can be shown to be exact within the framework of its assumptions. Any violation must be a result of applying it to situations in which its assumptions are violated, which may be the case in many crystallisation situations [39].

Experimental values of crystallinity for a BaO.2SiO<sub>2</sub> glass were compared with those predicted by the JMAK theory, using the equation for homogeneous nucleation – equation (12) –, which is the special case when the number of embryos is not exhausted until the end of the transformation [61]. The attempt was not successful due to the complex crystallisation behaviour of this system: spherulitic growth with large induction time.

Experimental tests were reported for the Na<sub>2</sub>O.2CaO.3SiO<sub>2</sub> (NC<sub>2</sub>S<sub>3</sub>) glass, which presents homogeneous nucleation, testing the validity of the JMAK theory [62]. The isothermal crystallisation of a nearly stoichiometric Na<sub>2</sub>O.2CaO.3SiO<sub>2</sub> glass was studied at 627 °C and 629 °C by optical microscopy, density measurements and X-ray diffraction. Both nucleation and growth rates were measured by single- and double-stage heat treatments up to very high volume fractions transformed and the

<sup>1</sup> Zanotto, E.D., *Personal communication*. 2011: Vitreous Materials Laboratory, Universidade Federal de São Carlos, São Carlos, Brazil.

experimental data for crystallinity were compared with the calculated values at the two temperatures. The early crystallisation stages were well described by theory for the limiting case of homogeneous nucleation and interface-controlled growth. For higher degrees of crystallinity, both growth and overall crystallisation decreased due to compositional changes of the glassy matrix, and the experimental kinetics could be described by theory if diffusion-controlled growth was assumed. It was demonstrated that it is required extra, detailed knowledge on the transformation mechanism to apply the JMAK theory, describing the transformation kinetics.

The  $\text{NC}_2\text{S}_3$  glass composition was chosen because it presents a measurable rate of internal (homogeneous) nucleation of spherical grains – single crystals – which apparently grow with constant velocity. Therefore, complicating features such as transient nucleation and growth, metastable phase formation, large compositional changes upon crystallisation, non-spherical or spherulitic growth and combined bulk and surface crystallisation were absent. However, even when using the  $\text{NC}_2\text{S}_3$  glass composition, the apparent value of  $n$  changes during transformation. The early stages ( $\zeta < 0.15$ ) are well described by simultaneous homogeneous nucleation and interface-controlled (constant) growth, with  $n = 4$  in the Avrami equation. The latter stages are better described by diffusion-controlled growth, with  $n = 2.5$  in the Avrami equation.

It was shown that the sole use of numerical fittings to analyse phase-transformation kinetics through the experimental values of  $n$ , as is very often reported in the literature, can provide misleading interpretations of the transformation mechanism. The JMAK theory describes well the transformation kinetics only if extra, detailed knowledge on the transformation mechanism is available. Because commercial materials are not perfectly stoichiometric and generally there are compositional differences between parent and new phase, the Avrami parameter  $n$  obtained from the sole use of numerical fits represents an average and can provide misleading interpretations for the phase transformation mechanism [62].

In summary, it can be concluded for the CST\_2 and CSTNA\_1 slags that the Avrami equation can represent the overall crystallisation kinetics. The typical S-shape is observed. However, it is not possible to obtain information regarding the transformation mechanism for the analysed slags, due to their complex crystallisation behaviour. The physical meaning of the values of  $n$  and  $K$  obtained from numerical fitting is unknown.

### 5.9 Relation between basicity index and crystallisation tendency

The basicity index Bi is given by the equation below [63]:

$$Bi = (1.53\%CaO + 1.51\%MgO + 1.94\%Na_2O + 3.55\%Li_2O + 1.53\%CaF_2) / (1.48\%SiO_2 + 0.10\%Al_2O_3)$$

(17)

It was reported that there is a good relation between Bi and alumina inclusions absorption rate for mould slags [63].

In Figure 45 it can be observed the relationship between the basicity index Bi and the incubation times measured in the present work for these slags.

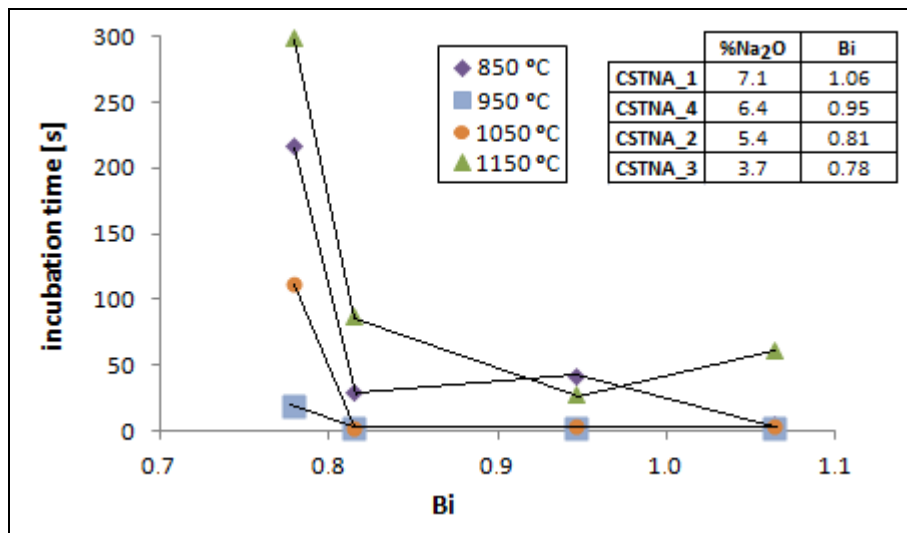


**Figure 45.** Relationship between the basicity index Bi and the incubation times measured in the present work, for four slags.

At each temperature different conditions for crystallisation exist, which can be related to thermodynamics (supercooling) and to kinetics (diffusion, viscosity of the liquid slag). It is interesting to note that even to different temperatures, above and below the noses of the TTT curves for the four slags, the relationship between Bi and incubation times is clear: the higher the Bi, the lower the incubation times. Besides, the higher the Na<sub>2</sub>O content, the higher the Bi.

In a work from literature DTA analysis was performed for different mould powders, determining the energy of activation for crystallisation ( $E_a$ ) [64]. According to the authors of this work the tendency of a mould powder to precipitate a crystalline phase depends on its  $E_a$  value, which relates physically to the viscosity and Bi [63] of the material. Relationships among  $E_a$ , Bi and mould slags' viscosity were found. High Bi resulted in facile crystallisation and low values for  $E_a$ . Besides, it was found that the lower the viscosity the lower the  $E_a$ .

### 5.10 Solidification behaviour of fluorine-free mould powders for billet casting

The choice of the mould powder for billet casting is very important in the achievement of a successful casting practice. Since the powder consumption demands for billet casting are not stringent, steelmakers frequently use high viscosity mould powders to overcome problems such as slag entrapment and SEN (Submerged Entry Nozzle) erosion [1, 65].

Commercial mould powders contain fluorine, typically as calcium fluoride ( $\text{CaF}_2$ ). Considering environmental and health questions, fluorine is undesirable because it creates problems for storage and utilisation of solid waste, and because it evolves easily from slags, producing health-injurious gaseous substances, such as hydrofluoric acid [12, 20-22, 25].

The hydrofluoric acid, which is generated during continuous casting process from mould powder, increases dramatically the corrosion rate especially below the mould where there is a high amount of water accelerating the corrosion process [12, 20-22, 25].

Fluorine can be substituted for  $\text{Na}_2\text{O}$  and/or  $\text{B}_2\text{O}_3$  in mould powders for billet casting. Regarding  $\text{Na}_2\text{O}$ -bearing raw materials, they are interesting to substitute fluorspar because  $\text{Na}_2\text{O}$  decreases viscosity, *liquidus* temperature and it also promotes inclusions absorption. It is theoretically possible to increase  $\text{Na}_2\text{O}$  content up to 20%; above this content the solid phase nefeline ( $\text{Na}_2\text{O} \cdot \text{Al}_2\text{O}_3 \cdot 2\text{SiO}_2$ ) precipitates. Frequently  $\text{Na}_2\text{O}$  content in industrial mould powders is high (>10%) [20, 25, 66].

A new F-free mould powder for billet casting was developed. During utilisation of a F-free mould powder at steelworks some benefits are expected: (i) benefits related to environmental and health questions, (ii) reduction of corrosion rate at the continuous casting machine, and (iii) reduction of SEN erosion.

Laboratory tests were performed in Stollberg do Brasil, using some Brazilian raw materials with fluxing ability, with new fluorine-free recipes [67]. From these laboratory tests the new mould powder Accutherm ST-SP/512SV-DS-1 (herein referred to as "F-free") was produced as granulated mould powder to replace the commercial Accutherm ST-SP/512SV-DS (herein referred to as "F-bearing"), which is produced by Stollberg Group and used at steelworks for billet casting. The laboratory tests and industrial tests results when using the new F-free mould powder are reported in the following.

#### 5.10.1 Laboratory tests

##### *Chemical composition*

The compositions of the F-bearing and F-free mould powders, determined through X-ray fluorescence, are shown in Table 14.

**Table 14.** Compositions and parameters for the F-bearing and F-free mould powders.

Mould powder	F-bearing	F-free
Basicity (V-ratio)	0.70	0.70
Bi – equation (17)	1.01	1.03
SiO <sub>2</sub> (wt%)	35.70	38.00
CaO (wt%)	24.98	26.50
MgO (wt%)	2.95	2.64
Al <sub>2</sub> O <sub>3</sub> (wt%)	12.07	7.82
TiO <sub>2</sub> (wt%)	0.47	0.29
Fe <sub>2</sub> O <sub>3</sub> (wt%)	2.61	2.22
MnO <sub>2</sub> (wt%)	0.09	0.12
Na <sub>2</sub> O (wt%)	4.11	7.28
K <sub>2</sub> O (wt%)	1.60	1.03
F (wt%)	4.20	0
B <sub>2</sub> O <sub>3</sub> (wt%)	0	0
Li <sub>2</sub> O (wt%)	0	0
C <sub>free</sub> (wt%)	6.02	6.05
CO <sub>2</sub> (wt%)	3.83	4.43
T <sub>melting</sub> [°C]	1188	1166
T <sub>flowing</sub> [°C]	1199	1172
Viscosity (1300 °C, IRSID) [P]	19.9	20.8

The basicity determines the rate of alumina inclusion absorption; it can be stated as either the V-ratio (%CaO/%SiO<sub>2</sub>) or a more complex term as Bi. It was reported that the alumina absorption rate ( $\text{g cm}^{-2} \text{s}^{-1}$ ) correlates well with the basicity index Bi [17, 63], according to the equation (17).

#### *Melting characteristics*

For the evaluation of melting characteristics it was used a heating microscope, increasing the temperature at 10 °C/min, obtaining the characteristic temperatures. The working method refers to the German standard DIN 51730 [68]. Regarding repeatability limit (same operator and same apparatus) results shall be considered acceptable if the characteristic temperatures do not differ by more than 30 °C. Regarding reproducibility limit (different operators or different apparatus) results shall be considered acceptable if the characteristic temperatures do not differ by more than 50 °C.

The results are in Table 14; each value is the average of two measurements. The F-free mould powder has similar characteristic temperatures.

As these measurements are carried out on powders during the heating cycle, they apply to the conditions in the upper mould, *i.e.*, the formation of the liquid slag pool but not to formation of the slag films in the mould/strand channels [1].

### Viscosity

The viscosity of the mould powders was calculated through the IRSID model for the F-bearing and for the F-free at 1300 °C: 19.9 P and 20.8 P respectively.

Then viscosity measurements were performed using a rotation viscometer at the Technische Universität Bergakademie Freiberg, for three samples extracted from the lot which was sent to the steelworks to execute the industrial test. The results for the F-free mould powder are shown in Figure 46. The viscosity at 1300 °C is 16.8 P (average of the three experiments), similar to the specification of the F-bearing (19.9 P). No break temperature ( $T_{br}$ ) was observed.

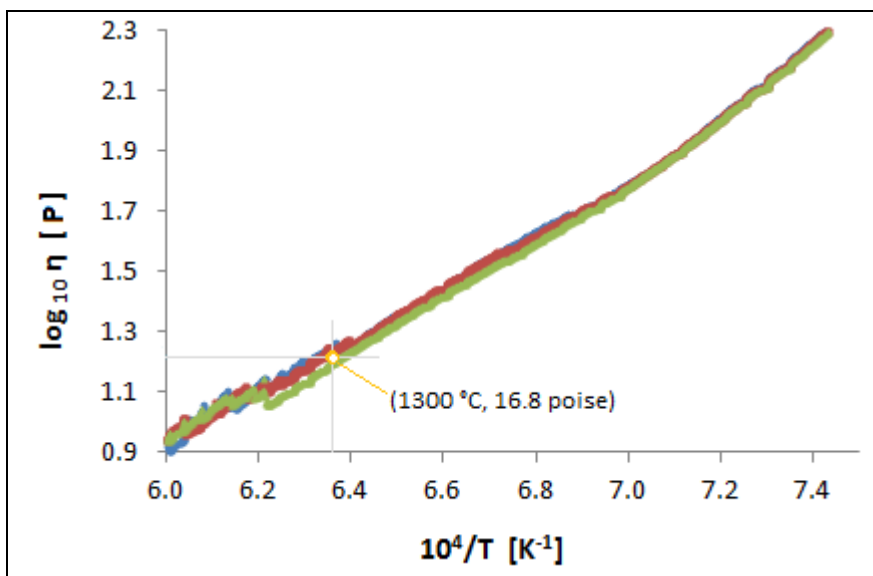


**Figure 46.** Viscosity measurements taken using a rotation viscometer for the F-free mould powder using three different samples.

Most conventional mould slags show a marked increase in viscosity when crystalline solids are formed at  $T_{br}$  on cooling. However, high viscosity slags form super-cooled liquids on cooling which persist down to their glass transition temperatures. A super-cooled liquid would move with the strand despite of having a high viscosity value [6].

Mould powder main function is the creation of a lubricant film at mould/strand interface. It is essential that the mould be lubricated throughout. Failure to do so could lead to a variety of problems, including sticker breakouts [1]. In terms of chemical composition, silica and alumina are the major constituents that determine mould slag viscosity. In addition to these oxides other components of mould slags – the so called network modifiers – such as  $\text{CaF}_2$ ,  $\text{Na}_2\text{O}$ ,  $\text{K}_2\text{O}$ ,  $\text{CaO}$ ,  $\text{MgO}$  lower the viscosity [18].

Additionally, the test herein referred to as Ramp Test was performed to evaluate fluidity, comparing the F-free and the F-bearing. In this test 0.5 grams of sample is placed inside an  $\text{Al}_2\text{O}_3$  boat with a fixed slope (15 °). The inclined boat with the sample on its higher part is heated in a furnace for 1-3 minutes at 1280 °C. The



molten slag flows down the boat. The length of the slag ribbon (molten mould powder) along the vessel is measured; it can be observed in Figure 47 that the length for all slag ribbons is similar.

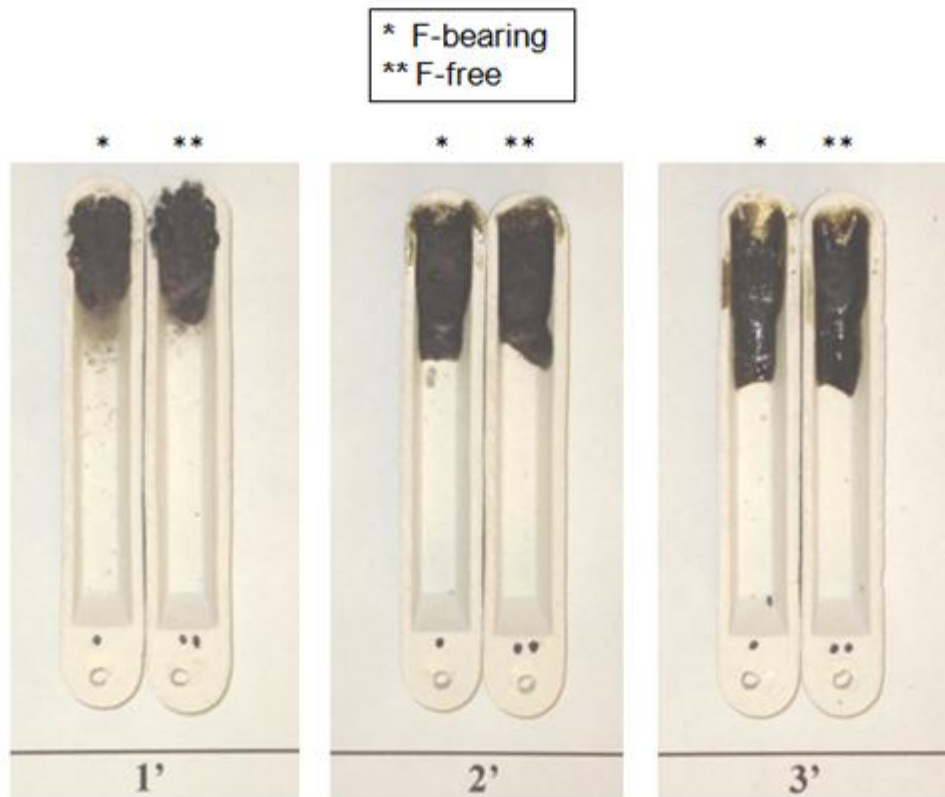


**Figure 47.** Ramp Test results at 1280 °C; 1, 2 and 3 minutes.

### *Melting behaviour*

Two kinds of tests were used to evaluate the melting behaviour, herein referred to as Boat Test and Box Test.

#### Boat Test

Different methods have been developed for obtaining melting rates. In combustion boat tests a known mass of powder is poured into an open sided porcelain combustion boat and then placed in a furnace at a known temperature; the time for the sample to melt provides an inverse ratio of the melting rate [1]. In the present work one gram of sample is placed inside an  $\text{Al}_2\text{O}_3$  boat and left in a temperature higher than *liquidus* for different periods up to complete fusion. Afterwards, the boats are examined for comparative purposes. This inspection is made visually.

The Boat Test was applied to F-bearing and F-free mould powders at different periods between 1 and 3 minutes, at 1280 °C. It can be observed in Figure 48 that both recipes show similar melting rates, since a vitreous aspect is observed in a gradual and similar way.

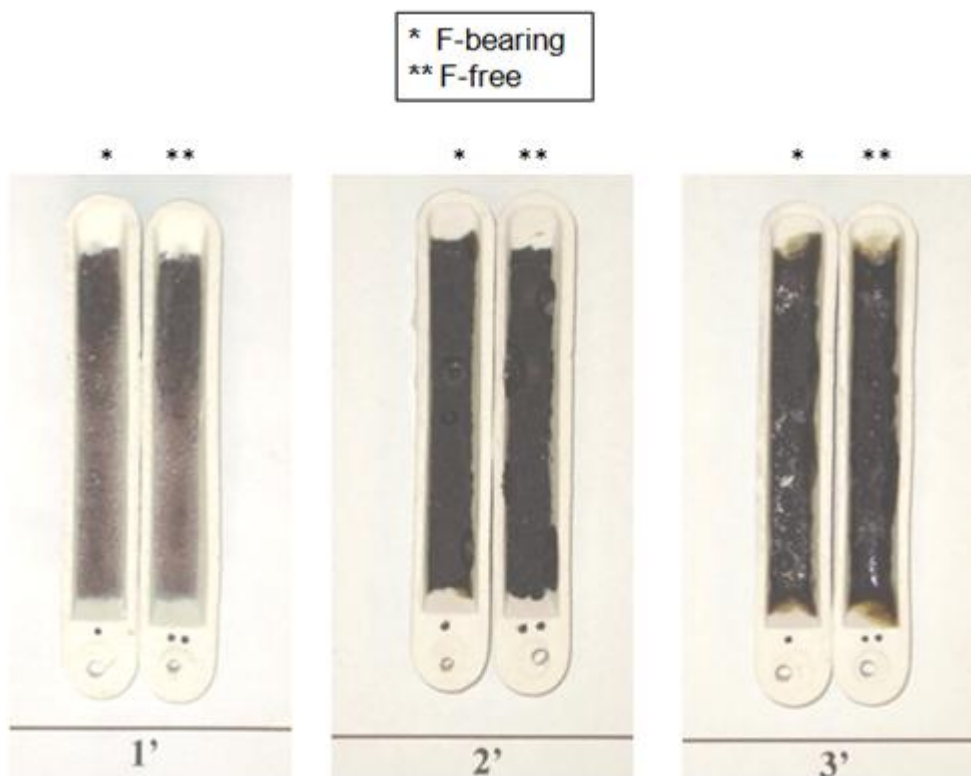


**Figure 48.** Boat Test results at 1280 °C - 1, 2 and 3 minutes.

The mould powder should melt at a rate that is compatible with the demand for liquid slag. The melting rate is controlled by several factors, such as [1]: (i) free carbon content of the mould powder, (ii) type and particle size of carbon, (iii) carbonate content of the mould powder, (iv) vertical heat flux, that is affected by various casting parameters such as casting speed, superheat, turbulence, *etc.*

Carbon type was the same for both recipes, with same particle size. Free carbon content and carbonate content are indicated in Table 14. Carbon particles separate the mineral particles and slow down the agglomeration of the molten slag globules. Thus, the more carbon is present, the more time is required to agglomerate and the slower the melting rate. For a given carbon content, the finer the carbon particles, the greater the separation of the partially molten particles, and hence the slower the melting rate [1].

Riboud and Larrecq have determined the melting rate of several mould powders and confirmed that the free carbon content of the mould powder has a profound influence on the rate of fusion. Moreover, their results showed that mould powders with similar overall chemical composition could have different rates of fusion; this fact led to the conclusion that the mineralogical nature of the mould powder constituents influences the melting rate [69]. In the present work different raw materials (different mineralogical natures) were used for the production of the mould powders.

### Box Test

Another test to investigate the melting performance of mould powders is the Box Test. It is based on visual inspection and the experience of the investigator. It is useful in giving additional information on melting behaviour. For this test, a deep-drawn metal pan is loaded with 50 grams of mould powder, and the containers are heated in a furnace at 1300 °C for different times. Then, the sintered and molten samples are visually inspected. In particular mould slag droplets and the presence of sintered layers and crusts indicate the melting properties of the mould powder. Figure 49 shows Box Test results for the mould powders F-bearing and F-free.

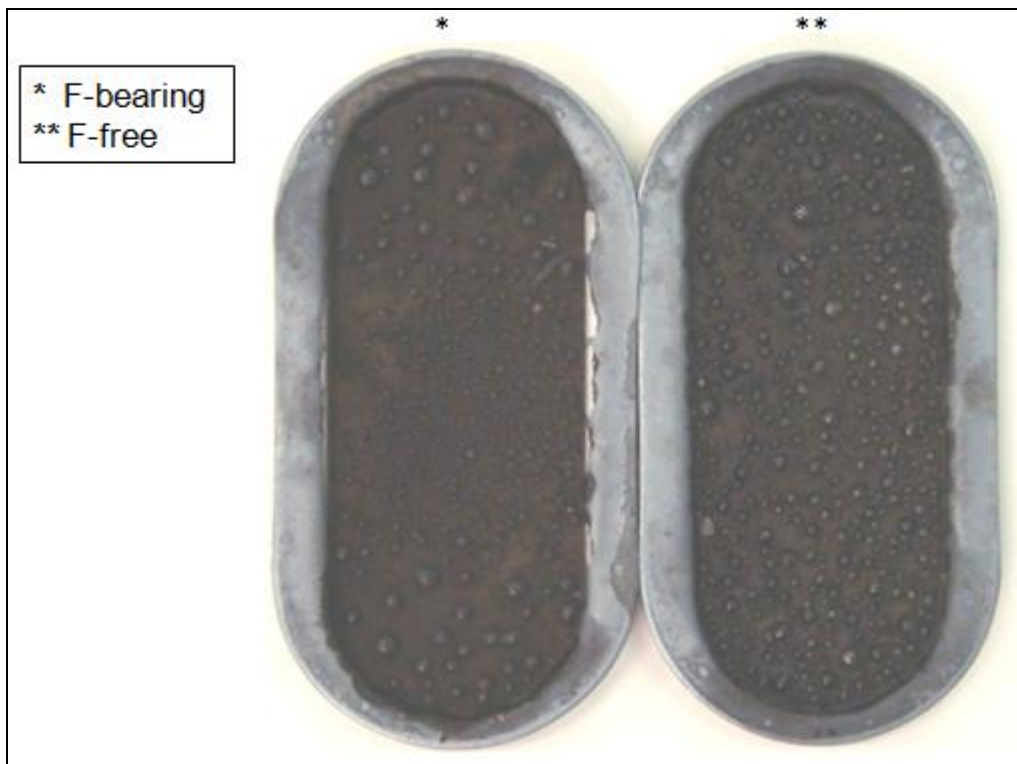


**Figure 49.** Box Test results at 1300 °C for 5 minutes.

### *Crystallinity analysis*

#### Test 1

Two kinds of crystallinity analysis were performed; the first one is described in the following (Test 1). Decarburized sample was placed in a platinum crucible and heated at 1300 °C for 20 minutes. The mould powder was then poured into a platinum mould at 950 °C and maintained at this temperature for 20 minutes for annealing. The samples were cut and the area of the crystalline fraction (%crystallinity) was determined using an optical microscope and a software program.

In Figure 50 it can be observed some crystallisation for the mould powders, for annealing at 950 °C for 20 minutes, after heating at 1300 °C for 20 minutes. The test was also repeated for annealing at 600 °C.

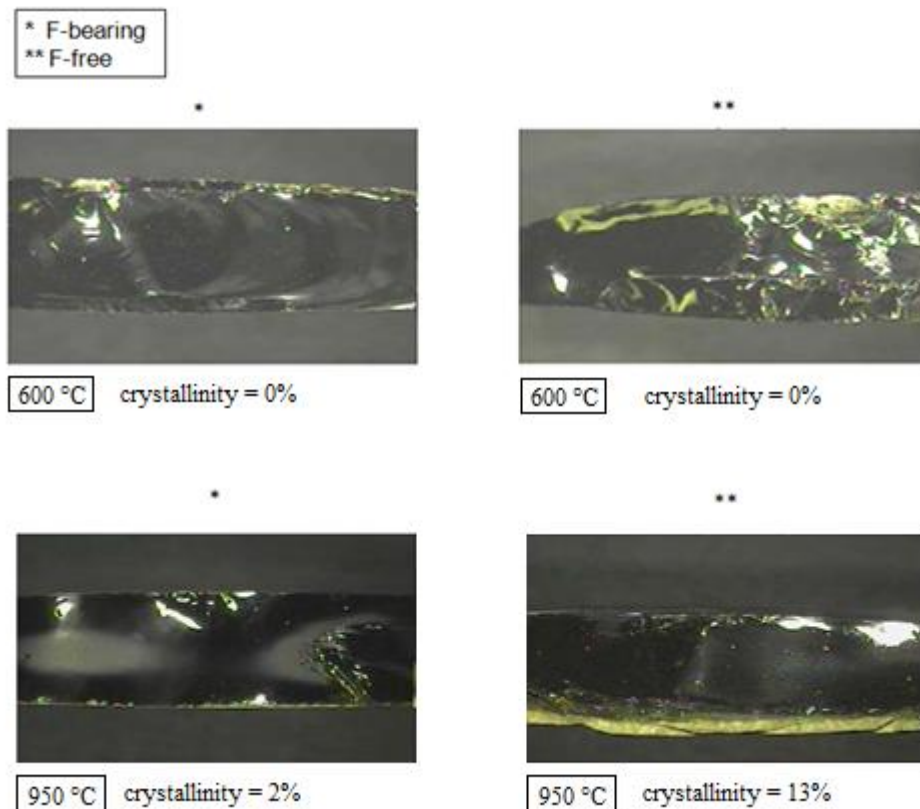


**Figure 50.** Test 1 (crystallinity analysis) results. At 600 °C both recipes (F-bearing and F-free) are 100% glassy. At 950 °C there are some crystals (layer at the bottom of the figures, which is the interface between mould and slag).

Original value of the image magnification which was got through the optical microscope is 20x. A yellow crystalline layer can be observed at the bottom of the figures (slag/mould interface). The pockets of crystals throughout the bead were also included in the %crystallinity determination. The samples were not etched. Thus, the %crystallinity for both recipes are close to each other.

From literature [70] it is known that  $\text{SiO}_2$ -rich slags can be cooled easily to form glasses in the temperature range where they should crystallize under equilibrium conditions. On the other hand, basic slags rich in CaO are difficult to quench as glasses. Most mould powders lie between these two extremes. The recipes of the present work are silica-rich slags *i.e.* vitreous phase is easily formed even at low cooling rates.

Li, Thackray and Mills [15] discussed a test to predict %crystallinity found in slag films formed between the steel strand and the mould. According to them, it should be noted that the slag film may be present in the mould/strand gap for a considerable time; thus, some of the crystallisation developed in the slag film may develop as a consequence of annealing in a temperature gradient: the hot face of the

slag film (against steel shell) will be between the steel *liquidus* and 1150 °C, but there has been some dispute concerning the temperature of the slag film on the mould side ranging from 300 °C lower down to the mould to above 600 °C although the temperature in the hot face of a copper plate slab mould is estimated between 260 °C and 110 °C. They recommended a holding time of 20 minutes at 610 °C in stainless steel crucible (after decarburisation and heating at 1300 °C for 20 minutes) to match with the %crystallinity found in slag films taken from the mould. In the present work the annealing temperature was higher (950 °C) since the recipes present low tendency to crystallize.

The crystalline fraction got from the F-free mould powder sample was milled and analysed by X-ray diffraction. The main phase is gehlenite ( $\text{Ca}_2\text{Al}_2\text{SiO}_7$ ); Figure 51.

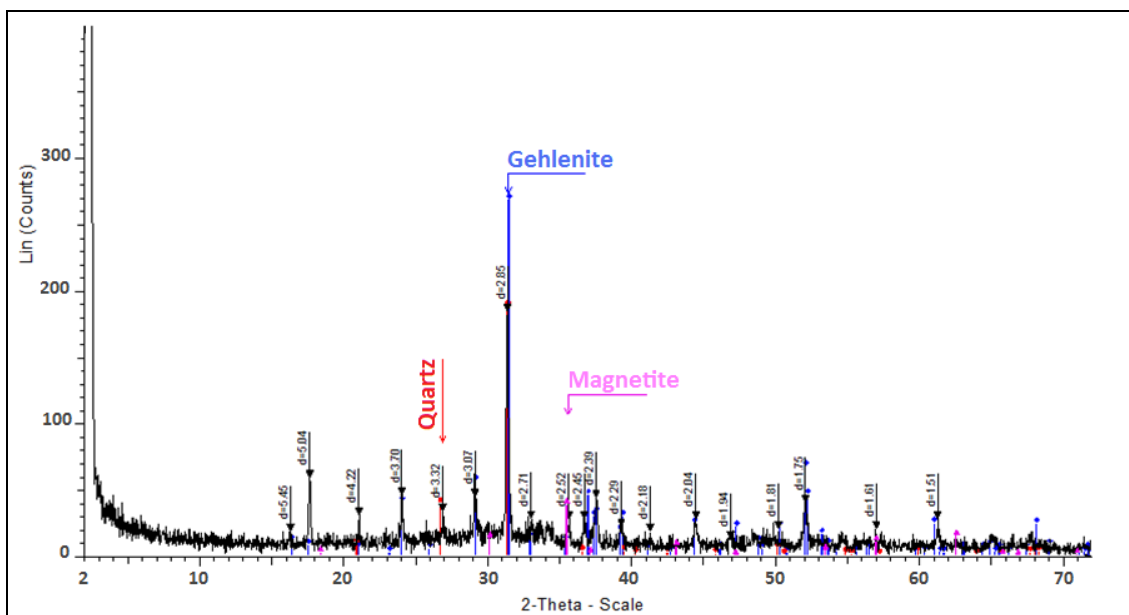


**Figure 51.** XRD analysis for the F-free sample after annealing at 950 °C for 20 minutes, according to Test 1 (crystalline part got from the F-free sample shown in Figure 50).

For industrial F-bearing mould powders for slab casting typically the main crystalline phase that is found when solid slag films are collected from the mould at the end of casting sequences is cuspidine ( $3\text{CaO}\cdot 2\text{SiO}_2\cdot \text{CaF}_2$ ). The films have a crystalline structure that either formed during cooling or via devitrification, i.e., crystallisation from the glassy state [2, 3].

In a work that was performed during slab casting [8] industrial slag samples were collected from mould. It was reported that depending on the composition different phases can exist, altering the registered friction force measured at the mould and the viscosity of the liquid slag. The phase gehlenite was detected in this study, and it was considered to be the phase which causes minimization of the friction force for the reported conditions. Besides gehlenite it was also detected cuspidine (typical in F-bearing industrial mould powders), combeite, nepheline and wollastonite. Thus, it was reported that in the gap between mould and strand the global friction force is not only

given by viscosity and thickness of the liquid slag layer, but also by the nature and proportion of the different mineralogical phases which can exist in the mould powders after solidification.

#### Crystallinity analysis - Test 2 (SHTT)

The second test related to the crystallisation behaviour – herein referred to as Test 2 – was in situ observation using the Single Hot Thermocouple Technique (SHTT), performed at the Technische Universität Bergakademie Freiberg. The crystallinity fraction at 950 °C was measured with images obtained from recorded video files. From these images (bitmap files), the area of the crystalline fraction (%crystallinity) was measured using a software program.

The thermal cycle used for the experiments was: a heating rate of 1000 °C/min up to 1600 °C; 60 seconds holding time at 1600 °C; and then quenching (> 3000 °C/min) down to 950 °C. Then, 20 min at 950 °C.

The results for the Test 2 are in Table 15, considering the average of three experiments per slag. Table 15 also shows results for Test 1.

**Table 15.** Crystallinity analysis results for Test 1 and Test 2 (SHTT).

	<b>Test 1</b> <b>[%crystallinity]</b>	<b>Test 2 (SHTT)</b> <b>[%crystallinity]</b>
<b>F-bearing</b>	2	7
<b>F-free</b>	13	24

Some results are shown in Figure 52 (besides, periods longer than 20 min are shown). With the evolution of the crystallisation the clear region of the samples (molten slag) become dark (crystals).

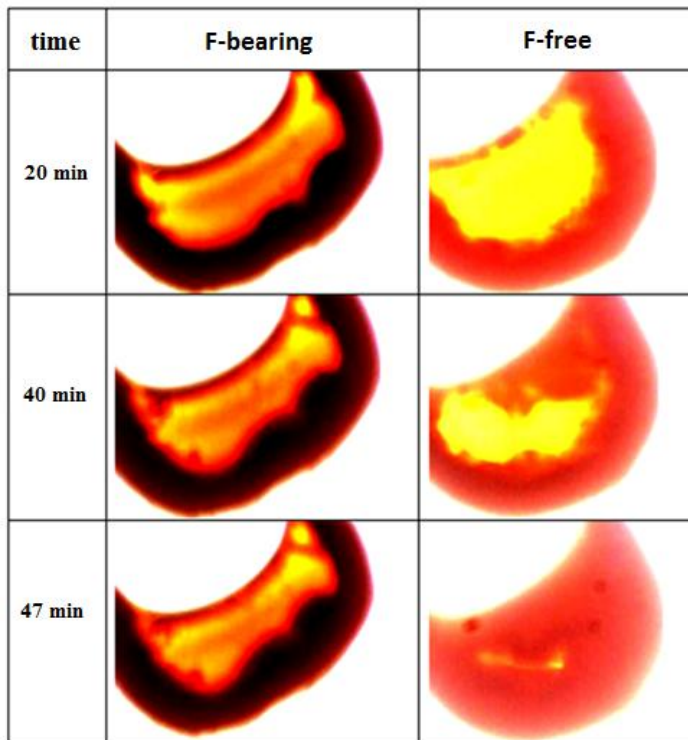


**Figure 52.** Some results for the Test 2 (in situ observation using the SHTT). With the evolution of the crystallisation the clear region of the samples (molten slag) become dark (crystals).

Crystallinity tests showed that both slags have low tendency to crystallisation, and that the F-free mould powder has a slightly higher crystallisation tendency. It seems that crystallisation of mould slag is not a so important parameter for these mould powders for billet casting. This was showed by the crystallinity tests, and also during the viscosity measurements because no break temperature ( $T_{br}$ ) was found. The main requirement is strand lubrication.

### 5.10.2 Industrial tests

From the aforementioned laboratory tests it was concluded that the F-free mould powder could be tested at steelworks, since its technological parameters are similar to the standard mould powder. Industrial tests were performed at a Brazilian steelworks with this new F-free mould powder, during continuous casting of billets (155x155 mm).

The compositions of the steels and the particular operational parameters which were used during the trials are in Table 16 and Table 17 respectively.

**Table 16.** Compositions of the steels used for the industrial tests (wt%).

	C	Si	Mn	P	S	Cr	Mo	Ni	Al sol
<b>Steel A</b>	0.39	0.24	0.78	0.02	0.02	0.93	0.17	0.08	0.010
<b>Steel B</b>	0.15	0.23	1.14	0.02	0.02	0.94	0.05	0.10	0.000
<b>Steel C</b>	0.53	0.27	0.74	0.02	0.02	0.16	0.03	0.07	0.023

**Table 17.** Operational parameters during the industrial trials.

	casting speed [m/min]	mould oscillation [cpm]	liquidus [°C]	superheating [°C]
<b>Steel A</b>	1.87	192	1486	45
<b>Steel B</b>	1.93-2.03	201-203	1512	53
<b>Steel C</b>	1.96-2.03	210	1485	45

Some evaluations performed during the trials for the steels A (one heat), B (two heats) and C (six heats) are reported in Table 18, comparing both mould powders, which were used simultaneously at different strands. Each heat lasted about one hour.

$\Delta T$ (°C) is the difference between the water inlet temperature and the water outlet temperature. The water flow in the mould is 1850-1860 L/min.

The slag pool thickness is related to mould powder consumption. Failure to maintain it can lead to lack of lubrication and ultimately to surface defects or sticker breakouts. The depth of the slag pool influences on the amount of liquid slag infiltrating into the mould/strand gap and the number of inclusions transferred from the steel to the slag [71]. The thickness measurements were performed by the three-wire method.

The billet temperature is measured before the straightener by means of a pyrometer.

**Table 18.** Evaluations during the industrial tests.

		$\Delta T$ [°C]	slag pool thickness [mm]	billet temp. [°C]
<b>Steel A</b>	F-bearing	6.7- 6.8	10-12	1124
	F-free	7.2-7.3	11-17	1124
<b>Steel B</b>	F-bearing	6.8-7.0	5-8	1158-1271
	F-free	7.1-7.4	6-10	1205
<b>Steel C</b>	F-bearing	7.1-9.1	5-9	1109-1257
	F-free	7.5-8.4	5-9	1117-1184

It was visually observed that the melting performance of the F-free mould powder is similar to the F-bearing. The melting behaviour depends on chemical and physical properties, like free carbon, CO<sub>2</sub> content, bulk density, and choice of the raw materials. The melting rate has a significant effect on powder performance since it determines the ability of the molten slag to maintain a stable liquid pool depth.

The powder consumption for the F-free mould slag was determined considering the amount used during the industrial trials with the steels B and C: 0.24 kg/t and 0.14 kg/t respectively. The average consumption at the steelworks for the F-bearing mould powder is 0.30 kg/t. The differences between the average consumption for the F-bearing and the measured consumption for the F-free can be related to variations in operational parameters. Mould oscillation is different for the steels B and C; see Table 17.



Table 19 shows compositions of F-free slag samples (Sample 1 and Sample 2) taken from two different heats during trials with steel grade C, analysed through X-ray fluorescence. In order to do a comparison for Al<sub>2</sub>O<sub>3</sub> increase, it is necessary to correct the original composition for the losses that happen during heating. The theoretical slag composition is shown in Table 19 as “F-free corrected”; it was calculated using the factor  $f$  [72]

$$f = \left[ 1 - \frac{\%C_{free}}{100} - \left( \frac{44}{12} \times \left\{ \frac{\%C_{total} - \%C_{free}}{100} \right\} \right) \right]$$

where:  $f$  is the fraction of the mould powder converted into slag;  $\%C_{free}$  and  $\%C_{total}$  are free carbon and total carbon respectively.

The results indicate %Al<sub>2</sub>O<sub>3</sub> increase of 3.6 % and 4.4 % for Sample 1 and Sample 2 respectively, due to mould slag Al<sub>2</sub>O<sub>3</sub> pick-up. For the mould powders F-bearing and F-free, the alumina absorption rate is expected to be similar since they have similar  $B_i$  [17, 63]; see Table 14.

**Table 19.** Compositions of F-free slag samples collected during continuous casting process, for steel grade C.

		F-free original [wt%]	F-free corrected [wt%]	F-free Sample 1 [wt%]	F-free Sample 2 [wt%]
<b>steel C</b>	SiO <sub>2</sub>	38.00	42.41	39.77	39.03
	CaO	26.50	29.58	30.12	31.82
	MgO	2.64	2.95	3.98	4.28
	Al <sub>2</sub> O <sub>3</sub>	7.82	8.73	12.28	13.12
	TiO <sub>2</sub>	0.29	0.32	0.39	0.47
	Fe <sub>2</sub> O <sub>3</sub>	2.22	2.48	0.98	0.77
	MnO <sub>2</sub>	0.12	0.13	2.75	2.37
	Na <sub>2</sub> O	7.28	8.13	6.79	7.37
	K <sub>2</sub> O	1.03	1.15	0.91	0.94

The amount of steel scrap produced during rolling process was linked to the quality of the billets, see Table 20. The %scrap produced with the F-free was not critical, indicating good surface quality. More industrial tests are under progress to confirm the effect on the quality of the steel.

SEN diameter measurements were got after the tests. A significant decrease of the SEN erosion was observed. According to Mills [1] the SENs usually contain an external band of ZrO<sub>2</sub>/C (Z band) in the interfacial region, since it has much better slag corrosion resistance than Al<sub>2</sub>O<sub>3</sub>/C refractories. The erosion and corrosion of refractories by slags is usually related to the fluidity (or reciprocal viscosity), but in the case of ZrO<sub>2</sub>/C erosion there is a second mechanism at work. ZrO<sub>2</sub> undergoes a high-temperature phase transition, and the zirconia is usually stabilized by additions of CaO

or  $Y_2O_3$ . However, it is thought that the fluorine and  $SiO_2$  in the mould slag tend to leach out the CaO and thereby destabilize it.

**Table 20.** %Scrap formed during rolling process, and SEN diameter reduction (initial SEN diameter is 65 mm).

		steel weight [kg]	%scrap (wt%)	SEN reduction (%)
<b>Steel A</b>	F-bearing	37980	0.05	-
	F-free	18990	2.00	-
<b>Steel B</b>	F-bearing	77422	0.24	11.0
	F-free	39590	0.35	0.0
<b>Steel C</b>	F-bearing	48536	1.75	6.2
	F-free	43100	1.90	3.1

Thus, regarding the performance of the new F-free mould powder in laboratory and in industrial tests, it can be summarised in the following:

(i) From laboratory tests it was concluded that the technological parameters are similar considering the standard F-bearing and the F-free mould powder: melting characteristics, viscosity, melting behaviour, and crystallisation tendency.

(ii) From tests at steelworks, during the continuous casting process some evaluations were made considering the following:  $\Delta T$  between water cooling inlet and outlet, slag pool thickness, billet temperature before straightener, melting performance, powder consumption, mould slag  $Al_2O_3$  pick-up. The behaviour of the F-free mould powder was considered adequate. Besides, a significant reduction of SEN erosion was registered.

(iii) The %scrap produced during rolling process for the F-free mould powder was not critical, indicating good surface quality.

(iv) More industrial tests are required to check the results reported in the present work.

## 6. CONCLUSIONS

By in situ observation using the Single Hot Thermocouple Technique (SHTT) the crystallisation behaviour of slags can be characterized, building time-temperature-transformation (TTT) or continuous-cooling-transformation (CCT) diagrams.

In the present work the following conclusions were obtained:

(i) The apparatus used for the Hot Thermocouple Technique – Single Hot Thermocouple Technique (SHTT) and Double Hot Thermocouple Technique (DHTT) – is accurate, according to the calibration that was performed using  $\text{CaF}_2$ ,  $\text{Na}_2\text{SO}_4$  and  $\text{K}_2\text{SO}_4$ .

(ii) The CCT diagram constructed for the basic slag CA – 44 %CaO , 56 %Al<sub>2</sub>O<sub>3</sub> (wt%) – showed large differences between *liquidus* temperature and the temperature for first crystals precipitation, even at low cooling rates, e.g., 168 °C below the *liquidus* temperature when cooling at a rate of 6 °C/min. In addition, for this slag a correspondence between break temperature obtained from viscometer and crystallisation temperature obtained from SHTT was found.

(iii) For the CS slag – %CaO/%SiO<sub>2</sub> (wt%) = 0.7 –, during isothermal experiments crystallisation was observed only at 1000 °C with an incubation time of 76 seconds (average of 6 experiments, standard deviation 27 seconds). For experiments with continuous cooling rates, no crystal is detected, even at low cooling rates (e.g., 10 °C/min). However, when increasing the temperature after reaching lower temperatures (< 1000 °C), intense crystallisation is observed; this may be explained by the fact that the optimum range of temperatures required for crystal nucleation is lower than the optimum range of temperatures required for crystal growth.

(iv) For the CST\_1 slag – 41.1 %CaO, 29.1 %SiO<sub>2</sub>, 29.8 %TiO<sub>2</sub> (wt%) –, that has high *liquidus* temperature (approximately 1600 °C), the effect of the duration of superheating (in the range 1650 °C - 1680 °C) on incubation time was studied. It was found that the longer the superheating is, the longer the incubation times become, i.e., the duration of superheating – for a slag that seems to be completely liquid – can strongly affect a slag's crystallisation behaviour. This may be explained by the fact that the invisible nuclei diminish more slowly than grains of measurable size (in the μm range).

(v) It was observed that the addition of Na<sub>2</sub>O in CaO-SiO<sub>2</sub>-TiO<sub>2</sub> slags dramatically shortens the crystals' incubation times, as shown in TTT diagrams, to the range of seconds. There is a clear effect of the %Na<sub>2</sub>O content on the critical cooling rate. It is possible to control the crystallisation kinetics in CaO-SiO<sub>2</sub>-TiO<sub>2</sub> slags by changing the Na<sub>2</sub>O content.

(vi) The slag CST\_2 – 35.6 %CaO, 46.3 %SiO<sub>2</sub>, 18.1 %TiO<sub>2</sub> (wt%) – presents complex crystallisation behaviour: more than one crystal phase, with different morphologies, which seem to be a combination of bulk and surface crystallisation. In this case, the physical meaning of the values of  $n$  and  $K$  of the Avrami equation obtained from numerical fitting is unknown. For the CSTNA slags, similar ambiguities arise.

(vii) The morphology of crystals varies with temperature. For CSTNA slags columnar grains (which seem to grow unidirectionally from surface to centre of the sample) and equiaxed grains (which seem to grow radially in the liquid slag) were observed. The crystals have dendritic appearance at higher temperatures and become small and dense at lower temperatures. When the temperature is low (< 900 °C) the crystals are very fine and the density of crystals increased until it appeared “cloud-like”.

(viii) A new fluorine-free mould powder for billet casting was developed by collaboration between universities, mould powder supplier and steel plant. Laboratory tests showed that the technological parameters for both, the commercial F-bearing mould powder and the new F-free mould powder, are similar. The crystallisation tendency for both is similar. From the tests performed at steelworks it was reported that comparable surface quality for the billets was obtained when using the F-free mould powder.

## REFERENCES

1. Mills, K., *The making, shaping and treating of steel (chapter 8)*. 2003, The AISE Steel Foundation: Pittsburgh.
2. Kromhout, J.A., *Mould powders for high speed continuous casting of steel*. 2011, Doctoral dissertation, Technische Universiteit Delft.
3. Hooli, P., *Study on the layers in the film originating from the casting powder between steel shell and mould and associated phenomena in continuous casting of stainless steel*. 2007, PhD dissertation, Helsinki University of Technology.
4. Garcia, A., Spim, J. A., Santos, C. A., Cheung, N., *Lingotamento contínuo de aços (Portuguese)*. 1 ed. 2006, São Paulo: Brazilian Association of Metallurgy, Materials and Mining.
5. Kashiwaya, Y., C.E. Cicutti, and A.W. Cramb, *An investigation of the crystallization of a continuous casting mold slag using the Single Hot Thermocouple Technique*. ISIJ International, 1998. **38**(4): p. 357-365.
6. Mills, K.C. and A.B. Fox, *The role of mould fluxes in continuous casting - so simple yet so complex*. ISIJ International, 2003. **43**(10): p. 1479-1486.
7. Pinheiro, C.A., I.V. Samarasekera, and J.K. Brimacombe, *Mold flux for continuous casting of steel, Part I*. Iron and Steelmaker, 1994(October).
8. Hering, L., H.P. Heller, and H.W. Fenzke, *Untersuchungen zur Giesspulverauswahl beim Brammenstranggießen (German)*. Stahl und Eisen, 1992. **112**(8): p. 61-65.
9. Hao, Z., Chen, W., Lippold, C., Mao, H., *Crystallization extent and phase constitution of slag films taken from continuous casting moulds for stainless steels*. Steel Research International, 2009. **80**(10).
10. Scheller, P.R., *Mass exchange at the metal-slag interface in the continuous casting process*, in *VII International Conference on Molten Slags Fluxes and Salts*. 2004: Cape Town, South Africa.
11. Pinheiro, C.A., I.V. Samarasekera, and J.K. Brimacombe, *Mold flux for continuous casting of steel, Part II*. Iron and Steelmaker, 1994. (November): p. 62.
12. Chilov, A., *Mass spectrometric study of volatile components in mould powders*. 2005, Doctoral dissertation, Helsinki University of Technology Espoo.
13. Orrling, C., Cramb, A. W., Tilliander, A., Kashiwaya, Y., *Observations of the melting and solidification behavior of mold slags*. I&SM, 2000(January).
14. Mizuno, H., Esaka, H., Shinozuka, K., Tamura, M., *Analysis of the crystallization of mold flux for continuous casting of steel*. ISIJ International, 2008. **48**(3): p. 277-285.
15. Li, Z., Thackray, R., Mills, K. C., *A test to determine crystallinity of mould fluxes*, in *VII International Conference on Molten Slags, Fluxes and Salts*. 2004: Cape Town, South Africa. p. 813-819.
16. Carli, R. and C. Righi, *Mould flux crystallization: a kinetic study*, in *VII International Conference on Molten Slags, Fluxes and Salts*. 2004: Cape Town, South Africa.
17. Branion, R.V., *Mold fluxes for continuous casting*. Iron and Steelmaker, 1986(September).
18. Pinheiro, C.A., I.V. Samarasekera, and J.K. Brimacombe, *Mold flux for continuous casting of steel, Part III*. Iron and Steelmaker, 1994(December).
19. Sridhar, S., Mills, K.C., Afrange, O.D.C., Lorz H.P., Carli R., *Break temperatures of mould fluxes and their relevance to continuous casting*. Ironmaking and Steelmaking, 2000. **27**(3): p. 238-242.
20. Schulz, T., Janke, D., Heller, H. P., Lychatz, B., *Entwicklung umweltfreundlicher Stranggießschlacken (German)*. Stahl Und Eisen, 2008. **128**(4,april): p. 65-78.
21. Heimbach, H., Schulz, K., Markardt, J., Ehrenberg, H., *Die Freisetzung von Fluorverbindungen aus Giessschlacken (German)*. Stahl und Eisen, 1997. **117**(12): p. 105-100 und 161.

22. Zaitsev, A.I., Leites, A. V., Litvina, A. D., Mogutnov, B. M., *Investigation of the mould powder volatiles during continuous casting*. Steel Research, 1994. **65**(9).
23. Janke, D., Schulz, T., Tonelli, T., Cimarelli, T., Holappa, L., Shilov, A., Havette, E., Viguet-Carrin, C., Valentin, P., Bruch, C., *Improvement of casting fluxes and slags by minimization of environment – polluting and corrosive constituents (fluorine, alkali components)*, in *EUR 20645 - Casting and Solidification, Technical Steel Research Series*. 2003, Office for Official Publications of the European Communities: Luxemburg.
24. Pinheiro, C.A., I.V. Samarasekera, and J.K. Brimacombe, *Mold flux for continuous casting of steel, Part VI*. Iron and Steelmaker, 1995(March).
25. Fox, A.B., Mills, K. C., Lever, D., Bezerra, C., Valadares, C., Unamuno, I., Laraudogoitia, J.J., Gisby, J., *Development of fluoride-free fluxes for billet casting*. ISIJ International, 2005. **45**(7): p. 1051-1058.
26. Nakada, H. and K. Nagata, *Crystallization of CaO–SiO<sub>2</sub>–TiO<sub>2</sub> slag as a candidate for fluoride free mold flux*. ISIJ International, 2006. **46**(3): p. 441-449.
27. Nakada, H., Susa, M., Seko, Y., Hayashi, M., Nagata, K., *Mechanism of heat transfer reduction by crystallization of mold flux for continuous casting*. ISIJ International, 2008. **48**(4): p. 446-453.
28. Wen, G., Sridhar, S., Tang, P., Qi, X., Liu, Y., *Development of fluoride-free mold powders for peritectic steel slab casting*. ISIJ International, 2007. **47**(8): p. 1117-1125.
29. Qi, X., G. Wen, and P. Tang, *Investigation on heat transfer performance of fluoride-free and titanium-bearing mold fluxes*. Journal of Non-Crystalline Solids, 2008. **354**: p. 5444-5452.
30. He, S., Wang, Q., Xie, D., Xu, C., Li, Z., Mills, K. C., *Solidification and crystallization properties of CaO–SiO<sub>2</sub>–Na<sub>2</sub>O based mould fluxes*. International Journal of Minerals, Metallurgy and Materials, 2009. **16**(3).
31. Zhang, Z., G. Wen, and Y. Zhang, *Crystallization behavior of F-free mold fluxes*. International Journal of Minerals, Metallurgy and Materials, 2011. **18**(2, April 2011).
32. Semykina, A., *Recovery of iron and manganese values from metallurgical slags by the oxidation route*, in *Division of Materials Process Science - Department of Materials Science and Engineering*. 2010, doctoral thesis, Royal Institute of Technology: Stockholm.
33. Wang, Q., S. He, and K.C. Mills, *Research on decreasing fluorine content from continuous casting mould fluxes*, in *4<sup>th</sup> International Conference on Continuous Casting of Steel in Developing Countries*. 2011: China.
34. Choi, S., Lee, D., Shin, D., Choi, S., *Properties of F-free glass system as a mold flux: viscosity, thermal conductivity and crystallization behavior*. Journal of Non-Crystalline Solids, 2004. **345&346**: p. 157-160.
35. Fang, Z., Yuan, C., Yici, W., Fang, D., *Influence of La<sub>2</sub>O<sub>3</sub> on crystallization behavior of free-fluoride mould flux and heat transfer of slag films*. Journal of Rare Earths, 2011. **29**(2).
36. Prapakorn, K. and A.W. Cramb, *Initial solidification behavior in continuous casting: the effect of MgO on the solidification behavior of CaO–Al<sub>2</sub>O<sub>3</sub> based slags*, in *MS&T Conference Proceedings*. 2004.
37. Orrling, C. and A.W. Cramb, *The effect of water vapor on mold slag crystallization*. Metallurgical and Materials Transactions B, 2000. **31B**(April ).
38. Fokin, V.M., Zanotto, E. D., Yuritsyn, N. S., Schmelzer, J. W. P., *Review - homogeneous crystal nucleation in silicate glasses: a 40 years perspective*. Journal of Non-Crystalline Solids, 2006. **352**: p. 2681-2714.
39. Zanotto, E.D., *Crystallization of liquids and glasses*. Brazilian Journal of Physics, 1992. **22**(2).
40. Zanotto, E.D. and M.L.G. Leite, *The nucleation mechanism of lithium disilicate glass revisited*. Journal of Non-Crystalline Solids, 1996. **202**: p. 145-152.

41. Christian, J.W., *The theory of transformations in metals and alloys - Part I*. Third edition ed. 2002: Elsevier Science Ltd.
42. Kashiwaya, Y., Cicutti, C. E., Cramb, A. W., Ishii, K., *Development of Double and Single Hot Thermocouple Technique for in situ observation and measurement of mold slag crystallization*. ISIJ International, 1998. **38**(4).
43. Lachmann, S. and P.R. Scheller, *Effect of  $Al_2O_3$  and  $CaF_2$  on the solidification of mould slags and the heat transfer through slag films*, in *VIII International Conference on Molten Slags, Fluxes and Salts*. 2009: Santiago, pp. 1101.
44. Patnaik, P., *Handbook of inorganic chemicals*, McGraw-Hill, Editor. 2003.
45. Gusarova, T., *Neue Messmethode zur Qualitätsprüfung von metallurgischen Schlacken (German)*, in *Institute of Iron and Steel Technology*. 2005, Diplomarbeit, Technische Universität Bergakademie Freiberg: Freiberg.
46. VDEh, ed. *Slag Atlas - 2nd edition*. 1995.
47. Wu, L., *Viscosity measurements of slags with rotation viscometer*, in *Institute of Iron and Steel Technology*. 2011, Diplomarbeit, Technische Universität Bergakademie Freiberg: Freiberg.
48. Strnad, Z., *Glass-ceramic materials*. Glass Science and Technology. Vol. 8. 1986: Elsevier Science Publishing Company.
49. Avrami, M., *Kinetics of phase change (Part II) - transformation-time relations for random distribution of nuclei*. Journal of Chemical Physics, 1940. **8**(February): p. 212-224.
50. Schenck, H. and M. Froberg, *Viskositätsmessungen an flüssigen Schlacken des Systems  $CaO-SiO_2-TiO_2$  im Temperaturbereich von 1300 bis 1600°C (German)*. Archiv für das Eisenhüttenwesen, 1962. **33**(7): p. 423-425.
51. Seetharaman, S., ed. *Fundamentals of metallurgy*. 2005, Woodhead Publishing and Maney Publishing on behalf of The Institute of Materials, Minerals and Mining.
52. Mutale, C.T., T. Claudon, and A.W. Cramb, *Observation of the crystallization behavior of a slag containing 46 wt pct CaO, 46 wt pct  $SiO_2$ , 6 wt pct  $Al_2O_3$ , and 2 wt pct  $Na_2O$  using the Double Hot Thermocouple Technique*. Metallurgical and Materials Transactions B, 2005. **36B**(June 2005).
53. Turkdogan, E.T., ed. *Physicochemical properties of molten slags and glasses*. 1983, The Metals Society, London.
54. Callister, W.D., *Materials science and engineering - an introduction (second edition)*.
55. Rocabois, P., Pontoire, J. N., Lehmann, J., Gaye, H., *Crystallization kinetics of  $Al_2O_3$ - $CaO-SiO_2$  based oxide inclusions*. Journal of Non-Crystalline Solids, 2001. **282**: p. 98-109.
56. Liu, H., G. Wen, and P. Tang, *Crystallization behaviors of mold fluxes containing  $Li_2O$  using Single Hot Thermocouple Technique*. ISIJ International, 2009. **49**(6): p. 843-850.
57. Zhou, L., Wang, W., Ma, F., Li, J., *A kinetic study of the effect of basicity on the mold fluxes crystallization*, in *Metallurgical and Materials Transactions B, published online on 27.10.2011*.
58. Li, J., X. Wang, and Z. Zhang, *Crystallization behavior of rutile in the synthesized Ti-bearing blast furnace slag using Single Hot Thermocouple Technique*. ISIJ International, 2011. **51**(9).
59. Avrami, M., *Kinetics of phase change (Part I) - general theory*. Journal of Chemical Physics, 1939. **7**(December): p. 1103-1112.
60. Avrami, M., *Kinetics of phase change (Part III) - granulation, phase change, and microstructure*. Journal of Chemical Physics, 1941. **9**(February): p. 177-184.
61. Zanotto, E.D. and P.F. James, *Experimental test of the general theory of transformation kinetics: homogeneous nucleation in a  $BaO.2SiO_2$  glass*. Journal of Non-Crystalline Solids, 1988. **104**(1): p. 70-72.

62. Zanotto, E.D. and A. Galhardi, *Experimental test of the general theory of transformation kinetics: homogeneous nucleation in a  $\text{Na}_2\text{O} \cdot 2\text{CaO} \cdot 3\text{SiO}_2$  glass*. Journal of Non-Crystalline Solids, 1988. **104**: p. 73-80.
63. Nakano, T., Kishi, T., Koyama, K., Komai, T., Naitoh, S., *Mold powder technology for continuous casting of aluminum-killed steel*. Transactions ISI, 1984. **24**: p. 950-956.
64. Dubrawski, J.V. and J.M. Camplin, *Crystallization of mould powders used in the continuous casting of steel*. Journal of Thermal Analysis, 1993. **40**: p. 329-334.
65. Unamuno, I., Ciriza, J., Arteaga, A., Laraudogoitia, J. J., *Mold powder properties characterisation for billet casting at Sidenor Basauri*, in *6th European Conference on Continuous Casting*. 2008.
66. Abratis, H., Höfer, F., Jünemann, M., Sardemann, J., Stoffel, H., *Einsatz von unterschiedlichen gießpulvern beim stranggießen von vorblöcken und knüppeln (German)*. Stahl Und Eisen, 1996. **116**(4): p. 85-91.
67. Klug, J.L., Freitas, S. L., Pereira, M. M. S. M., Heck, N. C., Silva, D. R., Vilela, A. C. F., Jung, D., *Fluorine-free mould powders for billet casting - technological parameters*, in *41<sup>st</sup> Steelmaking Seminar - International*. 2010, Brazilian Association of Metallurgy, Materials and Mining: Rio de Janeiro.
68. *DIN 51730: determination of fusibility of fuel ash*. 1998, Deutsches Institut für Normung.
69. Pinheiro, C.A., I.V. Samarasekera, and J.K. Brimacombe, *Mold flux for continuous casting of steel, Part X*. Iron and Steelmaker, 1995(July).
70. Pinheiro, C.A., I.V. Samarasekera, and J.K. Brimacombe, *Mold flux for continuous casting of steel, Part V*. Iron and Steelmaker, 1995(February).
71. Pinheiro, C.A., I.V. Samarasekera, and J.K. Brimacombe, *Mould flux for continuous casting of steel, Part XI*. Iron and Steel Maker, 1995(August).
72. Fox, A.B., Mills, K. C., Sridhar, S., Lee, P. D., *Mould powder selection model for continuous casting*, in *85th Steelmaking Conference, ISS-AIME*. 2002: Warrendale, PA. p. 133-144.



## EXTENDED ABSTRACT

Good understanding and control of phenomena in the mould during production of steel are essential to the success of the continuous casting process. The presence of crystals in mould slags has a decisive effect on both the lubrication and the heat transfer rate between the mould and the steel strand.

Considering the development of fluorine-free mould powders for slab casting and thin slab casting, the control of crystallisation is imperative. Therefore, mould powders crystallisation behaviour should be characterised. Time-temperature-transformation (TTT) or continuous-cooling-transformation (CCT) diagrams provide a fundamental understanding of the transformation kinetics. These diagrams can be constructed using the Single Hot Thermocouple Technique (SHTT).

The main problem related to the development of fluorine-free mould powders is effectively controlling the heat transfer between the steel shell and the mould. In industrial F-bearing mould powders, the crystallisation of cuspidine from mould slag is thought to be the most effective way of exerting heat-transfer control. Although the mechanism of heat-transfer control via the crystallisation of cuspidine has not yet been determined, two ideas have been proposed. One idea is that radiation heat flux is decreased by scattering at the boundary between the crystalline and the liquid layers; the other idea is that the total heat flux is reduced by the large thermal resistance of the air gap formed as a result of the solidification shrinkage of the solidified slag layer. In any case, the crystallisation of cuspidine from mould slag has a great effect on heat-transfer control [26].

Several papers report on the possibilities of replacing the cuspidine phase by the formation of different crystals to allow for heat-transfer control. Some papers indicate that  $\text{TiO}_2$ -bearing raw materials can be used by forming  $\text{TiO}_2$  crystals [26, 28, 29]. Moreover, there are also other reports on the solidification behaviour of mould fluxes without fluorine or with relatively low fluorine contents using different crystals, such as  $\text{Na}_2\text{O} \cdot \text{CaO} \cdot 3\text{SiO}_2$  [30];  $\text{Na}_2\text{O} \cdot 2\text{CaO} \cdot 3\text{SiO}_2$  [33];  $\text{CaSiO}_3$ ,  $\text{Ca}_3\text{Si}_2\text{O}_7$  and  $\text{Ca}_2\text{SiO}_4$  [31] and  $\text{CaB}_2\text{SiO}_7$  and  $\text{CaAl}_{14}\text{B}_2[\text{SiO}_4]_8$  [34].

The motivation for the present work is to provide fundamental information related to crystallisation control for the development of fluorine-free mould powders for continuous casting of steel, studying the crystallisation behaviour of slags through the Single Hot Thermocouple Technique (SHTT).

The objectives are the following:

(i) To perform a basic and systematic study evaluating the crystallisation behaviour of slags in the systems  $\text{CaO}-\text{Al}_2\text{O}_3$ ,  $\text{CaO}-\text{SiO}_2$ ,  $\text{CaO}-\text{SiO}_2-\text{TiO}_2$ , and  $\text{CaO}-\text{SiO}_2-\text{TiO}_2-\text{Na}_2\text{O}$ , building TTT and CCT curves, analysing the kinetics of crystals growth and crystals morphology;

(ii) To study the solidification behaviour of a new industrial fluorine-free mould powder to be used at steelworks during continuous casting of billets.

### Experimental work

The SHTT is a unique apparatus that enables measurement of the slag sample temperature using a thermocouple while the sample is heated simultaneously. The sample is placed on a thermocouple tip and it can be subjected to rapid cooling rates or heating rates, or to be held under isothermal conditions. The advantage of the SHTT is that it allows for the in situ observation of melting and solidification under various thermal conditions. Due to the low heat capacity of the system (sample and thermocouple) very high heating and cooling rates can be easily obtained ( $> 3000^{\circ}\text{C}/\text{min}$ ). The SHTT can be applied to slags which are optically transparent or translucent, while the crystalline phase which precipitates upon cooling should be opaque.

The slags used in the present work for the SHTT were produced from reagent-grade  $\text{CaCO}_3$ ,  $\text{SiO}_2$ ,  $\text{TiO}_2$ ,  $\text{Na}_2\text{CO}_3$  and  $\text{Al}_2\text{O}_3$ . Table 1 shows their compositions.

**Table 1.** Compositions of the slags used for analyses with the SHTT (wt%). B is the ratio  $\% \text{CaO} / \% \text{SiO}_2$ .

	$\% \text{CaO}$	$\% \text{SiO}_2$	$\% \text{TiO}_2$	$\% \text{Na}_2\text{O}$	$\% \text{Al}_2\text{O}_3$	$\% \text{C}$	B
CA	43.7				56.3	0.074	
CS	41.7	58.3				0.063	0.7
CST_1	41.1	29.1	29.8			-	1.4
CST_2	35.6	46.3	18.1			0.590	0.8
CSTNA_1	33.6	41.3	16.5	7.1	1.5	0.073	0.8
CSTNA_2	30.1	46.8	16.4	5.4	1.3	0.034	0.6
CSTNA_3	31.6	48.1	15.5	3.7	1.1	0.032	0.7
CSTNA_4	30.9	42.3	15.2	6.4	5.2	0.038	0.7

The apparatus used in the present work was constructed at the Technische Universität Bergakademie Freiberg [43]; see Figure 1. It consists of two systems: an observation system and a thermocouple system. In a vacuum chamber, there are two water-cooled inserts, one on the left and another on right. Both of them hold a B-type thermocouple at the tips. Each thermocouple is connected to a separate thermocouple controller. The material under study is melted directly on the thermocouple in the vacuum chamber. The thermocouples remain inside an additional heating element (i.e., a kanthal coil), which reduces heat losses from the sample to the surroundings, maintaining a temperature of approximately  $500^{\circ}\text{C}$  around the sample.

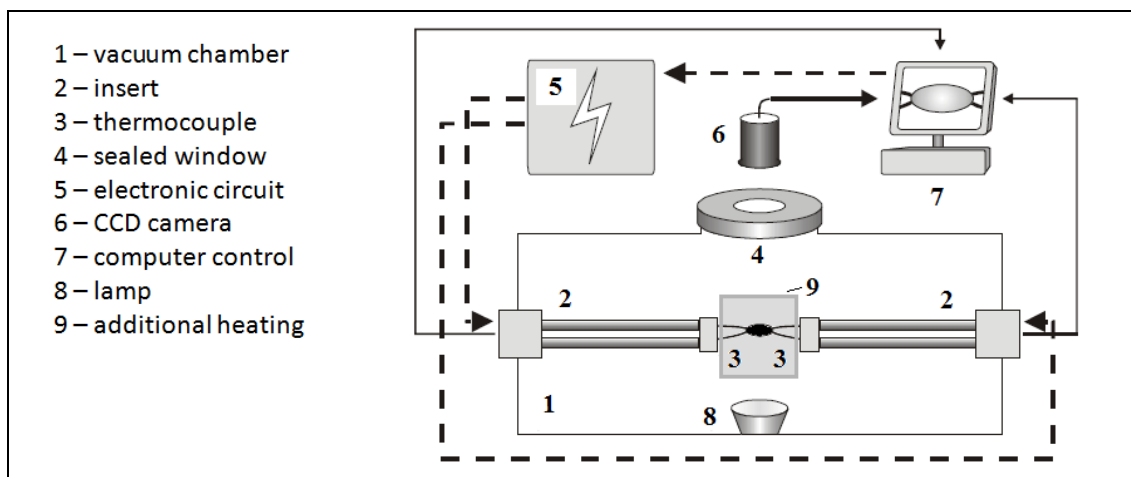


**Figure 1.** Schematic view of the experimental set-up used in the present work.

The B-type thermocouple (up to 1800°C) is built using two platinum wires measuring 0.5 mm in diameter and approximately 25 mm in length: Pt30Rh and Pt6Rh.

The accuracy of the apparatus was verified by measuring the crystallisation temperature ( $T_{\text{cryst.}}$ ) of  $\text{CaF}_2$ ,  $\text{Na}_2\text{SO}_4$  and  $\text{K}_2\text{SO}_4$ . The  $T_{\text{cryst.}}$  is defined here as the temperature at which the first crystals can be observed at a particular cooling rate. With the substances in the vacuum chamber, a pressure of 10 mbar was applied for 5 minutes. Then, the vessel was filled with Ar, maintaining a flux of 300 L/h during the measurements. Afterwards, the substances were melted at 100°C above their melting points and cooled at a rate of 30 °C/min. Their melting points are  $\text{CaF}_2$  - 1418 °C,  $\text{Na}_2\text{SO}_4$  - 884 °C, and  $\text{K}_2\text{SO}_4$  - 1069 °C [44].

Figure 2 shows the differences between the reported melting points [44] and  $T_{\text{cryst.}}$ . Twelve experiments were performed for each substance (experiments 1-6 with the left thermocouple and experiments 7-12 with the right thermocouple).

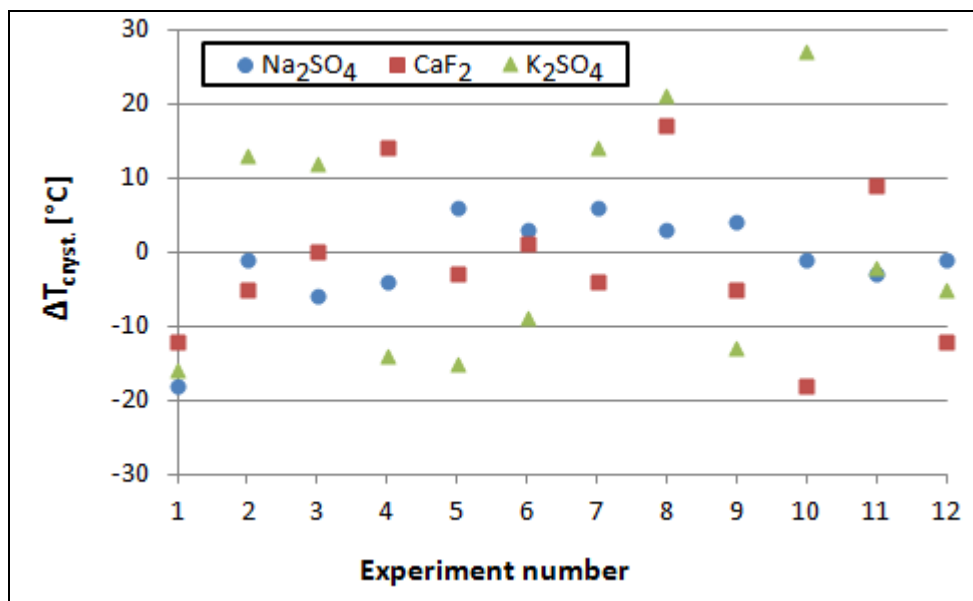


**Figure 2.** Comparison between literature results [44] and the results of the present work.  $\Delta T_{\text{cryst.}}$  is the difference between the reported melting point and the crystallisation temperature that was measured by SHTT.

Assuming a normal distribution for  $\Delta T_{\text{cryst.}}$ , the average values of  $T_{\text{cryst.}}$  for the three substances used for calibration can be calculated; see Table 2. The average values of  $T_{\text{cryst.}}$  are very close to the melting points reported in the literature, and the scattering is low.

**Table 2.** Comparison between the literature-reported [44] melting points and the crystallisation temperatures measured by SHTT ( $T_{\text{cryst.}}$ ). For each substance, 12 measurements were performed.

	m.p. literature [44]	average $T_{\text{cryst.}}$	standard deviation $T_{\text{cryst.}}$
$\text{CaF}_2$	1418 °C	1417 °C	10.6 °C
$\text{Na}_2\text{SO}_4$	884 °C	883 °C	6.6 °C
$\text{K}_2\text{SO}_4$	1069 °C	1071 °C	15.4 °C

The results summarised in Table 2 were obtained through video-file analysis. The apparatus also registers the evolution of temperature with time, in a similar manner to differential thermal analysis (DTA). It was verified during calibration that the visually observed crystallisation corresponds to peaks in the T versus t diagrams.

It was observed that it is important to apply suitable vacuum times, for this apparatus approximately 10 mbar for 5 minutes, before the measurements. When working with lower vacuum times, e.g., 1 minute at 10 mbar, the  $\text{CaF}_2$  crystallisation temperatures tend to fall outside of the  $1418 \pm 20$  °C range, most likely because of the reaction between water vapour and  $\text{CaF}_2$ .

To perform the experiments using SHTT small portions of premelted slags (5-10 mg) are pressed and placed on thermocouple tips. With the substances in the vacuum chamber, a pressure of 10 mbar is applied for 5 minutes. Then, the vessel is filled with

Ar, maintaining a flux of 300 L/h during the measurements. The additional heating element is turned on, maintaining a temperature of approximately 500 °C around the thermocouple.

To produce time-temperature-transformation (TTT) diagrams, after melting, very high cooling rates (higher than 3000 °C/min) are applied down to the desired temperature. Then, the incubation time, i.e., the time required to obtain the first crystals, is measured by direct observation. Using the incubation times for different temperatures, TTT diagrams are constructed. To create continuous-cooling-transformation (CCT) diagrams, after melting, a particular cooling rate is applied. Then, the solidification behaviour is observed. Using different cooling rates, a CCT curve can be constructed.

Viscosity measurements were performed using a rotation viscometer (Anton Paar MC 301) at the Technische Universität Bergakademie Freiberg. The materials used for these measurements have compositions close to that of the slags used for the SHTT analyses (whose compositions are in Table 1).

## **Results and discussion**

### *CaO-Al<sub>2</sub>O<sub>3</sub> slag (CA)*

The CaO-Al<sub>2</sub>O<sub>3</sub> slag, herein referred to as CA, containing 43.7% CaO and 56.3% Al<sub>2</sub>O<sub>3</sub>, was studied with the SHTT. The *liquidus* temperature for this slag according to FactSage 6.1 is 1518 °C, and the first crystal during cooling is CaAl<sub>2</sub>O<sub>4</sub>. The second crystal during cooling is Ca<sub>3</sub>Al<sub>2</sub>O<sub>6</sub>, which precipitates at 1362 °C (*solidus* temperature).

It was constructed a CCT diagram for the CA slag using the SHTT. The samples were maintained at 1700 °C for 60 seconds before the cooling at different cooling rates. It was observed that the crystallisation starts far from the *liquidus*. The crystallisation temperature (i.e., the temperature where the first crystals are observed) is a function of the cooling rate. The critical cooling rate for the CA slag is 1700 °C/min, i.e. with higher cooling rates no crystal is observed.

From the viscosity measurements it can be observed that the break temperature, i.e., the point where there is a sudden increase of the viscosity due to crystals precipitation, is in the range 1350 - 1375 °C. According to the SHTT the point where the first crystals were detected for this CA slag at a cooling rate of 6 °C/min is 1350 °C. Therefore, for this slag there is a correspondence between break temperature obtained from viscometer and crystallisation temperature obtained from SHTT.

### *CaO-SiO<sub>2</sub> slag (CS)*

The CaO-SiO<sub>2</sub> slag with basicity %CaO/%SiO<sub>2</sub> = 0.7, herein referred to as CS, has the following characteristics according to FactSage 6.1: *liquidus* temperature, 1500 °C;

first solid phase during cooling,  $\text{CaSiO}_3$ ; and *solidus* temperature, 1437 °C, where the second crystal ( $\text{SiO}_2$ ) precipitates.

Regarding the CCT experiments (continuous cooling), no crystallisation is observed, even at very low cooling rates. This result is in agreement with the results of other reports for CaO-SiO<sub>2</sub> slags with basicity 0.8, 1.0 and 1.2, in which no crystal was detected when performing CCT experiments [43].

For TTT experiments (isothermal transformation), the samples were completely melted and then maintained at 1700 °C for 5 minutes. Then, a very high cooling rate (> 3000 °C/min) was applied. When the desired temperatures were reached – 900 °C, 950 °C, 1000 °C, 1050 °C, 1100°C, 1150°C, and 1200 °C – the samples were maintained at those temperatures for up to 1000 seconds. Crystallisation was observed only at 1000 °C, occurring at 76 seconds (average for 6 experiments, standard deviation 27 seconds).

In addition to the CCT and TTT experiments, one special thermal cycle was applied: (i) the sample was maintained at 1700 °C for 5 minutes, i.e., completely melted; (ii) quenching (> 3000 °C/min) down to particular temperatures (900 °C, 950 °C, 975 °C, 1000 °C, 1025 °C, 1050 °C, 1100°C, 1150 °C, 1200 °C, and 1300 °C); (iii) maintenance at the particular temperature for 60 seconds, and (iv) heating again at a rate of 1000 °C/min up to 1700 °C.

With respect to the aforementioned special thermal cycle, crystallisation was observed to occur intensely during heating at a rate of 1000 °C/min but only when starting (after quenching) at 1000 °C or below. The crystallisation occurs intensely in the range 1069 - 1125 °C when starting at 900 °C, 950 °C, 975 °C, and 1000 °C. Therefore, it is clear that when increasing the temperature after reaching a particular range of lower temperatures, good conditions for crystals growth can be obtained for the CS slag. This intense crystallisation can be explained by the fact that the optimum range of temperatures for crystal nucleation is lower than the optimum range of temperatures for crystal growth. This is related to the fact that the rate of crystal growth is not the only factor determining the ability of a melt to form crystals because crystals grow from a certain number of nuclei, and in many respects, the nucleation stage determines the pathways of overall crystallisation in silicate glasses [38]. It is well known that crystallisation can be divided into two processes: (i) formation of nuclei and (ii) crystal growth. The rates of both processes are temperature-dependent, with maxima at certain supercooling values. These maxima are separated in glass-forming materials suitable for the preparation of glass ceramics, allowing for control over glass crystallisation [48].

The observation of crystals during isothermal experiments at 1000 °C for the CS slag is explained by the fact that 1000 °C is an intermediate temperature at which both the nucleation rate and growth rate are sufficiently high.

*CaO-SiO<sub>2</sub>-TiO<sub>2</sub> slag (CST\_1)*

The slag of the CaO-SiO<sub>2</sub>-TiO<sub>2</sub> system, herein referred to as CST\_1, was used to study the effect of the duration of superheating on incubation times. The composition (wt%) of CST\_1 is 41.1 %CaO, 29.1 %SiO<sub>2</sub>, and 29.8 %TiO<sub>2</sub>. The *liquidus* temperature for this slag is very high, approximately 1600 °C. The first phase formed during cooling from liquid slag is CaO.TiO<sub>2</sub>.

A special thermal cycle, which was repeated several times for each sample, was applied and it is described in the following: (i) the samples were held in the temperature range of 1650 °C - 1680 °C for different periods (the samples always completely melted and became transparent within a few seconds); (ii) quenching down to 1400 °C at the highest cooling rate (> 3000 °C/min); (iii) measurement of the incubation time, i.e., when the first crystals could be observed; (iv) quenching down to a temperature of 1200 °C, which was held for 60 seconds to guarantee full crystallisation of the sample; (v) heating up to 1650 °C - 1680 °C.

It was observed that the duration of superheating completely changed the crystallisation behaviour of the CST\_1 slag, assuming that the initial conditions before melting were the same. When the holding time is 60 s, the incubation times tend to be much shorter (5-12 seconds) than when the holding time is 600 s (it is notable that no crystal was observed up to 1000 seconds). Two samples were analysed, one with a mass of 1.4 mg and the other with a mass of 2.3 mg.

It is known that a new phase is nucleated by nuclei that already exist in the old phase and whose effective number per unit nucleation region can be altered by the temperature of superheating and the duration of superheating. There are indications that, for given supercooling or superheating, the nuclei grow or diminish considerably more slowly than grains of visible size. These nuclei, which may be heterogeneities of any sort, would usually consist of small particles of the subcritical phase or tough films of the latter surrounding foreign inclusions [49].

Therefore, there is a relation between the duration of superheating, incubation times, and number of nuclei. The longer the duration of superheating is, the lower the number of nuclei per unit nucleation region is, and consequently, the longer the incubation time becomes.

*CaO-SiO<sub>2</sub>-TiO<sub>2</sub> slag (CST\_2) and CaO-SiO<sub>2</sub>-TiO<sub>2</sub>-Na<sub>2</sub>O-Al<sub>2</sub>O<sub>3</sub> slags (CSTNA)*

The compositions for the CST\_2 and for the CSTNA slags are shown in Table 1.

The TTT diagram for the slag CST\_2, which was constructed using SHTT, is shown in Figure 3. It is required that the crystals of the CaO-SiO<sub>2</sub>-TiO<sub>2</sub> system precipitate as the phase cuspidine in commercial mould powders, replacing the system CaO-SiO<sub>2</sub>-CaF<sub>2</sub>. However, the incubation times for the slag CST\_2 are much longer than of the F-bearing industrial slag, whose TTT diagram is also shown in the figure – it is a commercial mould powder normally employed in the continuous casting of stainless steels, which contains CaF<sub>2</sub> and Na<sub>2</sub>O, without TiO<sub>2</sub>.

The slag CSTNA\_1 was designed to have basicity and TiO<sub>2</sub> content similar to the slag CST\_2; its TTT diagram is shown in Figure 3. The Na<sub>2</sub>O-bearing slag CSTNA\_1 has higher crystallisation rate.

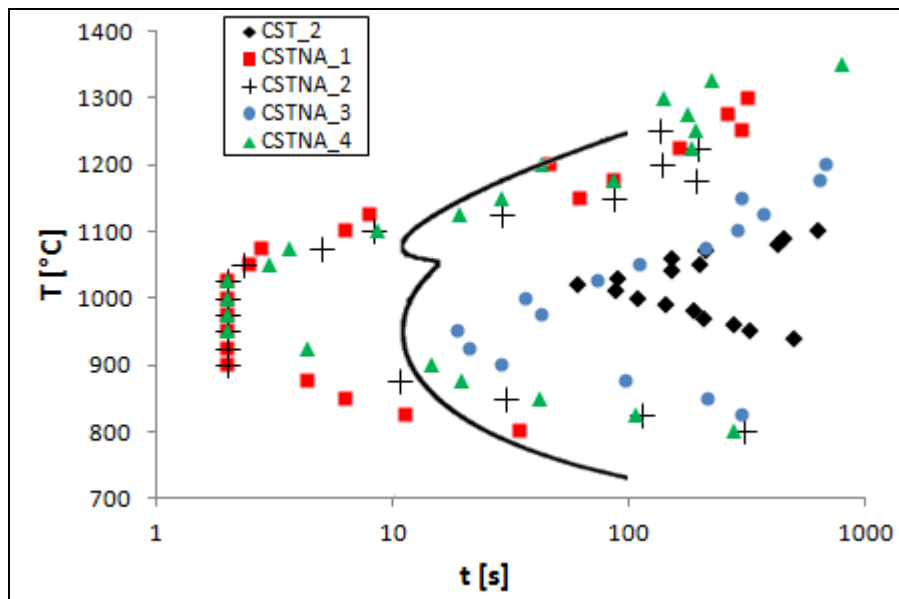


**Figure 3.** TTT diagrams for slags in the CaO-SiO<sub>2</sub>-TiO<sub>2</sub>-Na<sub>2</sub>O-Al<sub>2</sub>O<sub>3</sub> system (compositions in Table 1) obtained from SHTT and for a F-bearing industrial slag [5] (continuous line also obtained from SHTT).

With this new finding, i.e., the fact that there is a great increase of the crystallisation rate when adding Na<sub>2</sub>O in the CaO-SiO<sub>2</sub>-TiO<sub>2</sub> system, other slags were produced with lower Na<sub>2</sub>O content to study the possibility of controlling the crystallisation: CSTNA\_2, CSTNA\_3, and CSTNA\_4. The TTT diagrams for the CSTNA slags show that it is possible to control the crystallisation tendency changing the Na<sub>2</sub>O content in CaO-SiO<sub>2</sub>-TiO<sub>2</sub> slags.

It was observed for all the slags that the morphology of the crystals varies with temperature. Columnar grains (which seem to grow unidirectionally from surface to centre of the sample) and equiaxed grains (which seem to grow radially in the liquid slag) were observed. The crystals show dendritic structure at higher temperatures and become small and dense at lower temperatures. For these last crystals, which are formed in the middle of the liquid slag for higher degree of undercooling, they can be explained by homogeneous nucleation.

Na<sub>2</sub>O also has an important role regarding mould slag viscosity. It is known that the lower the viscosity the easier the crystallisation. It was observed that (i) when adding TiO<sub>2</sub> in a CaO-SiO<sub>2</sub> slag (43.3 %CaO, 56.7 %SiO<sub>2</sub>), the viscosity decreases for all the range of temperatures, and (ii) afterwards, when adding Na<sub>2</sub>O in a CaO-SiO<sub>2</sub>-TiO<sub>2</sub> slag (36,4 %CaO, 45,9 %SiO<sub>2</sub>, 17,7 %TiO<sub>2</sub>) obtaining in this way a CaO-SiO<sub>2</sub>-TiO<sub>2</sub>-Na<sub>2</sub>O slag (33.5 %CaO, 41.9 %SiO<sub>2</sub>, 16.3 %TiO<sub>2</sub>, 8.2 %Na<sub>2</sub>O, 0.1 %Al<sub>2</sub>O<sub>3</sub>) the viscosity decreases more, for all the range of temperatures, and the slope of the curve becomes lower.



Industrial mould slags would be more complex than the CSTNA slags, since they have more components. Anyway, the present study can be used as a reference for future developments when designing fluorine-free mould powders for slab casting, where the control of crystallisation is imperative.

#### *Critical cooling rates*

The critical cooling rates ( $R_c$ ) for the slags studied using the SHTT were determined. They were calculated by obtaining  $T_{nose}$  and  $t_{nose}$  from the TTT curves and calculating  $T_{liquidus}$  using FactSage 6.1. The influence of sodium on increasing critical cooling rate is clear; the higher the sodium content is, the higher the critical cooling rate becomes.

Because the cooling rates during continuous casting range from less than 1 °C/s to 100 °C/s [2, 43], it can be concluded that for Na<sub>2</sub>O-bearing slags with higher sodium content (CSTNA\_1, CSTNA\_2, CSTNA\_4) crystallisation during cooling cannot be avoided.

#### *Kinetics of crystal growth*

The kinetics of crystal growth for the CST\_2 and CSTNA\_1 slags (composition in Table 1) were analysed. The overall crystallisation can be described by determining the volume fraction of the transformed phase during isothermal transformation,  $\zeta(t)$ . Images were obtained from videos files and from these images the area of the crystallised fraction was measured using a software program. The particles were treated as spheres. For the CST\_2 slag the Avrami equation obtained at 1070 °C is

$$\zeta(t) = 1 - \exp(-0.00135t^{1.57}).$$

For the slag CSTNA\_1, during isothermal transformation at different temperatures, the results are summarised in Figure 4.

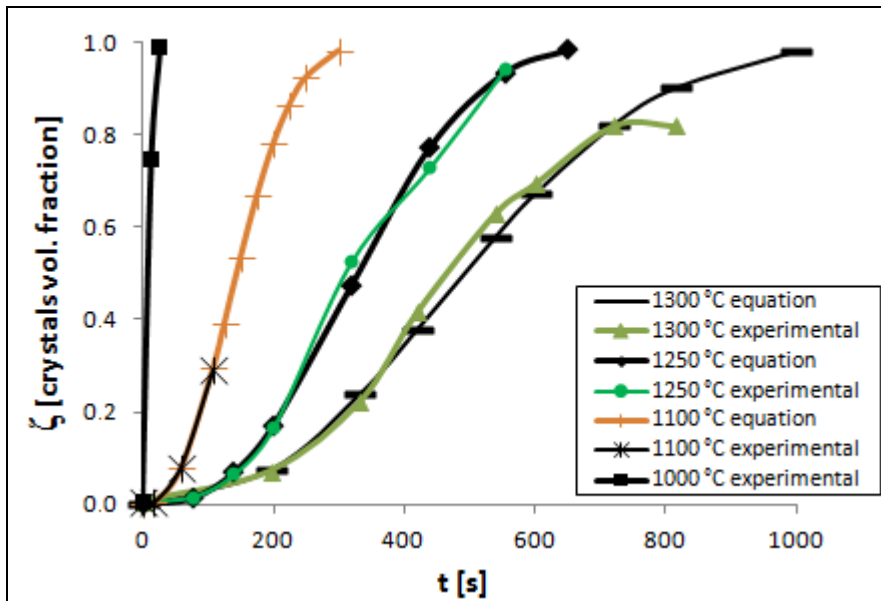


**Figure 4.** Crystals volume fraction versus time for the isothermal transformation at different temperatures, for the slag CSTNA\_1.

The CST\_2 slag presents complex crystallisation behaviour, i.e., more than one crystal phase, with different morphologies that seem to be a combination of bulk and surface crystallisation. In this case, the physical meaning of the values of  $n$  and  $K$  of the Avrami equation obtained from numerical fitting is unknown. Thus, it is not possible to obtain information regarding the transformation mechanism, which makes it unclear whether the crystal growth is controlled by the interface or by diffusion. For the CSTNA slags, similar ambiguities arise.

The Avrami parameter  $n$  obtained from the sole use of numerical fits represents an average and can provide misleading interpretations for the phase transformation mechanism [62]. The JMAK theory can be shown to be exact within the framework of its assumptions. Any violation must be a result of applying it to situations in which its assumptions are violated, which may be the case in many crystallisation situations. It was demonstrated that it is required extra, detailed knowledge on the transformation mechanism to apply the JMAK theory, describing the transformation kinetics [39].

#### *Solidification behaviour of fluorine-free mould powders for billet casting*

The choice of the mould powder for billet casting is very important in the achievement of a successful casting practice. Since the powder consumption demands for billet casting are not stringent, steelmakers frequently use high viscosity mould powders to overcome problems such as slag entrapment and SEN (Submerged Entry Nozzle) erosion [1, 65].

Laboratory tests were performed with new fluorine-free recipes [67]. From these laboratory tests the new mould powder Accutherm ST-SP/512SV-DS-1 (herein referred to as “F-free”) was produced as granulated mould powder to replace the commercial Accutherm ST-SP/512SV-DS (herein referred to as “F-bearing”), which is

produced by Stollberg Group and used at steelworks for billet casting. Industrial trials were performed using the new F-free mould powder.

The performance of the new F-free mould powder in laboratory and in industrial tests can be summarised in the following:

(i) From laboratory tests it was concluded that the technological parameters are similar considering the standard F-bearing and the F-free mould powder: melting characteristics, viscosity, melting behaviour, and crystallisation tendency.

(ii) From tests at steelworks, during the continuous casting process some evaluations were made considering the following:  $\Delta T$  between water cooling inlet and outlet, slag pool thickness, billet temperature before straightener, melting performance, powder consumption, mould slag  $\text{Al}_2\text{O}_3$  pick-up. The behaviour of the F-free mould powder was considered adequate. Besides, a significant reduction of SEN erosion was registered.

(iii) The %scrap produced during rolling process for the F-free mould powder was not critical, indicating good surface quality.

(iv) More industrial tests are required to check the results reported in the present work.

### Conclusions

The following conclusions were obtained in the present work:

(i) The apparatus used for the Hot Thermocouple Technique – Single Hot Thermocouple Technique (SHTT) and Double Hot Thermocouple Technique (DHTT) – is accurate, according to the calibration that was performed using  $\text{CaF}_2$ ,  $\text{Na}_2\text{SO}_4$  and  $\text{K}_2\text{SO}_4$ .

(ii) By in situ observation using the SHTT the crystallisation behaviour of slags can be characterized, building time-temperature-transformation (TTT) or continuous-cooling-transformation (CCT) diagrams.

(iii) The CCT diagram constructed for the basic slag CA – 44 %CaO , 56 % $\text{Al}_2\text{O}_3$  (wt%) – showed large differences between *liquidus* temperature and the temperature for first crystals precipitation, even at low cooling rates, e.g., 168 °C below the *liquidus* temperature when cooling at a rate of 6 °C/min. In addition, for this slag a correspondence between break temperature obtained from viscometer and crystallisation temperature obtained from SHTT was found.

(iv) For the CS slag – %CaO/% $\text{SiO}_2$  (wt%) = 0.7 –, during isothermal experiments crystallisation was observed only at 1000 °C with an incubation time of 76 seconds (average of 6 experiments, standard deviation 27 seconds). For experiments with continuous cooling rates, no crystal is detected, even at low cooling rates (e.g., 10 °C/min). However, when increasing the temperature after reaching lower temperatures (< 1000 °C), intense crystallisation is observed; this may be explained by the fact that the optimum range of temperatures required for crystal nucleation is lower than the optimum range of temperatures required for crystal growth.

(v) For the CST\_1 slag (41.1 %CaO, 29.1 %SiO<sub>2</sub>, 29.8 %TiO<sub>2</sub> (wt%)), that has a high *liquidus* temperature (approximately 1600 °C), the effect of the duration of superheating (in the range 1650 °C - 1680 °C) on incubation time was studied. It was found that the longer the superheating is, the longer the incubation times become, i.e., the duration of superheating – for a slag that seems to be completely liquid – can strongly affect a slag's crystallisation behaviour. This may be explained by the fact that the invisible nuclei diminish more slowly than grains of measurable size (in the µm range).

(vi) It was observed that the addition of Na<sub>2</sub>O in CaO-SiO<sub>2</sub>-TiO<sub>2</sub> slags dramatically shortens the crystals' incubation times, as shown in TTT diagrams, to the range of seconds. There is a clear effect of the %Na<sub>2</sub>O content on the critical cooling rate. It is possible to control the crystallisation kinetics in CaO-SiO<sub>2</sub>-TiO<sub>2</sub> slags by changing the Na<sub>2</sub>O content.

(vii) The slag CST\_2 presents complex crystallisation behaviour: more than one crystal phase, with different morphologies, which seem to be a combination of bulk and surface crystallisation. In this case, the physical meaning of the values of *n* and *K* of the Avrami equation obtained from numerical fitting is unknown. For the CSTNA slags, similar ambiguities arise.

(viii) The morphology of crystals varies with temperature. For CSTNA slags columnar grains (which seem to grow unidirectionally from surface to centre of the sample) and equiaxed grains (which seem to grow radially in the liquid slag) were observed. The crystals have dendritic appearance at higher temperatures and become small and dense at lower temperatures. When the temperature is low (< 900 °C) the crystals are very fine and the density of crystals increases until it appeared "cloud-like".

(ix) A new fluorine-free mould powder for billet casting was developed by collaboration between universities, mould powder supplier and steel plant. Laboratory tests showed that the technological parameters for both, the commercial F-bearing mould powder and the new F-free mould powder, are similar. The crystallisation tendency for both is similar. From the tests performed at steelworks it was reported that comparable surface quality for the billets was obtained when using the F-free mould powder.

## RESUMO ESTENDIDO

No processo de lingotamento contínuo, é importante entender e controlar os fenômenos que ocorrem no molde durante a produção de aço. A presença de cristais em escórias de molde tem efeito decisivo, tanto na lubrificação como na taxa de transferência de calor entre o molde e a casca sólida de aço em formação.

Considerando o desenvolvimento de escórias de molde sem flúor para o lingotamento de placas e para o lingotamento de placas finas, o controle da cristalização é muito importante. Assim, o comportamento de cristalização de escórias de molde deve ser caracterizado. Diagramas TTT (transformação-tempo-temperatura) ou CCT (transformação em resfriamento contínuo) permitem um entendimento fundamental da cinética de transformação. Esses diagramas podem ser construídos utilizando a técnica Single Hot Thermocouple Technique (SHTT).

O principal problema relacionado ao desenvolvimento de escórias de molde sem flúor é efetivamente controlar a transferência de calor entre a casca sólida de aço em formação e o molde. Em pós fluxantes industriais que contêm flúor, promover a cristalização de cuspidina na escória de molde é aceita como a forma mais eficaz para controlar a transferência horizontal de calor. Embora o mecanismo de controle da transferência de calor através da cristalização da fase cristalina cuspidina ainda não tenha sido determinado, duas idéias tem sido propostas. A primeira idéia diz que o fluxo de calor via radiação é diminuído por dispersão entre a camada cristalina e a camada de escória líquida. A segunda idéia diz que o fluxo total de calor é reduzido pela maior resistência térmica dos vãos de ar, que são formados como resultado da contração durante a solidificação da escória. De qualquer forma, a cristalização de cuspidina a partir da escória líquida tem grande efeito no controle da transferência de calor [26].

Há diversos trabalhos na literatura mostrando possibilidades para substituir o cristal cuspidina por outros cristais, mantendo o controle da transferência de calor. Alguns trabalhos indicam que matérias-primas contendo  $\text{TiO}_2$  podem ser utilizadas, formando cristais de  $\text{TiO}_2$  [26, 28, 29]. Além disso, há também outros trabalhos sobre o comportamento de solidificação de escórias de molde sem flúor ou com relativamente baixo teor de flúor, estudando diversos cristais, tais como  $\text{Na}_2\text{O} \cdot \text{CaO} \cdot 3\text{SiO}_2$  [30];  $\text{Na}_2\text{O} \cdot 2\text{CaO} \cdot 3\text{SiO}_2$  [33];  $\text{CaSiO}_3$ ,  $\text{Ca}_3\text{Si}_2\text{O}_7$  e  $\text{Ca}_2\text{SiO}_4$  [31] e  $\text{CaB}_2\text{SiO}_7$  e  $\text{CaAl}_{14}\text{B}_2[\text{SiO}_4]_8$  [34].

A motivação para o presente trabalho é prover informações fundamentais sobre controle de cristalização, para o desenvolvimento de escórias de molde sem flúor para o lingotamento contínuo de aço, estudando o comportamento de cristalização de escórias através da técnica Single Hot Thermocouple Technique (SHTT).

Os objetivos são os seguintes:

(i) Realizar um estudo básico e sistemático para avaliar o comportamento de cristalização de escórias nos sistemas  $\text{CaO-Al}_2\text{O}_3$ ,  $\text{CaO-SiO}_2$ ,  $\text{CaO-SiO}_2\text{-TiO}_2$ , e  $\text{CaO-SiO}_2\text{-TiO}_2\text{-Na}_2\text{O}$ , construindo curvas TTT e CCT;

(ii) Estudar o comportamento de solidificação de uma nova escória de molde industrial sem flúor, para ser utilizada em siderúrgica durante o lingotamento contínuo de tarugos.

### **Trabalho experimental**

A técnica SHTT é um aparato único, que permite medir a temperatura de uma amostra de escória utilizando um termopar, ao mesmo tempo em que a amostra é aquecida pelo próprio termopar. A amostra é posicionada sobre a ponta de um termopar, e pode ser submetida a altas taxas de resfriamento ou aquecimento, ou ser mantida em condições isotérmicas. A vantagem da SHTT é o fato de que é possível observação *in situ* da fusão e solidificação sob diversas condições térmicas. Devido à baixa capacidade térmica do sistema (amostra e termopar) altíssimas taxas de aquecimento e resfriamento podem ser facilmente obtidas (> 3000°C/min). A SHTT pode ser aplicada a escórias que são transparentes ou translúcidas, enquanto que a fase cristalina que precipita ao se resfriar a amostra deve ser opaca.

As escórias utilizadas no presente trabalho, para a SHTT, foram produzidas a partir de materiais *reagent grade*: CaCO<sub>3</sub>, SiO<sub>2</sub>, TiO<sub>2</sub>, Na<sub>2</sub>CO<sub>3</sub> e Al<sub>2</sub>O<sub>3</sub>. A Tabela 1 mostra as suas composições.

**Tabela 1.** Composições das escórias utilizadas para análises com a SHTT (wt%). B é %CaO/%SiO<sub>2</sub>.

	%CaO	%SiO <sub>2</sub>	%TiO <sub>2</sub>	%Na <sub>2</sub> O	%Al <sub>2</sub> O <sub>3</sub>	%C	B
CA	43.7				56.3	0.074	
CS	41.7	58.3				0.063	0.7
CST_1	41.1	29.1	29.8			-	1.4
CST_2	35.6	46.3	18.1			0.590	0.8
CSTNA_1	33.6	41.3	16.5	7.1	1.5	0.073	0.8
CSTNA_2	30.1	46.8	16.4	5.4	1.3	0.034	0.6
CSTNA_3	31.6	48.1	15.5	3.7	1.1	0.032	0.7
CSTNA_4	30.9	42.3	15.2	6.4	5.2	0.038	0.7

O aparato utilizado no presente trabalho foi construído na Technische Universität Bergakademie Freiberg [43]; ver Figura 1. O aparato consiste de dois sistemas: um sistema de observação e um sistema de termopares. Em uma câmara de vácuo, há duas barras refrigeradas a água, uma na esquerda e outra na direita. Na ponta de cada uma das barras é inserido um termopar tipo B. Cada termopar é conectado a um diferente sistema de controle. O material sob estudo é fundido diretamente na ponta do termopar dentro de uma câmara de vácuo. Os termopares permanecem dentro de um elemento de aquecimento extra (uma espiral de kanthal), que reduz as perdas de calor da amostra para os arredores, mantendo temperaturas em torno de 500 °C próximo à amostra.

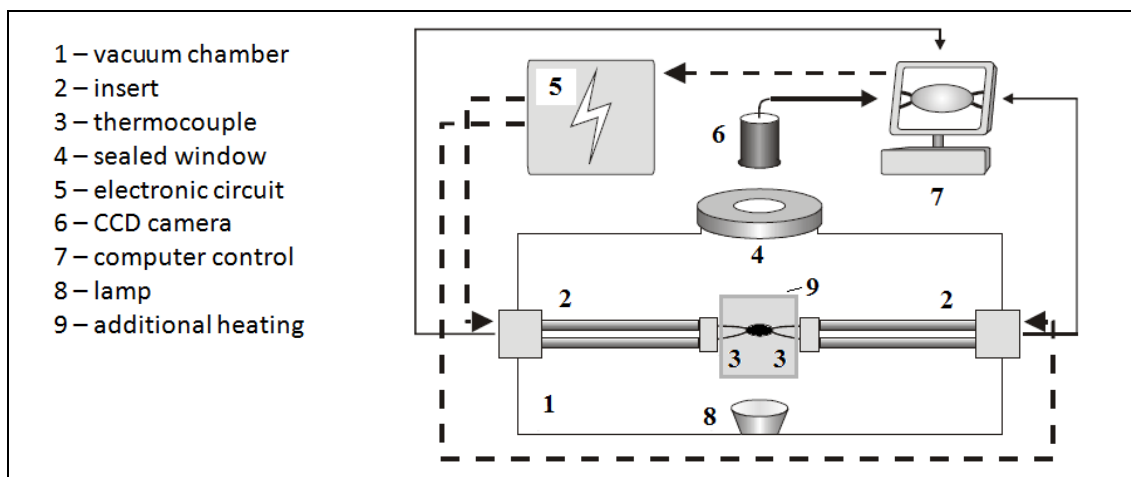


**Figura 1.** Diagrama esquemático do aparato experimental utilizado no presente trabalho.

O termopar tipo B (até 1800 °C) é construído utilizando dois fios de platina com 0.5 mm de diâmetro e aproximadamente 25 mm de comprimento: Pt30Rh and Pt6Rh.

A precisão do aparato foi verificada medindo a temperatura de cristalização ( $T_{\text{cryst.}}$ ) de  $\text{CaF}_2$ ,  $\text{Na}_2\text{SO}_4$  e  $\text{K}_2\text{SO}_4$ . A  $T_{\text{cryst.}}$  é definida aqui como a temperatura na qual os primeiros cristais podem ser observados em uma taxa de resfriamento específica. Com as substâncias na câmara de vácuo, uma pressão de 10 mbar durante 5 minutos é aplicada. Então, a câmara é preenchida com Ar, mantendo fluxo de 300 L/h durante os experimentos. Em seguida, as substâncias foram fundidas 100 °C acima dos seus pontos de fusão, e resfriadas a uma taxa de 30 °C/min. Seus pontos de fusão são  $\text{CaF}_2$  - 1418 °C,  $\text{Na}_2\text{SO}_4$  - 884 °C, e  $\text{K}_2\text{SO}_4$  - 1069 °C [44].

A Figura 2 mostra as diferenças entre os pontos de fusão da literatura [44] e  $T_{\text{cryst.}}$ . Doze experimentos foram realizados para cada substância (os experimentos 1-6 para o termopar do lado esquerdo, e os experimentos 7-12 para o termopar do lado direito).

Assumindo uma distribuição normal para  $\Delta T_{\text{cryst.}}$ , os valores médios da  $T_{\text{cryst.}}$  para as três substâncias utilizadas para calibração podem ser calculados; ver Tabela 2. Os valores médios da  $T_{\text{cryst.}}$  são muito próximos dos pontos de fusão reportados na literatura, e o desvio padrão é baixo.

**Tabela 2.** Comparação entre os pontos de fusão reportados na literatura [44] e as temperaturas de cristalização medidas com a SHTT ( $T_{\text{cryst.}}$ ). Para cada substância, 12 medidas foram realizadas.

	p. f. literatura [44]	média $T_{\text{cryst.}}$	desvio-padrão $T_{\text{cryst.}}$
$\text{CaF}_2$	1418 °C	1417 °C	10.6 °C
$\text{Na}_2\text{SO}_4$	884 °C	883 °C	6.6 °C
$\text{K}_2\text{SO}_4$	1069 °C	1071 °C	15.4 °C

Os resultados sumarizados na Tabela 2 foram obtidos através de análise de arquivos de vídeo. O aparato também registra a evolução da temperatura com o

tempo, de uma forma similar à análise térmica diferencial (DTA). Foi verificado durante a calibração que a visualmente observada cristalização corresponde a picos em diagramas T versus t.

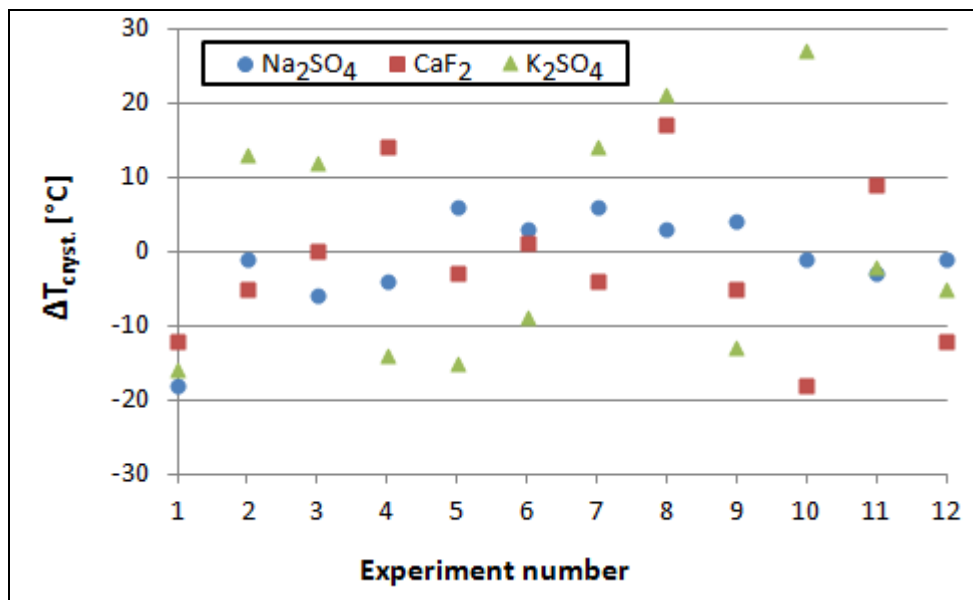


**Figura 2.** Comparação entre resultados da literatura [44] e os resultados do presente trabalho.  $\Delta T_{\text{cryst.}}$  é a diferença entre o ponto de fusão da literatura e a temperatura de cristalização que foi medida via SHTT.

Observou-se que é importante aplicar períodos adequados de vácuo, no caso desse aparato aproximadamente 10 mbar durante 5 minutos, antes dos experimentos. Ao se trabalhar com períodos mais curtos, por exemplo 1 minuto a 10 mbar, as temperaturas de cristalização de  $\text{CaF}_2$  tendem a estar fora do intervalo  $1418 \pm 20$   $^{\circ}\text{C}$ , provavelmente devido à reação entre vapor de água e  $\text{CaF}_2$ .

Para executar os experimentos utilizando a SHTT pequenas porções de escórias pré-fundidas (5-10 mg) são prensadas e posicionadas nas pontas dos termopares. Com as substâncias na câmara de vácuo, uma pressão de 10 mbar é aplicada durante 5 minutos. Então, a câmara é preenchida com Ar, mantendo-se um fluxo de 300 L/h durante as medições. O elemento de aquecimento adicional é ligado, mantendo uma temperatura de aproximadamente 500  $^{\circ}\text{C}$  em torno do termopar.

Para produzir diagramas TTT (transformação-tempo-temperatura), após a fusão taxas de resfriamento bastante altas (maiores que 3000  $^{\circ}\text{C}/\text{min}$ ) são aplicadas até a temperatura desejada. Em seguida, o tempo de incubação, isto é, o tempo necessário para obter os primeiros cristais, é medido via observação direta. Com os tempos de incubação para diferentes temperaturas, diagramas TTT são construídos. Para criar diagramas CCT (transformação em resfriamento contínuo), após a fusão uma específica taxa de resfriamento é aplicado. Em seguida, o comportamento de



solidificação é observado. Utilizando diferentes taxas de resfriamento, uma curva CCT pode ser construída.

Medidas de viscosidade foram realizadas utilizando um viscosímetro rotativo (Anton Paar MC 301) na Technische Universität Bergakademie Freiberg. Os materiais utilizados para essas medições possuem composições próximas às das escórias utilizadas para as análises com a SHTT (cujas composições estão na Tabela 1).

## **Resultados e discussão**

### *Escória CaO-Al<sub>2</sub>O<sub>3</sub> (CA)*

A escória CaO-Al<sub>2</sub>O<sub>3</sub> denominada CA, contendo 43.7% CaO and 56.3% Al<sub>2</sub>O<sub>3</sub>, foi estudada com a SHTT. A temperatura *liquidus* para essa escória de acordo com FactSage 6.1 é 1518 °C, e o primeiro cristal durante o resfriamento é CaAl<sub>2</sub>O<sub>4</sub>. O segundo cristal durante o resfriamento é Ca<sub>3</sub>Al<sub>2</sub>O<sub>6</sub>, que precipita a 1362 °C (temperatura *solidus*).

Um diagrama CCT foi construído para a escória CA através da SHTT. As amostras foram mantidas a 1700 °C durante 60 segundos antes do resfriamento, a diferentes taxas de resfriamento. Observou-se que a cristalização começa distante da *liquidus*. A temperatura de cristalização (ou seja, a temperatura na qual os primeiros cristais são observados) é função da taxa de resfriamento. A taxa de resfriamento crítica para a escória CA é 1700 °C/min, ou seja, com taxas de resfriamento mais elevadas nenhum cristal é observado. Para baixas taxas de resfriamento em alguns segundos a amostra é 100% cristalina.

A partir das medidas de viscosidade observa-se que a *break temperature*, ou seja, o ponto no qual há um repentino aumento da viscosidade devido à precipitação de cristais, está no intervalo 1350 - 1375 °C. De acordo com a SHTT o ponto no qual os primeiros cristais são detectados para a escória CA na taxa de resfriamento de 6 °C/min é 1350 °C. Dessa forma, há para essa escória uma correspondência entre a *break temperature* obtida do viscosímetro e a temperatura de cristalização obtida através da SHTT.

### *Escória CaO-SiO<sub>2</sub> (CS)*

A escória CaO-SiO<sub>2</sub> com basicidade %CaO/%SiO<sub>2</sub> = 0.7, denominada como CS, tem as seguintes características de acordo com FactSage 6.1: temperatura *liquidus*, 1500 °C; primeira fase sólida durante resfriamento, CaSiO<sub>3</sub>; e temperatura *solidus*, 1437 °C, onde o segundo cristal (SiO<sub>2</sub>) precipita.

Considerando os experimentos CCT (resfriamento contínuo), cristalização não é observada mesmo a baixas taxas de resfriamento. Esse resultado está de acordo com outros resultados da literatura para escórias CaO-SiO<sub>2</sub> com basicidade 0.8, 1.0 e 1.2, onde também nenhum cristal foi observado em experimentos CCT [43].

Para experimentos TTT (transformação isotérmica), as amostras foram completamente fundidas e mantidas a 1700 °C durante 5 minutos. Em seguida, uma taxa de resfriamento muito alta (> 3000 °C/min) foi aplicada. Quando as temperaturas desejadas foram atingidas – 900 °C, 950 °C, 1000 °C, 1050 °C, 1100°C, 1150°C, e 1200 °C – as amostras foram mantidas nessas temperaturas por até 1000 segundos. Cristalização foi observada somente a 1000 °C, ocorrendo em 76 segundos (média de 6 experimentos, desvio-padrão 27 segundos).

Além dos experimentos CCT e TTT, um ciclo térmico especial foi aplicado: (i) amostra mantida a 1700 °C durante 5 minutos, ou seja, completamente fundida; (ii) resfriamento rápido (> 3000 °C/min) para determinadas temperaturas (900 °C, 950 °C, 975 °C, 1000 °C, 1025 °C, 1050 °C, 1100°C, 1150 °C, 1200 °C, e 1300 °C); (iii) manutenção na temperatura específica por 60 segundos, e (iv) reaquecimento a uma taxa de 1000 °C/min até 1700 °C.

Considerando o ciclo térmico especial supracitado, intensa cristalização foi observada durante aquecimento na taxa de 1000 °C/min, mas somente ao começar o aquecimento (após o resfriamento rápido) a 1000 °C ou a temperaturas mais baixas. A cristalização ocorre intensamente no intervalo 1069 - 1125 °C ao se começar a 900 °C, 950 °C, 975 °C, e 1000 °C. Desse forma, é evidente que ao se aumentar a temperatura após atingir determinados intervalos de baixas temperaturas, boas condições para o crescimento de cristais podem ser obtidas para escórias CS. Essa intensa cristalização pode ser explicada pelo fato de que o intervalo ótimo de temperaturas para a nucleação de cristais é mais baixo do que o intervalo ótimo de temperaturas para o crescimento de cristais. Isso está relacionado ao fato de que a taxa de crescimento de cristais não é o único fator que determina a habilidade da escória líquida de formar cristais, porque cristais crescem a partir de um certo número de núcleos, e em muitos aspectos o estágio de nucleação determina a evolução do processo global de cristalização em silicatos [38]. Sabe-se que a cristalização pode ser dividida em dois processos: (i) formação de núcleos, e (ii) crescimento de cristais. As taxas de ambos os processos são dependentes da temperatura, com máximos a certos valores de super-resfriamento. Esses máximos são separados em materiais que são utilizados para a produção de vitro-cerâmicos, permitindo o controle da cristalização a partir de vidros [48].

A observação de cristais durante experimentos isotérmicos a 1000 °C para a escória CS é explicada pelo fato de que 1000 °C é uma temperatura intermediária, na qual tanto a taxa de nucleação como a taxa de crescimento são suficientemente elevadas.

#### *Escória CaO-SiO<sub>2</sub>-TiO<sub>2</sub> (CST\_1)*

A escória do sistema CaO-SiO<sub>2</sub>-TiO<sub>2</sub>, aqui denominada como CST\_1, foi utilizada para estudar o efeito da duração do super-aquecimento nos tempos de incubação. A composição (wt%) da CST\_1 é 41.1 %CaO, 29.1 %SiO<sub>2</sub>, e 29.8 %TiO<sub>2</sub>. A temperatura

*liquidus* para essa escória é muito alta, aproximadamente 1600 °C. A primeira fase formada durante o resfriamento a partir da escória líquida é  $\text{CaO}\cdot\text{TiO}_2$ .

Um ciclo térmico especial foi aplicado e repetido diversas vezes para cada amostra: (i) as amostras foram mantidas no intervalo de temperaturas 1650 °C - 1680 °C por diferentes períodos (as amostras sempre fundiram completamente e tornaram-se transparentes em alguns segundos); (ii) resfriamento rápido até 1400 °C na mais alta taxa de resfriamento (> 3000 °C/min); (iii) medida dos tempos de incubação, ou seja, quando os primeiros cristais podem ser observados; (iv) resfriamento até a temperatura de 1200 °C, que foi mantida por 60 segundos para garantir completa cristalização da amostra; (v) aquecimento até 1650 °C - 1680 °C.

Observou-se que a duração do super-aquecimento mudou completamente o comportamento de cristalização da escória CST\_1, assumindo que as condições iniciais antes da fusão foram as mesmas. Quando o tempo de manutenção é 60 segundos, os tempos de incubação tendem a ser bem mais curtos (5-12 segundos) do que quando o tempo de manutenção é 600 segundos – nenhum cristal foi observado até 1000 segundos. Duas amostras foram analisadas, uma com massa de 1.4 mg e a outra com massa de 2.3 mg.

Sabe-se que uma nova fase é nucleada através de núcleos que já existem na fase antiga, e cujo número efetivo por unidade de volume pode ser alterado modificando a temperatura de super-aquecimento, e a duração do super-aquecimento. Há indicações de que, para um dado super-resfriamento ou super-aquecimento, os núcleos crescem ou diminuem bem mais lentamente do que grãos de tamanho visível. Esses núcleos, que podem ser heterogeneidades de qualquer tipo, seriam usualmente pequenas partículas da fase sub-crítica ou filmes da fase sub-crítica envolvendo inclusões de outros materiais [49].

Dessa forma, há uma relação entre duração do super-aquecimento, tempos de incubação, e número de núcleos. Quanto mais longo o super-aquecimento for, menor o número de núcleos por unidade de volume e, conseqüentemente, mais longos os tempos de incubação se tornam.

#### *Escória $\text{CaO-SiO}_2\text{-TiO}_2$ (CST\_2) e escórias $\text{CaO-SiO}_2\text{-TiO}_2\text{-Na}_2\text{O-Al}_2\text{O}_3$ (CSTNA)*

As composições das escórias CST\_2 e CSTNA podem ser vistas na Tabela 1.

O diagrama TTT da escória CST\_2, que foi construído utilizando a SHTT, é mostrado na Figura 3. É necessário que os cristais no sistema  $\text{CaO-SiO}_2\text{-TiO}_2$  precipitem como a fase cuspidina em pós fluxantes comerciais, substituindo o sistema  $\text{CaO-SiO}_2\text{-CaF}_2$ . No entanto, os tempos de incubação da escória CST\_2 são muito mais longos do que os da escória industrial que contém flúor, cujo diagrama TTT é também mostrado na figura – trata-se de um pó fluxante comercial normalmente empregado durante o lingotamento contínuo de aços inoxidáveis, o qual contém  $\text{CaF}_2$  e  $\text{Na}_2\text{O}$ , e não contém  $\text{TiO}_2$ .

A escória CSTNA\_1 foi projetada para ter basicidade e teor de  $\text{TiO}_2$  similares aos da escória CST\_2; o seu diagrama TTT é mostrado na Figura 3. A escória CSTNA\_1, que contém  $\text{Na}_2\text{O}$ , tem taxa de cristalização mais elevada.

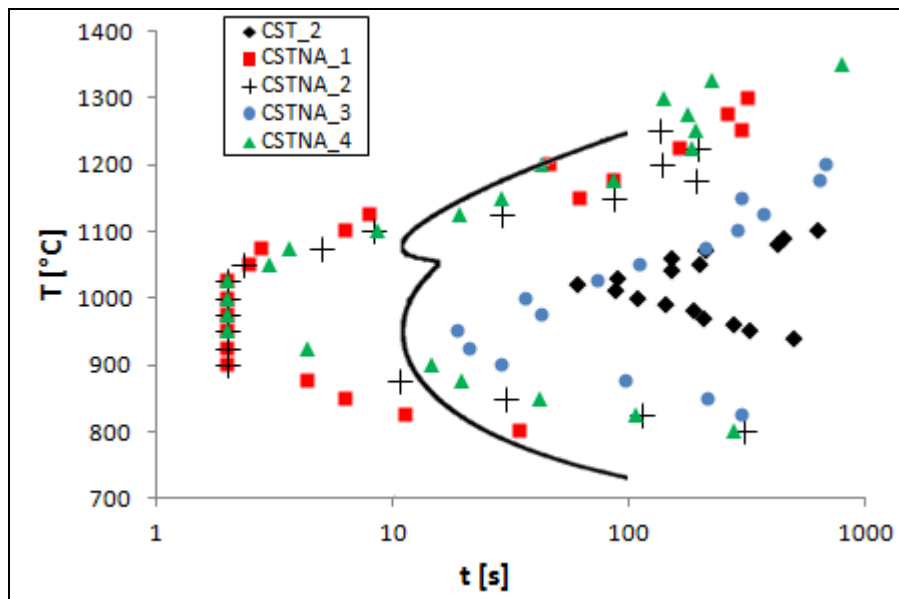


**Figura 3.** Diagramas TTT para escórias no sistema  $\text{CaO-SiO}_2\text{-TiO}_2\text{-Na}_2\text{O-Al}_2\text{O}_3$  (composições na Tabela 1) obtidas através da SHTT e para uma escória industrial que contém flúor [5] (linha contínua obtida também através da SHTT).

Com esse novo resultado, ou seja, o fato de que há um grande aumento da taxa de cristalização ao se adicionar  $\text{Na}_2\text{O}$  no sistema  $\text{CaO-SiO}_2\text{-TiO}_2$ , outras escórias foram produzidas com teor de  $\text{Na}_2\text{O}$  mais baixos para estudar a possibilidade de controlar a cristalização: CSTNA\_2, CSTNA\_3, e CSTNA\_4. Os diagramas TTT das escórias CSTNA mostram que é possível controlar a tendência à cristalização modificando o teor de  $\text{Na}_2\text{O}$  em escórias  $\text{CaO-SiO}_2\text{-TiO}_2$ .

Observou-se para todas as escórias que a morfologia dos cristais varia com a temperatura. Grãos colunares (que crescem unidirecionalmente da superfície para o centro da amostra) e grãos equiaxiais (que crescem radialmente na escória líquida) foram observados. Os cristais têm estrutura dendrítica nas temperaturas mais elevadas e se tornam pequenos e densos em temperaturas mais baixas. Para esses últimos, que se formam no meio da escória líquida em maior nível de super-resfriamento, eles podem ser explicados considerando nucleação homogênea.

$\text{Na}_2\text{O}$  também tem um papel importante em relação à viscosidade da escória de molde. Sabe-se que quanto mais baixa a viscosidade mais fácil é a cristalização. Observou-se que (i) ao se adicionar  $\text{TiO}_2$  em uma escória  $\text{CaO-SiO}_2$  (43.3 % $\text{CaO}$ , 56.7 % $\text{SiO}_2$ ) a viscosidade diminui para todo o intervalo de temperaturas, e que (ii) ao se adicionar em seguida  $\text{Na}_2\text{O}$  em uma escória  $\text{CaO-SiO}_2\text{-TiO}_2$  (36.4 % $\text{CaO}$ , 45.9 % $\text{SiO}_2$ , 17.7 % $\text{TiO}_2$ ) obtendo-se dessa forma uma escória  $\text{CaO-SiO}_2\text{-TiO}_2\text{-Na}_2\text{O}$  (33.5 % $\text{CaO}$ , 41.9 % $\text{SiO}_2$ , 16.3 % $\text{TiO}_2$ , 8.2 % $\text{Na}_2\text{O}$ , 0.1 % $\text{Al}_2\text{O}_3$ ) a viscosidade diminui ainda mais, para todo o intervalo de temperaturas, e a inclinação da curva se torna menor.

Escórias de molde industriais seriam mais complexas do que as escórias CSTNA, porque têm maior número de componentes. De qualquer forma, o presente estudo pode ser utilizado como uma referência para desenvolvimentos futuros ao se projetar pós fluxantes sem flúor para o lingotamento de placas, onde o controle da cristalização é imperativo.

#### *Taxas de resfriamento críticas*

As taxas de resfriamento críticas ( $R_c$ ) para as escórias estudadas com a SHTT foram determinadas. Elas foram calculadas obtendo-se  $T_{nose}$  and  $t_{nose}$  das curvas TTT e calculando  $T_{liquidus}$  com FactSage 6.1. A influência do sódio no aumento da taxa de resfriamento crítico é clara; quando mais alto o teor de sódio, mais alta se torna a taxa de resfriamento crítico.

Devido ao fato de que as taxas de resfriamento durante o lingotamento contínuo variam de menos de 1 °C/s até 100 °C/s [2, 43], pode-se concluir que, para escórias que contêm teor relativamente mais alto de Na<sub>2</sub>O (CSTNA\_1, CSTNA\_2, CSTNA\_4), cristalização durante o resfriamento não pode ser evitada.

#### *Cinética do crescimento de cristais*

A cinética do crescimento de cristais para as escórias CST\_2 e CSTNA\_1 (composição na Tabela 1) foi analisada. A cristalização global pode ser descrita determinando-se a fração de volume de fase transformada durante a transformação isotérmica,  $\zeta(t)$ . Imagens foram obtidas de arquivos de vídeo e a partir dessas imagens a área da fração de fase cristalina foi medida através de um programa de computador. As partículas foram tratadas como esferas. Para a escória CST\_2 a equação de Avrami obtida a 1070 °C é

$$\zeta(t) = 1 - \exp(-0.00135t^{1.57}) .$$

Para a escória CSTNA\_1, os resultados para transformação isotérmica em diferentes temperaturas estão sumarizados na Figura 4.

A escória CST\_2 apresenta comportamento de cristalização complexo, ou seja, mais do que uma fase cristalina, com diferentes morfologias que parecem ser uma combinação de cristalização superficial e volumétrica. Nessa situação, o significado físico dos valores de  $n$  e  $K$  na equação de Avrami, obtidos através de ajuste numérico, é desconhecido. Assim, não é possível obter informações sobre o mecanismo de transformação; não é claro se o crescimento de cristais é controlado por difusão ou por interface. Para as escórias CSTNA, há questões similares.

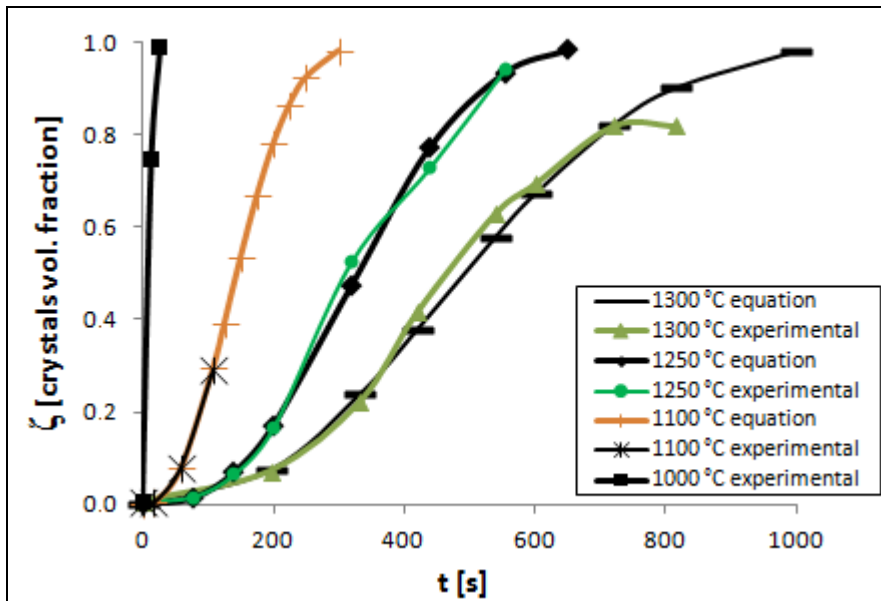


**Figura 4.** Fração volumétrica de cristais versus tempo na transformação isotérmica em diferentes temperaturas, para a escória CSTNA\_1.

O parâmetro de Avrami  $n$  obtido somente a partir de ajuste numérico representa uma média; interpretações equivocadas podem ser obtidas ao se considerar esse parâmetro, em relação ao mecanismo de transformação de fase [62]. A teoria JMAK é eficaz dentro de suas hipóteses. Resultados não previstos pela teoria acontecem quando ela é aplicada a situações em que suas hipóteses são violadas, o que pode acontecer em muitas situações envolvendo cristalização. Tem sido demonstrado que é necessário conhecimento detalhado sobre o mecanismo de transformação para aplicar a teoria JMAK, para que a cinética da transformação seja descrita [39].

#### *Comportamento de solidificação de pós fluxantes sem flúor para o lingotamento de tarugos*

A escolha do pó fluxante para o lingotamento de tarugos é muito importante para o lingotamento contínuo. Visto que o consumo de pó fluxante no lingotamento de tarugos é relativamente baixo, nas aciarias frequentemente são utilizados pós fluxantes de alta viscosidade para lidar com problemas como arraste de escória e corrosão da válvula submersa [1, 65].

Testes de laboratório foram realizados com novas fórmulas sem flúor [67]. A partir desses testes laboratoriais o novo pó fluxante Accutherm ST-SP/512SV-DS-1 (aqui denominado como “F-free”) foi produzido na forma granulada, para substituir o pó fluxante comercial Accutherm ST-SP/512SV-DS (aqui denominado como “F-bearing”), que é utilizado pelo grupo siderúrgico Stollberg e utilizado em aciarias para o lingotamento de tarugos. Testes industriais foram realizados utilizando o novo pó fluxante sem flúor.

A performance do novo pó fluxante sem flúor em laboratório e em testes industriais pode ser resumida da seguinte forma:

(i) A partir dos testes de laboratório concluiu-se que os parâmetros tecnológicos são similares entre o pó fluxante padrão com flúor, e o pó fluxante sem flúor: temperaturas características, viscosidade, comportamento de fusão, e tendência à cristalização.

(ii) A partir dos testes em aciaria, durante o processo de lingotamento contínuo avaliações foram realizadas considerando o seguinte:  $\Delta T$  entre entrada e saída da água de resfriamento do molde, profundidade da piscina de escória líquida, temperatura do billet antes do endireitador, comportamento de fusão, consumo de pó, absorção de  $Al_2O_3$  pela escória de molde. O comportamento do pó fluxante sem flúor foi considerado adequado. Além disso, significativa redução do desgaste da válvula submersa foi registrado.

(iii) o %sucata produzido durante o processo de laminação usando o pó fluxante sem flúor não foi crítico, indicando boa qualidade superficial.

(iv) Mais testes industriais são necessários para confirmar os resultados do presente trabalho.

### **Conclusões**

As seguintes conclusões foram obtidas no presente trabalho:

(i) O aparato utilizado para a Hot Thermocouple Technique – Single Hot Thermocouple Technique (SHTT) e Double Hot Thermocouple Technique (DHTT) – é preciso, de acordo com a calibração que foi realizada usando  $CaF_2$ ,  $Na_2SO_4$  e  $K_2SO_4$ .

(ii) Através de observação in situ utilizando a Single Hot Thermocouple Technique (SHTT) o comportamento de cristalização de escórias pode ser caracterizado, construindo diagramas time-temperature-transformation (TTT) ou diagramas continuous-cooling-transformation (CCT) diagrams.

(iii) o diagrama CCT construído para a escória simples CA – 44 %CaO , 56 % $Al_2O_3$  (wt%) – mostrou grandes diferenças entre a temperatura *liquidus* e a temperatura onde os primeiros cristais precipitam, mesmo a baixas taxas de resfriamento, por exemplo, 168 °C abaixo da temperatura *liquidus* ao se resfriar a uma taxa de 6 °C/min. Além disso, para essa escória encontrou-se uma correspondência entre a break temperature obtida com o viscosímetro e a temperatura de cristalização obtida com o SHTT.

(iv) Para a escória CS – %CaO/% $SiO_2$  (wt%) = 0.7 –, durante experimentos isotérmicos cristalização foi observada somente a 1000 °C com um tempo de incubação de 76 segundos (média de 6 experimentos, desvio-padrão 27 segundos). Para experimentos a resfriamento contínuo, nenhum cristal é detectado, mesmo a baixas taxas de resfriamento (por exemplo, 10 °C/min). No entanto, ao se aumentar a temperatura após atingir temperaturas mais baixas (< 1000 °C), intensa cristalização é observada; isso pode ser explicado pelo fato de que o intervalo ótimo de temperaturas

relacionado à nucleação de cristais é menor do que o intervalo ótimo de temperaturas relacionado ao crescimento de cristais.

(v) Para a escória CST\_1 (41.1 %CaO, 29.1 %SiO<sub>2</sub>, 29.8 %TiO<sub>2</sub> (wt%)), que possui alta temperatura *liquidus* (aproximadamente 1600 °C), o efeito da duração do super-aquecimento (no intervalo 1650 °C - 1680 °C) sobre os tempos de incubação foi estudado. Observou-se que quanto mais longo o super-aquecimento for, mais longos se tornam os tempos de incubação, ou seja, a duração do super-aquecimento – para uma escória que aparentemente é completamente líquida – pode afetar fortemente o comportamento de cristalização de uma escória. Isso pode ser explicado pelo fato de que núcleos invisíveis diminuem de tamanho mais lentamente do que grãos maiores (na ordem de μm).

(vi) Observou-se que a adição de Na<sub>2</sub>O em escórias CaO-SiO<sub>2</sub>-TiO<sub>2</sub> diminui drasticamente os tempos de incubação dos cristais, como pode ser visto nos diagramas TTT, para a escala de segundos. Há um claro efeito do teor de %Na<sub>2</sub>O na taxa de resfriamento crítica. É possível controlar a cinética de cristalização em escórias CaO-SiO<sub>2</sub>-TiO<sub>2</sub> modificando o teor de Na<sub>2</sub>O.

(vii) A escória CST\_2 apresenta comportamento de cristalização complexo: mais do que uma fase cristalina, com diferentes morfologias, que aparentemente são uma combinação de cristalização superficial e volumétrica. Nesse caso, o significado físico dos valores de *n* e de *K* da equação de Avrami obtidos a partir de ajuste numérico são desconhecidos. Para as escórias CSTNA, há questões similares.

(viii) A morfologia de cristais varia com a temperatura. Para escórias CSTNA grão colunares (que crescem unidirecionalmente da superfície para o centro da amostra) e grãos equiaxiais (que crescem radialmente na escória líquida) foram observados. Os cristais têm aparência dendrítica em temperaturas mais elevadas e se tornam pequenos e densos em temperaturas mais baixas. Quando a temperatura é baixa (< 900 °C) os cristais são muito finos e a densidade dos cristais aumenta até terem “aspecto de nuvem”.

(ix) Um novo pó fluxante sem flúor para o lingotamento de tarugos foi desenvolvido através de uma colaboração entre universidades, fabricante de pó fluxante e usina siderúrgica. Testes de laboratório mostraram que os parâmetros tecnológicos para ambos – o pó fluxante comercial que contém flúor e o novo pó fluxante sem flúor – são similares. A tendência à cristalização para ambos os pós fluxantes é similar. A partir dos testes realizados em usina siderúrgica observou-se que ao se utilizar o pó fluxante sem flúor qualidade superficial comparável foi obtida para os lingotes produzidos.



## ERWEITERTER ABSTRACT

Ein gutes Verständnis und die Kontrolle von Phänomenen in der Gießform während der Stahlproduktion sind für das Gelingen des kontinuierlichen Gießprozesses erforderlich. Die Gegenwart von Kristallen in Gießschlacken hat sowohl auf die Schmierung als auch auf die Wärmeübergangsrate zwischen Gießform und Stahlstrang einen maßgeblichen Einfluss.

Bei Betrachtung der Entwicklung von Fluor-freien Gießpulvern für das Brammengießen und Dünnbrammengießen ist die Kontrolle der Kristallisation unumgänglich. Aus diesem Grund soll das Kristallisationsverhalten von Gießpulvern charakterisiert werden. Zeit-Temperatur-Umwandlungs-Schaubilder – „time-temperature-transformation“, TTT, oder „continuous-cooling-transformation“, CCT – liefern ein grundlegendes Verständnis der Umwandlungskinetik. Diese Diagramme können unter Anwendung der SHTT (Single Hot Thermocouple Technique) erstellt werden.

Das Hauptproblem bezüglich der Entwicklung von Fluor-freien Gießpulvern liegt in der effektiven Kontrolle des Wärmeübergangs zwischen der Strangschale und der Gießform. In industriellen fluorhaltigen Gießpulvern wird die Kristallisation von Cuspidin aus der Gießschlacke als effektivste Methode zur Kontrolle des Wärmeübergangs betrachtet. Obwohl der Mechanismus der Wärmeübergangskontrolle mithilfe der Kristallisation von Cuspidin noch nicht bestimmt wurde, wurden bereits zwei Ideen diesbezüglich vorgeschlagen. Eine Idee ist, dass der Fluss der Wärmestrahlung durch Streuung an der Grenzfläche zwischen den kristallinen und den flüssigen Schichten abgesenkt wird. Die andere Idee ist, dass der totale Wärmestrahlungsfluss durch den hohen thermischen Widerstand des Luftspaltes reduziert wird, wobei der Luftspalt Ergebnis des Schrumpfens bei Erstarrung der Schlackeschicht ist. In jedem Fall hat die Kristallisation von Cuspidin aus der Gießschlacke einen großen Einfluss auf die Kontrolle des Wärmeüberganges [26].

Einige Fachartikel berichten von Möglichkeiten, die Cuspidinphase durch die Bildung eines anderen Kristalles zu ersetzen, um die Kontrolle des Wärmeübergangs zu ermöglichen. Einige Artikel besagen, dass  $\text{TiO}_2$ -haltiges Rohmaterial unter Bildung von  $\text{TiO}_2$ -Kristallen verwendet werden kann [26, 28, 29]. Darüber hinaus gibt es andere Berichte bezüglich des Erstarrungsverhaltens von Gießschlacken ohne Fluor oder mit relativ niedrigen Fluorgehalten unter Verwendung verschiedener Kristalle wie beispielsweise  $\text{Na}_2\text{O}\cdot\text{CaO}\cdot 3\text{SiO}_2$  [30];  $\text{Na}_2\text{O}\cdot 2\text{CaO}\cdot 3\text{SiO}_2$  [33];  $\text{CaSiO}_3$ ,  $\text{Ca}_3\text{Si}_2\text{O}_7$  und  $\text{Ca}_2\text{SiO}_4$  [31] und  $\text{CaB}_2\text{SiO}_7$  and  $\text{CaAl}_{14}\text{B}_2[\text{SiO}_4]_8$  [34].

Motivation für die vorliegende Arbeit ist es, grundlegende Informationen bezüglich der Kristallisationskontrolle für die Entwicklung von Fluor-freien Gießpulvern für das kontinuierliche Gießen von Stahl bereitzustellen, indem das Kristallisationsverhalten von Schlacken mithilfe der SHTT untersucht wird.

Ziele dieser Arbeit sind folgende:

(i) Ein Grundlage und systematische Studie zu leisten, die das Kristallisationsverhalten von Schlacken der Systeme  $\text{CaO-Al}_2\text{O}_3$ ,  $\text{CaO-SiO}_2$ ,  $\text{CaO-SiO}_2\text{-TiO}_2$  und  $\text{CaO-SiO}_2\text{-TiO}_2\text{-Na}_2\text{O}$  mittels der Erstellung von Zeit-Temperatur-Umwandlungs-Schaubilder – „time-temperature-transformation“, TTT, oder „continuous-cooling-transformation“, CCT –, einer Analyse zur Kinetik des Kristallwachstums und der Kristallmorphologie bewertet.

(ii) Das Erstarrungsverhalten eines neuen industriellen Fluor-freien Gießpulvers für die Anwendung in Stahlwerken während des kontinuierlichen Gießens von Knüppeln zu untersuchen.

### **Experimentelle Arbeit**

Die Anlage zur SHTT ist eine einzigartige Apparatur, die mittels eines Thermoelementes Messungen der Schlackeprobentemperatur ermöglicht, während die Probe gleichzeitig erhitzt wird. Die Probe wird auf die Spitze des Thermoelementes gelegt und sie kann schnellen Abkühl- oder Aufheizraten ausgesetzt werden oder unter isothermen Bedingungen gehalten werden. Der Vorteil der SHTT ist, dass sie die in-situ-Beobachtung des Schmelzens und Erstarrens unter diversen thermischen Bedingungen ermöglicht. Es ist möglich sehr hohe Aufheiz- und Abkühlraten erreichen ( $> 3000 \text{ }^\circ\text{C/Min}$ ). Die SHTT kann für Schlacken angewendet werden, die optisch durchsichtig oder durchscheinend sind, während die kristalline Phase, welche bei der Abkühlung entsteht, undurchsichtig sein soll.

Die Schlacken, die in der vorliegenden Arbeit für die SHTT verwendet werden, wurden von dem sog. reagent-grade  $\text{CaCO}_3$ ,  $\text{SiO}_2$ ,  $\text{TiO}_2$ ,  $\text{Na}_2\text{CO}_3$  und  $\text{Al}_2\text{O}_3$  hergestellt. Tabelle 1 zeigt deren Zusammensetzungen.

**Tabelle 1:** Zusammensetzungen der für die Analyse mit der SHTT verwendeten Schlacken (Gew.-%). B ist das Verhältnis  $\% \text{CaO} / \% \text{SiO}_2$ .

	$\% \text{CaO}$	$\% \text{SiO}_2$	$\% \text{TiO}_2$	$\% \text{Na}_2\text{O}$	$\% \text{Al}_2\text{O}_3$	$\% \text{C}$	B
CA	43,7				56,3	0,074	
CS	41,7	58,3				0,063	0,7
CST_1	41,1	29,1	29,8			-	1,4
CST_2	35,6	46,3	18,1			0,590	0,8
CSTNA_1	33,6	41,3	16,5	7,1	1,5	0,073	0,8
CSTNA_2	30,1	46,8	16,4	5,4	1,3	0,034	0,6
CSTNA_3	31,6	48,1	15,5	3,7	1,1	0,032	0,7
CSTNA_4	30,9	42,3	15,2	6,4	5,2	0,038	0,7

Die im Rahmen dieser Arbeit verwendete Anlage (siehe Abbildung 1) wurde an der Technischen Universität Bergakademie Freiberg konstruiert [43]. Sie besteht aus zwei Systemen: einem System zur Beobachtung und einem aus dem Thermoelement bestehendem System. In einer Vakuumkammer gibt es zwei wassergekühlte Einsätze, einen auf der linken und einen auf der rechten Seite. Beide dieser Einsätze halten ein

Thermoelement des Typs B an den jeweiligen Spitzen fest. Jedes Thermoelement ist mit einem separaten Thermoelement-Kontrollgerät verbunden. Das zu untersuchende Material wird direkt auf dem Thermoelement in der Vakuumkammer aufgeschmolzen. Die Thermoelemente verbleiben innerhalb eines zusätzlichen Heizelementes (d. h. einer Kanthal-Spule), das den Wärmeverlust von der Probe an die Umgebung reduziert, indem es eine Temperatur von ca. 500 °C um die Probe herum aufrecht erhält.

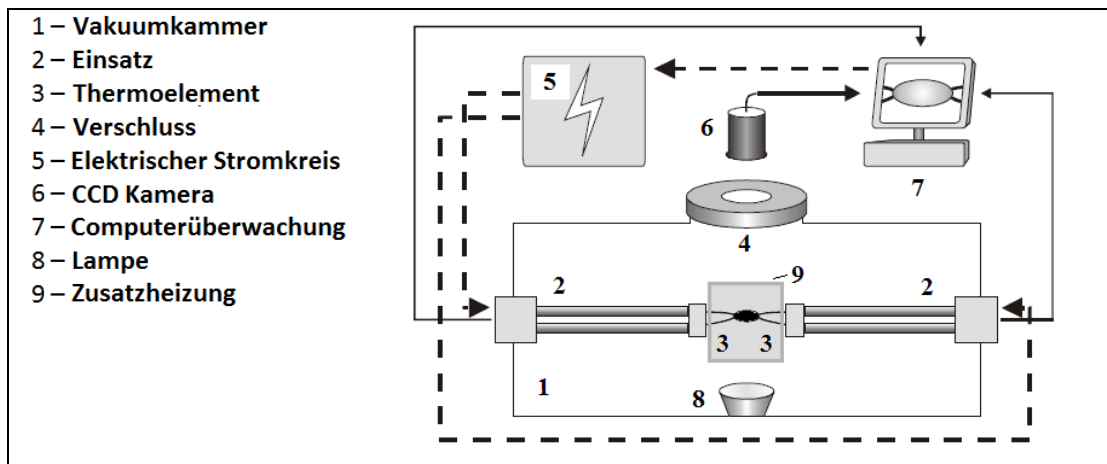


**Abbildung 1:** Schematische Ansicht der im Rahmen dieser Arbeit verwendeten experimentellen Vorrichtung.

Das Thermoelement ist vom Typ B (bis zu 1800°C). Es wird aus zwei Platindrähten mit einem Durchmesser von 0,5 mm und einer Länge von ca. 25 mm hergestellt: Pt30Rh und Pt6Rh.

Die Genauigkeit des Gerätes wurde mithilfe von Messungen der Kristallisationstemperatur ( $T_{\text{cryst.}}$ ) von  $\text{CaF}_2$ ,  $\text{Na}_2\text{SO}_4$  und  $\text{K}_2\text{SO}_4$  überprüft. Die  $T_{\text{cryst.}}$  wird hier als die Temperatur definiert, bei welcher unter Verwendung einer bestimmten Abkühlrate die ersten Kristalle beobachtet werden können. Mit der Probesubstanz in der Vakuumkammer wurde innerhalb von fünf Minuten ein Druck von 10 mbar eingestellt. Anschließend wurde der Behälter mit Ar gefüllt, wobei eine Durchflussrate von 300 L/h während der Messungen beibehalten wurde. Danach wurden die Substanzen auf 100 °C oberhalb ihrer Schmelzpunkte geschmolzen und bei einer Rate von 30 °C/Min abgekühlt. Die Schmelzpunkte der Substanzen sind folgende:  $\text{CaF}_2$  - 1418 °C,  $\text{Na}_2\text{SO}_4$  - 884 °C, und  $\text{K}_2\text{SO}_4$  - 1069 °C [44].

Abbildung 2 zeigt die Unterschiede zwischen den beschriebenen Schmelzpunkten [44] und der  $T_{\text{cryst.}}$ . Zwölf Experimente wurden für jede Substanz durchgeführt (Die Experimente 1-6 mit dem linken Thermoelement und die Experimente 7-12 mit dem rechten Thermoelement).

Unter Annahme einer Normalverteilung für  $\Delta T_{\text{cryst.}}$  können die Durchschnittswerte von  $T_{\text{cryst.}}$  der für die Kalibration verwendeten drei Substanzen

berechnet werden, siehe Tabelle 2. Die Durchschnittswerte von  $T_{\text{cryst}}$  liegen sehr nahe zu den in der Literatur beschriebenen Schmelzpunkten und die Streuung ist niedrig.

**Tabelle 2:** Vergleich zwischen den in der Literatur beschriebenen [44] Schmelzpunkten und der mittels SHTT gemessenen Kristallisationstemperaturen ( $T_{\text{cryst}}$ ). Für jede Substanz wurden 12 Messungen durchgeführt.

	Literatur [44]	Durchschnittswert $T_{\text{cryst}}$	Streuung (standard deviation) $T_{\text{cryst}}$
$\text{CaF}_2$	1418 °C	1417 °C	10,6 °C
$\text{Na}_2\text{SO}_4$	884 °C	883 °C	6,6 °C
$\text{K}_2\text{SO}_4$	1069 °C	1071 °C	15,4 °C

Die in Tabelle 2 zusammengefassten Ergebnisse wurden mittels Analyse einer Videodatei erzielt. Das Gerät zur SHTT registriert auch die Temperaturentwicklung in Abhängigkeit von der Zeit, ähnlich der Differenzialthermoanalyse (DTA). Es wurde während der Kalibration nachgewiesen, dass die optisch beobachtete Kristallisation den Peaks in den Diagrammen zur Darstellung der Temperatur in Abhängigkeit von der Zeit entspricht.

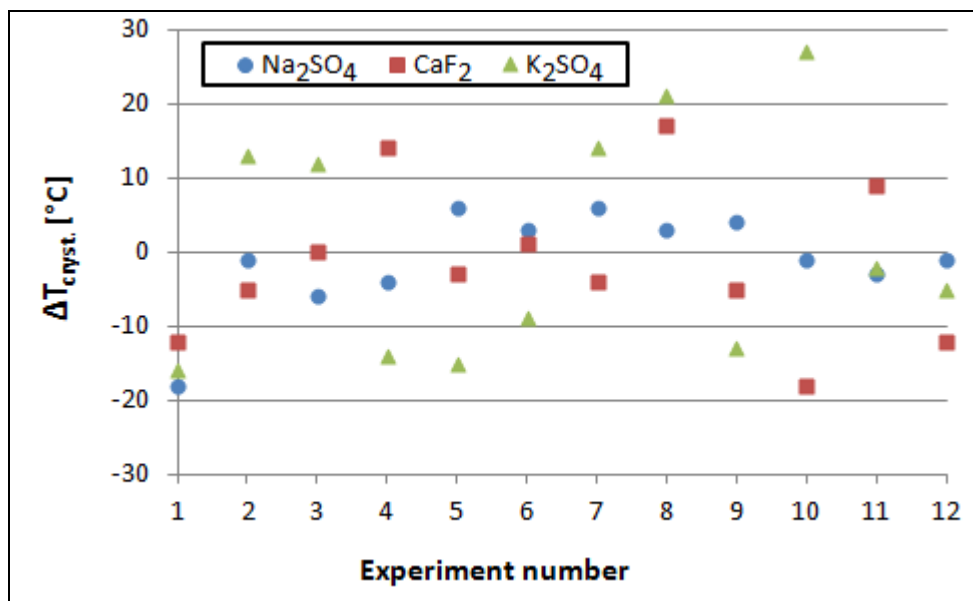


**Abbildung 2:** Vergleich der Ergebnisse aus der Fachliteratur [44] und der Ergebnisse der vorliegenden Arbeit.  $\Delta T_{\text{cryst}}$  ist die Differenz zwischen dem beschriebenen Schmelzpunkt und der mittels der SHTT gemessenen Kristallisationstemperatur.

Es wurde beobachtet, dass es wichtig ist, geeignete Vakuumzeiten vor Beginn der Messungen anzuwenden. Sie liegen für dieses Gerät bei ca. 10 mbar für fünf Minuten. Wenn mit kürzeren Vakuumzeiten gearbeitet wird, beispielsweise von einer Minute bei 10 mbar, tendiert die Kristallisationstemperatur von  $\text{CaF}_2$  dazu, außerhalb des Bereiches von  $1418 \pm 20$  °C zu fallen, wahrscheinlich aufgrund der Reaktion von Wasserdampf und  $\text{CaF}_2$ .

Um die Experimente mit der SHTT durchzuführen, werden kleine Mengen vorgeschmolzener Schlacke (5-10 mg) gepresst und auf die Spitze des Thermoelements plaziert. Mit der Substanz in der Vakuumkammer wird innerhalb von fünf Minuten ein Druck von 10 mbar eingestellt. Anschließend wird der Behälter mit Ar gefüllt, wobei während der Messungen eine Durchflussrate von 300 L/h beibehalten wird. Das zusätzliche Heizelement wird eingeschaltet und eine Temperatur von ca. 500 °C wird um das Thermoelement herum aufrecht erhalten.

Zur Erstellung von Zeit-Temperatur-Umwandlungsschaubildern (isothermisch) werden nach dem Schmelzen sehr hohe Abkühlraten (größer als 3000 °C/Min) bis zum Erreichen der gewünschten Temperatur angewandt. Anschließend wird die Inkubationszeit, also die bis zur Beobachtung der ersten Kristalle benötigte Zeit, mittels direkter Beobachtung ermittelt. Unter Anwendung der Inkubationszeiten für verschiedene Temperaturen werden ZTU-Schaubilder konstruiert. Zur Erstellung von kontinuierlichen Abkühlkurven wird nach dem Schmelzen eine bestimmte Abkühlrate angewandt. Anschließend wird das Erstarrungsverhalten beobachtet. Unter Anwendung verschiedener Abkühlraten kann eine kontinuierliche Abkühlkurve erstellt werden.

Viskositätsmessungen wurden unter Verwendung eines Rotationsviskosimeters (Anton Paar MC 301) an der Technischen Universität Bergakademie Freiberg durchgeführt. Die für diese Messungen verwendeten Materialien haben eine der für die SHTT-Analyse verwendeten Schlacken (vgl. Tabelle 1) ähnliche Zusammensetzung.

## ***Ergebnisse und Diskussion***

### *CaO-Al<sub>2</sub>O<sub>3</sub>-Schlacke (CA)*

Die CaO-Al<sub>2</sub>O<sub>3</sub> Schlacke, hier als CA bezeichnet, mit 43,7 % CaO and 56,3 % Al<sub>2</sub>O<sub>3</sub> wurde mittels SHTT untersucht. Die Liquidustemperatur für diese Schlacke liegt laut FactSage 6.1 bei 1518 °C und der erste Kristall während der Abkühlung ist CaAl<sub>2</sub>O<sub>4</sub>. Der zweite Kristall während der Abkühlung ist Ca<sub>3</sub>Al<sub>2</sub>O<sub>6</sub>, der bei einer Temperatur von 1362 °C (Solidustemperatur) entsteht.

Eine kontinuierliche Abkühlkurve wurde mittels der SHTT erstellt. Die Proben wurden vor der Abkühlung bei verschiedenen Abkühlraten für 60 Sekunden auf einer Temperatur von 1700 °C gehalten. Es wurde beobachtet, dass die Kristallisation weit von der Liquidustemperatur entfernt beginnt. Die Kristallisationstemperatur (d. h. die Temperatur, bei der die ersten Kristalle beobachtet werden) ist von der Abkühlrate abhängig. Die kritische Abkühlrate für die CA-Schlacke liegt bei 1700 °C/Min, d. h. bei einer höheren Abkühlrate werden keine Kristalle beobachtet.

Von den Viskositätsmessungen kann festgestellt werden, dass der sog. Breakpoint, d. h. der Punkt, an dem ein plötzlicher Viskositätsanstieg aufgrund der Kristallbildung zu verzeichnen ist, in einem Bereich zwischen 1350 – 1375 °C liegt. Entsprechend der Ergebnisse von der SHTT liegt der Punkt, an dem die ersten Kristalle

für diese CA-Schlacke entdeckt wurden bei einer Abkühlrate von 6 °C/Min bei 1350 °C. Daher gibt es für diese Schlacke eine Übereinstimmung zwischen der mittels Viskosimeter ermittelten Breakpoint und der durch die SHTT ermittelten Kristallisationstemperatur.

#### *CaO-SiO<sub>2</sub>-Schlacke (CS)*

Die CaO-SiO<sub>2</sub>-Schlacke mit einer Basizität von %CaO/%SiO<sub>2</sub> = 0,7, hier als CS bezeichnet, hat laut FactSage 6.1 folgende Charakteristika: Liquidustemperatur 1500 °C; erste feste Phase während der Abkühlung CaSiO<sub>3</sub>; und Solidustemperatur 1437 °C, bei der die zweiten Kristalle (SiO<sub>2</sub>) auftreten.

Bezüglich der Experimente mit kontinuierlicher Abkühlung wird keine Kristallisation beobachtet, sogar bei sehr niedrigen Abkühlraten. Dieses Ergebnis stimmt mit den Ergebnissen anderer Berichte für CaO-SiO<sub>2</sub>-Schlacken mit Basizitäten von 0,8 , 1,0 and 1,2 überein, in welchen kein Kristall bei Experimenten mit kontinuierlicher Abkühlung entdeckt wurden [43].

Für Experimente mit isothermischer Umwandlung („TTT diagrams“) wurden die Proben vollständig aufgeschmolzen und dann bei 1700 °C für fünf Minuten lang gehalten. Anschließend wurde eine sehr hohe Abkühlrate (> 3000 °C/min) angewandt. Sobald die gewünschten Temperaturen – 900 °C, 950 °C, 1000 °C, 1050 °C, 1100 °C, 1150 °C und 1200 °C – erreicht waren, wurden die Proben für bis zu 1000 Sekunden auf dieser Temperatur gehalten. Für die isotherme Umwandlung wurde eine Kristallisation erst bei 1000 °C nach einer Haltedauer von 76 Sekunden (Durchschnitt von sechs Experimenten, Standardabweichung 27 Sekunden) beobachtet und diese wurde innerhalb weniger Sekunden abgeschlossen.

Zusätzlich zu den kontinuierlichen und isothermen Experimenten wurde ein spezieller thermischer Zyklus angewandt: (i) Die Probe wurde bei 1700 °C für fünf Minuten gehalten, d. h. vollständig aufgeschmolzen; (ii) Abschrecken (> 3000 °C/Min) bis auf eine bestimmten Temperatur (900 °C, 950 °C, 975 °C, 1000 °C, 1025 °C, 1050 °C, 1100 °C, 1150 °C, 1200 °C, 1300 °C); (iii) Halten auf der bestimmten Temperatur für 60 Sekunden; und (iv) Erneutes Aufheizen bei einer Rate von 1000 °C/Min bis zu 1700 °C.

Was den oben genannten thermischen Zyklus anbelangt, wurde beobachtet, dass die Kristallisation während des Aufheizens bei einer Rate von 1000 °C/Min intensiv auftritt, aber nur wenn (nach dem Abschrecken) bei 1000 °C oder niedriger begonnen wird. Die Kristallisation tritt intensiv im Bereich zwischen 1069 – 1125 °C auf, wenn bei 900 °C, 950 °C, 975 °C und 1000 °C begonnen wird. Daher wird deutlich, dass beim Erhöhen der Temperatur nach Erreichen eines bestimmten Bereiches niedrigerer Temperaturen gute Bedingungen für das Kristallwachstum für CS-Schlacken erzielt werden können. Diese intensive Kristallisation kann durch die Tatsache erklärt werden, dass der optimale Temperaturbereich für die Keimbildung zur Kristallisation niedriger als der optimale Temperaturbereich für das Kristallwachstum liegt. Dies ist

verbunden mit der Tatsache, dass die Kristallwachstumsrate nicht der einzige Parameter zur Bestimmung der Fähigkeit einer Schmelze, Kristalle zu bilden ist, da die Kristalle aus einer bestimmten Anzahl von Keimen wachsen und in vielerlei Hinsicht der Keimbildungsabschnitt den Ablauf der gesamten Kristallisation in silikatischen Gläsern bestimmt [38]. Es ist bekannt, dass die Kristallisation in zwei Prozesse unterteilt werden kann: (i) Die Keimbildung und (ii) Das Kristallwachstum. Die Geschwindigkeiten beider Prozesse sind temperaturabhängig mit Maxima bei bestimmten Unterkühlungswerten. Diese Maxima sind in glassbildende Materialien, die für die Herstellung von Glaskeramik geeignet sind und die Kontrolle der Kristallisation ermöglichen, voneinander getrennt [48].

Die Beobachtung von Kristallen während Experimenten unter isothermen Bedingungen bei 1000 °C für die CS-Schlacke wird durch die Tatsache erklärt, dass 1000 °C eine intermediäre Temperatur ist, bei der sowohl die Keimbildungs- als auch die Keimwachstumsrate ausreichend hoch sind.

#### *CaO-SiO<sub>2</sub>-TiO<sub>2</sub>-Schlacke (CST\_1)*

Die Schlacke des CaO-SiO<sub>2</sub>-TiO<sub>2</sub> Systems, hier als CST\_1 bezeichnet, wurde verwendet, um den Effekt der Überhitzungsdauer auf die Inkubationszeiten zu untersuchen. Die Zusammensetzung (Gew.-%) der CST\_1 ist 41,1 % CaO, 29,1 % SiO<sub>2</sub>, and 29,8 % TiO<sub>2</sub>. Die Liquidustemperatur ist für diese Schlacke ca. 1600 °C – sehr hoch. Die erste während der Abkühlung gebildete Phase aus der flüssigen Schlacke ist CaO.TiO<sub>2</sub>.

Ein spezieller thermischer Zyklus, der mehrmals für jede Probe wiederholt wurde, wurde angewandt und wird im Folgenden beschrieben: (i) Die Proben wurden in einem Temperaturbereich zwischen 1650 – 1680 °C mit unterschiedliche Dauer gehalten (die Proben waren immer komplett aufgeschmolzen und wurden innerhalb weniger Sekunden transparent); (ii) Bei der höchsten Abkühlrate (> 3000 °C/min) bis auf 1400 °C abschrecken; (iii) Messung der Inkubationszeit, d. h. wann die ersten Kristalle beobachtet werden konnten; (iv) Abschrecken bis auf eine Temperatur von 1200 °C, die für 60 Sekunden gehalten wurde, um eine vollständige Kristallisation der Probe zu gewährleisten; (v) Erhitzen bis auf eine Temperatur zwischen 1650 – 1680 °C.

Es wurde beobachtet, dass die Überhitzungsdauer das Kristallisationsverhalten der CST\_1-Schlacke vollständig verändert hat, unter der Annahme, dass vor dem Schmelzen äquivalente Anfangsbedingungen herrschten. Wenn die Haltezeit 60 Sekunden beträgt, so tendiert die Inkubationszeit zu deutlich kürzeren Zeiten (5-12 Sekunden) im Vergleich zu einer Haltezeit von 600 Sekunden (es ist bemerkenswert, dass bis zu einer Wartezeit von 1000 Sekunden kein Kristall beobachtet wurde). Zwei Proben wurden analysiert, eine mit einer Masse von 1,4 mg und die andere mit einer Masse von 2,3 mg.

Es ist bekannt, dass eine neue Phase von Keimen, die bereits in der alten Phase existiert, gebildet wird und deren effektive Anzahl pro Keimbildungsflächeneinheit

durch die Überhitzungstemperatur und die Überhitzungsdauer verändert werden kann. Es gibt Hinweise darauf, dass die Keime für eine gegebene Unterkühlung oder Überhitzung bedeutend langsamer als Körner von sichtbarer Größe wachsen oder schrumpfen. Diese Keime, die Inhomogenitäten jeglicher Art sein können, bestünden normalerweise aus kleinen Partikeln der subkritischen Phase oder aus festen Schichten der vorhergehenden umgebenden Fremdeinschlüsse [49].

Deshalb gibt es eine Beziehung zwischen der Überhitzungsdauer, den Inkubationszeiten und der Keimzahl. Je länger die Überhitzungsdauer ist, umso niedriger ist die Anzahl an Keimen pro Keimbildungsflächeneinheit und infolgedessen wird die Inkubationszeit umso länger.

#### *CaO-SiO<sub>2</sub>-TiO<sub>2</sub>-Schlacke (CST\_2) und CaO-SiO<sub>2</sub>-TiO<sub>2</sub>-Na<sub>2</sub>O-Al<sub>2</sub>O<sub>3</sub>-Schlacken (CSTNA)*

Die Zusammensetzung für die CST\_2 und für die CSTNA-Schlacken sind in Tabelle 1 dargestellt.

Das ZTU-Diagramm (isothermisch) für die Schlacke CST\_2, das unter Anwendung der SHTT erstellt wurde, ist in Abbildung 3 dargestellt. Es ist erforderlich, Kristalle des Systems CaO-SiO<sub>2</sub>-TiO<sub>2</sub> ausscheiden, indem sie das System CaO-SiO<sub>2</sub>-CaF<sub>2</sub> ersetzen. Jedoch sind die Inkubationszeiten für die Schlacke CST\_2 deutlich länger als jene der Fluor-haltigen industriellen Schlacke, deren ZTU-Diagramm auch in der Abbildung dargestellt ist – es ist ein kommerzielles Gießpulver, das für gewöhnlich für das Stranggießen von nichtrostenden Stählen angewendet wird, das CaF<sub>2</sub> und Na<sub>2</sub>O ohne TiO<sub>2</sub> beinhaltet.

Die Schlacke CSTNA\_1 wurde entwickelt, um eine Basizität sowie einen TiO<sub>2</sub> Gehalt ähnlich der Schlacke CST\_2 zu erhalten; ihr ZTU-Diagramm ist in Abbildung 3 dargestellt. Die Na<sub>2</sub>O-haltige Schlacke CSTNA\_1 hat eine höhere Kristallisationsrate.

Mit diesem neuen Ergebnis, d. h. der Tatsache, dass es unter Zugabe von Na<sub>2</sub>O in das System CaO-SiO<sub>2</sub>-TiO<sub>2</sub> zu einem bedeutenden Anstieg der Kristallisationsrate kommt, wurden andere Schlacken mit niedrigerem Na<sub>2</sub>O Gehalt hergestellt, um die Möglichkeit der Kristallisationskontrolle zu untersuchen: CSTNA\_2, CSTNA\_3 und CSTNA\_4. Die ZTU-Diagramme (isothermisch) für die CSTNA-Schlacken zeigen, dass es mittels Variation des Gehaltes an Na<sub>2</sub>O in CaO-SiO<sub>2</sub>-TiO<sub>2</sub> Schlacken möglich ist, die Kristallisationstendenz zu kontrollieren.

Es wurde für alle Schlacken beobachtet, dass die Kristallmorphologie mit der Temperatur variiert. Stängelförmige Körner (die in eine einheitliche Richtung von der Oberfläche zum Zentrum der Probe hin zu wachsen scheinen) und gleichachsige Körner (die radial in die flüssige Schlacke zu wachsen scheinen) wurden beobachtet. Die Kristalle zeigen bei höheren Temperaturen eine dendritische Struktur und werden bei niedrigeren Temperaturen klein und massiv. Diese letzten Kristalle, die bei höherem Unterkühlungsgrad in der Mitte der flüssigen Schlacke gebildet werden, können mithilfe der homogenen Keimbildungstheorie erklärt werden.



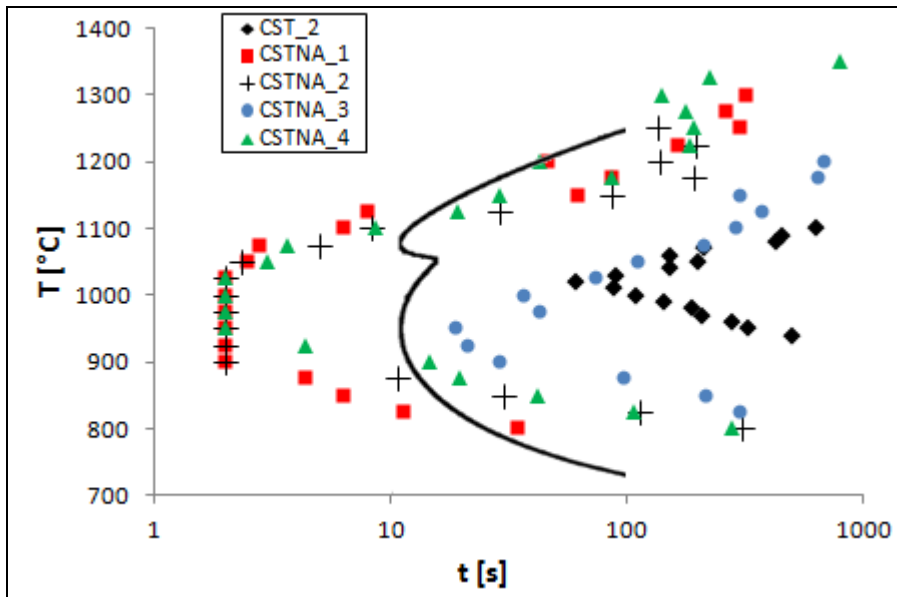


**Abbildung 3:** ZTU-Diagramm (isothermisch) für Schlacken des Systems  $\text{CaO-SiO}_2\text{-TiO}_2\text{-Na}_2\text{O-Al}_2\text{O}_3$  (Zusammensetzung siehe Tabelle 1) ermittelt mithilfe der SHTT und für eine Fluor-haltige industrielle Schlacke [5] (kontinuierliche Linie ebenfalls mittels SHTT ermittelt).

$\text{Na}_2\text{O}$  hat auch einen großen Einfluss hinsichtlich der Viskosität der Gießschlacke. Es ist bekannt, dass die Kristallisation umso einfacher abläuft, je niedriger die Viskosität ist. Es wurde beobachtet, dass (i) bei Zugabe von  $\text{TiO}_2$  in eine  $\text{CaO-SiO}_2$  Schlacke (43,3 %  $\text{CaO}$ , 56,7 %  $\text{SiO}_2$ ) die Viskosität für den gesamten Temperaturbereich absinkt und (ii) danach, wenn  $\text{Na}_2\text{O}$  in die  $\text{CaO-SiO}_2\text{-TiO}_2$  Schlacke (36,4 %  $\text{CaO}$ , 45,9 %  $\text{SiO}_2$ , 17,7 %  $\text{TiO}_2$ ) hinzugefügt wird und auf diese Weise eine  $\text{CaO-SiO}_2\text{-TiO}_2\text{-Na}_2\text{O}$  Schlacke (33,5 %  $\text{CaO}$ , 41,9 %  $\text{SiO}_2$ , 16,3 %  $\text{TiO}_2$ , 8,2 %  $\text{Na}_2\text{O}$ , 0,1 %  $\text{Al}_2\text{O}_3$ ) entsteht, die Viskosität für den gesamten Temperaturbereich weiter absinkt und die Neigung der Kurve geringer wird.

Industrielle Gießschlacken wären aufwändiger als die CSTNA-Schlacken, da sie mehr Komponenten besitzen. In jedem Fall kann die vorliegende Studie als Referenz für zukünftige Entwicklungen bei der Herstellung von Fluor-freien Gießpulvern für das Brammengießen verwendet werden, für das die Kontrolle der Kristallisation unumgänglich ist.

#### Kritische Abkühlraten

Die kritischen Abkühlraten ( $R_c$ ) für mithilfe der SHTT untersuchten Schlacken wurden bestimmt. Sie wurden berechnet durch Ermittlung der  $T_{\text{nose}}$  und der  $t_{\text{nose}}$  aus dem ZTU-Schaubild („TTT curves“) und Berechnung der  $T_{\text{liquidus}}$  mittels FactSage 6.1. Der Einfluss von Natrium auf steigende kritische Abkühlraten ist deutlich; je höhere Gehalt an Natrium ist, umso höher wird die kritische Abkühlrate.

Da die Abkühlraten während des Stranggießens von weniger als  $1\text{ °C/s}$  bis zu  $100\text{ °C/s}$  [2, 43] variieren, kann gefolgert werden, dass für  $\text{Na}_2\text{O}$ -haltige Schlacken mit

höherem Natriumgehalt (CSTNA\_1, CSTNA\_2, CSTNA\_4) die Kristallisation während der Abkühlung nicht vermieden werden kann.

#### *Kinetik des Kristallwachstums*

Die Kinetik des Kristallwachstums für die CST\_2 und CSTNA\_1 Schlacken (Zusammensetzung siehe Tabelle 1) wurden analysiert. Die allgemeine Kristallisation kann mittels der Bestimmung des Volumenanteils der umgewandelten Phase während der isothermen Umwandlung  $\zeta(t)$  beschrieben werden. Bilder wurden von Videodateien entnommen und von diesen Bildern wurde der Bereich des kristallinen Anteils mithilfe einer Software gemessen. Die Partikel wurden als Kugeln behandelt. Für die CST\_2 Schlacke lautet die Avrami-Gleichung bei 1070 °C folgendermaßen:

$$\zeta(t) = 1 - \exp(-0.00135t^{1.57})$$

Für die Schlacke CSTNA\_1 sind die Ergebnisse während isothermer Umwandlung bei verschiedenen Temperaturen in Abbildung 4 zusammengefasst.

Die CST\_2-Schlacke zeigt ein komplexes Kristallisationsverhalten, d. h. mehr als eine Kristallphase, mit unterschiedlichen Morphologien auf, die eine Kombination von Volumen- und Oberflächenkristallisation zu sein scheinen. In diesem Fall ist die physikalische Bedeutung der aus der numerischen Angleichung erhaltenen Werte von  $n$  und  $K$  aus der Avrami-Gleichung unbekannt. Dadurch ist es nicht möglich, Informationen bezüglich des Umwandlungsmechanismus zu ermitteln, wodurch nicht deutlich ist, ob das Kristallwachstum von der Grenzfläche oder durch Diffusion kontrolliert wird. Für die CSTNA-Schlacke entstehen ähnliche Schwierigkeiten.

Der Avrami-Parameter  $n$ , der aus der alleinigen Nutzung von numerischen Methoden ermittelt wurde, repräsentiert einen Durchschnitt und kann zu fehlerhaften Interpretationen für den Mechanismus der Phasenumwandlung führen [62]. Die JMAK-Theorie kann innerhalb des Rahmens ihrer Annahmen als exakt nachgewiesen werden. Jeder Widerspruch muss Ergebnis ihrer Anwendung auf Situationen sein, in welchen ihren Annahmen widersprochen wird, was in vielen Situationen der Kristallisation der Fall sein kann. Es wurde gezeigt, dass es zusätzlich erforderlich ist, eine detaillierte Kenntnis bezüglich des Umwandlungsmechanismus zu besitzen, um die JMAK-Theorie anzuwenden, welche die Transformationskinetik beschreibt [39].

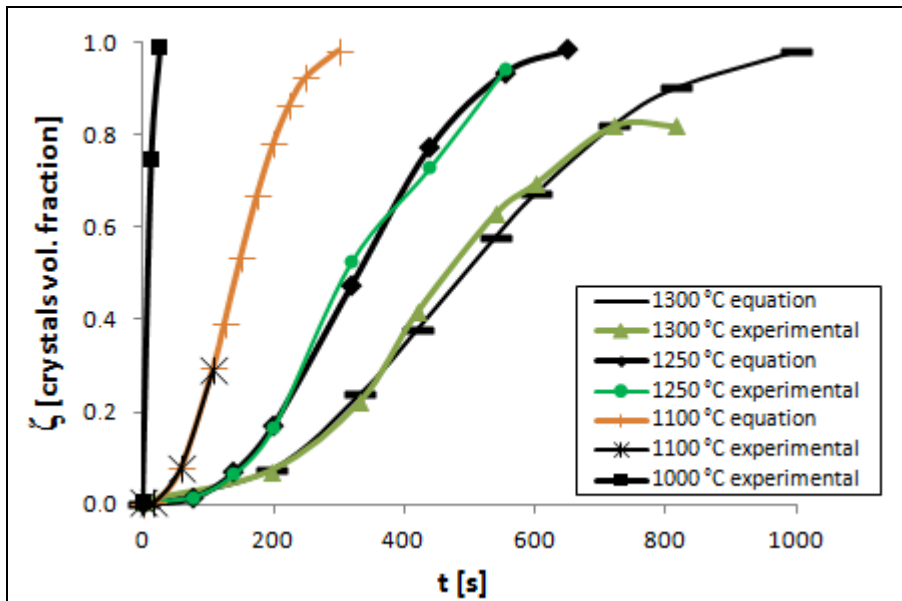


**Abbildung 4:** Volumenanteil der Kristalle in Abhängigkeit von der Zeit für die isotherme Umwandlung bei unterschiedlichen Temperaturen für die Schlacke CSTNA\_1.

#### *Erstarrungsverhalten von Fluor-freien Gießpulvern für das Gießen von Knüppeln*

Die Wahl des Gießpulvers für das Gießen von Knüppeln ist zum Erzielen einer erfolgreichen Gießpraxis sehr wichtig. Da die Nachfrage nach dem Gießpulververbrauch für das Gießen von Knüppeln nicht hoch sind, verwenden Stahlhersteller häufig hochviskose Gießschlacken, um Probleme wie die Ansammlung von Schlacke und die Erosion des Tauchausgusses zu verhindern [1, 65].

Laborversuche wurden mit neuen Fluor-freien Rezepturen durchgeführt [67]. Aus diesen Labortest heraus wurde das neue Gießpulver Accutherm ST-SP/512SV-DS-1 (hier bezeichnet als „Fluor-frei“) als granuliertes Gießpulver hergestellt, um die kommerzielle Accutherm ST-SP/512SV-DS (hier bezeichnet als „Fluor-haltig“) zu ersetzen, die von der Stollberg Gruppe produziert und in Stahlwerken für das Gießen von Knüppeln verwendet wird.

Das Verhalten des neuen Fluor-freien Gießpulvers aus Labortests und industriellen Versuchen kann folgendermaßen zusammengefasst werden:

(i) Aus den Laborversuchen wurde geschlossen, dass die technologischen Parameter bei Betrachtung des Fluor-haltigen Standardgießpulvers und des Fluor-freien Gießpulvers ähnlich sind: Schmelzcharakteristika, Viskosität, Aufschmelzverhalten und Kristallisationstendenz.

(ii) Aus den Versuchen in Stahlwerken, während des Stranggießprozesses wurden einige Bewertungen bezüglich folgender Parameter gemacht:  $\Delta T$  zwischen dem Ein- und Auslauf der Wasserkühlung, Dicke des Schlackepools, Strangtemperatur vor dem Richten, Aufschmelzverhalten, Gießpulververbrauch, Aufnahme von  $\text{Al}_2\text{O}_3$  durch die Gießschlacke. Das Verhalten des Fluor-freien Gießpulvers wurde als adäquat bewertet. Außerdem wurde eine signifikante Reduzierung der Tauchausgusserosion registriert.

(iii) Der Ausschussanteil, der während des Walzprozesses für das Fluor-freie Gießpulver entstand, war nicht kritisch und es zeigte sich eine gute Oberflächenqualität.

(iv) Weitere industrielle Versuche sind notwendig, um die im Rahmen dieser Arbeit beschriebenen Ergebnisse zu überprüfen.

### **Zusammenfassung**

Folgende Ergebnisse wurden im Rahmen der vorliegenden Arbeit ermittelt:

(i) Das Gerät, das für die Heißthermoelementmethode – SHTT (Single Hot Thermocouple Technique) und DHTT (Double Hot Thermocouple Technique) – genutzt wird, ist entsprechend der mit  $\text{CaF}_2$ ,  $\text{Na}_2\text{SO}_4$  und  $\text{K}_2\text{SO}_4$  durchgeführten Kalibration exakt.

(ii) Durch die in-situ Beobachtung unter Anwendung der SHTT kann das Kristallisationsverhalten von Schlacken charakterisiert werden, indem ZTU-Schaubilder (isothermisch) oder kontinuierliche Abkühlkurven erstellt werden.

(iii) Die kontinuierliche Abkühlkurve für die Basisschlacke CA – 44 % CaO , 56 %  $\text{Al}_2\text{O}_3$  (Gew.-%) – zeigte eine große Differenz zwischen der Liquidustemperatur und der Temperatur des Auftretens der ersten Kristalle, sogar bei niedrigen Abkühlraten, d. h. 168 °C unter der Liquidustemperatur bei einer Abkühlrate von 6 °C/Min. Des Weiteren wurde für diese Schlacke ein Zusammenhang zwischen der mittels Viskosimeter ermittelten Breakpoint und der mittels SHTT ermittelten Kristallisationstemperatur gefunden.

(iv) Für die CS-Schlacke – %CaO/% $\text{SiO}_2$  (Gew.-%) = 0,7 – wurde während der isothermen Experimente erst bei 1000 °C eine Kristallisation mit einer Inkubationszeit von 76 Sekunden (Mittelwert aus 6 Experimenten, Standardabweichung 27 Sekunden) beobachtet. Für Versuche mit kontinuierlichen Abkühlraten kann sogar bei niedrigen Abkühlraten (z. B. 10 °C/Min) kein Kristall entdeckt werden. Jedoch wird eine intensive Kristallisation beobachtet, wenn die Temperatur nach dem Erreichen niedriger Temperaturen (< 1000 °C) erhöht wird, dies kann durch die Tatsache erklärt werden, dass der optimale für die Keimbildung erforderliche Temperaturbereich niedriger als der für das Kristallwachstum erforderliche Temperaturbereich liegt.

(v) Für die CST\_1-Schlacke – 41,1 % CaO, 29,1 %  $\text{SiO}_2$ , 29,8 %  $\text{TiO}_2$  (Gew.-%) – die eine hohe Liquidustemperatur besitzt (ca. 1600 °C), wurde der Effekt der Überhitzungsdauer (im Bereich von 1650 – 1680 °C) auf die Inkubationszeit untersucht. Es wurde entdeckt, dass die Inkubationszeit umso länger wird, je länger die Überhitzungsdauer war, d. h. die Überhitzungsdauer kann – für eine Schlacke, die vollständig flüssig zu sein scheint – das Kristallisationsverhalten einer Schlacke stark beeinflussen. Dies kann durch die Tatsache erklärt werden, dass die unsichtbaren Keime langsamer als Körner einer messbaren Größe schrumpfen (im  $\mu\text{m}$ -Bereich)

(vi) Es wurde beobachtet, dass die Zugabe von  $\text{Na}_2\text{O}$  in CaO- $\text{SiO}_2$ - $\text{TiO}_2$ -Schlacken die Inkubationszeit für die Kristalle drastisch auf den Bereich von Sekunden verkürzt,

wie im ZTU-Schaubild (isothermisch) gezeigt ist. Es gibt einen deutlichen Effekt des Gehaltes an  $\text{Na}_2\text{O}$  auf die kritische Abkühlrate. Es ist möglich, die Kristallisationskinetik in  $\text{CaO-SiO}_2\text{-TiO}_2$ -Schlacken durch die Veränderung des Gehaltes an  $\text{Na}_2\text{O}$  zu kontrollieren.

(vii) Die Schlacke CST\_2 zeigt ein komplexes Kristallisationsverhalten auf: mehr als eine Kristallphase mit unterschiedlichen Morphologien, die eine Kombination von Volumen- und Oberflächenkristallisation zu sein scheinen. In diesem Fall ist die physikalische Bedeutung der aus numerischen Methoden ermittelten Werte  $n$  und  $K$  aus der Avrami-Gleichung unbekannt. Für die CSTNA-Schlacke entstehen ähnliche Schwierigkeiten.

(viii) Die Morphologie der Kristalle variiert mit der Temperatur. Für CSTNA-Schlacken wurden stängelförmige Körner (die von der Oberfläche gerichtet in das Zentrum der Probe zu wachsen scheinen) und gleichachsige Körner (die radial in die flüssige Schlacke zu wachsen scheinen) beobachtet. Die Kristalle haben bei höheren Temperaturen ein dendritisches Aussehen und werden bei niedrigeren Temperaturen klein und kompakt. Bei niedriger Temperatur ( $< 900\text{ °C}$ ) sind die Kristalle sehr fein und die Kristalldichte stieg an, bis sie „wolkenartig“ aussah.

(ix) Ein neues Fluor-freies Gießpulver für das Stranggießen wurde durch die Zusammenarbeit zwischen Universitäten, Gießpulverlieferanten und Stahlwerken entwickelt. Laboruntersuchungen zeigten, dass die technologischen Parameter für sowohl das kommerzielle Fluor-haltige Gießpulver als auch für das neue Fluor-freie Gießpulver ähnlich sind. Die Kristallisationstendenz für beide ist ähnlich. Von den in den Stahlwerken durchgeführten Versuchen wurde berichtet, dass eine vergleichbare Oberflächenqualität für die unter Verwendung des Fluor-freien Gießpulvers erzeugten Stränge erzielt wurde.



## **CURRICULUM VITAE**

Jeferson Leandro Klug (born on October 31<sup>st</sup> 1978 in Camaquã, Brazil) is a Metallurgical Engineer who got his graduation at Universidade Federal do Rio Grande do Sul (UFRGS), Brazil. He started working in Brazilian metallurgical industries. Afterwards, he got a MSc title from the Program of Postgraduate Studies in Mining, Metallurgical and Materials Engineering of the UFRGS.

His bi-national doctorate was performed at UFRGS and at Technische Universität Bergakademie Freiberg (TUBAF), according to a joint doctorate agreement. Main partners were the Brazilian Science and Technology National Council (CNPq), the Laboratory of Iron and Steel Technology of the UFRGS, the Laboratory of Computational Thermodynamics for Metallurgy of the UFRGS, the Institute of Iron and Steel Technology of the TUBAF, the Institute for Nonferrous Metallurgy and Purest Materials of the TUBAF, the company Stollberg (in Brazil and in Germany), and a Brazilian steel producer.

In his doctorate work, at TUBAF a basic study was performed with slags using the Single Hot Thermocouple Technique, with the aim of controlling their crystallisation behaviour. In Brazil the focus was industrial research, in a collaborative work established with the universities, the leading mould powder producer and the steel producer, with the aim of developing a new fluorine-free mould powder for the continuous casting of billets. The results when doing tests at steelworks with this new industrial mould powder have been successful.

Results of his doctoral work have been sent to recognized journals and to international conferences.

Currently he is working as a professor at Universidade Federal do Ceará, Brazil, in the Department of Metallurgical and Materials Engineering.